Exciton and Polaron Dynamics in Thin Oligo- and Polythiophene Films

Exziton- und Polarondynamik
in dünnen Oligo- und Polythiophenfilmen

Am Fachbereich Physik
der Freien Universität zu Berlin
eingereichte kumulative Dissertation

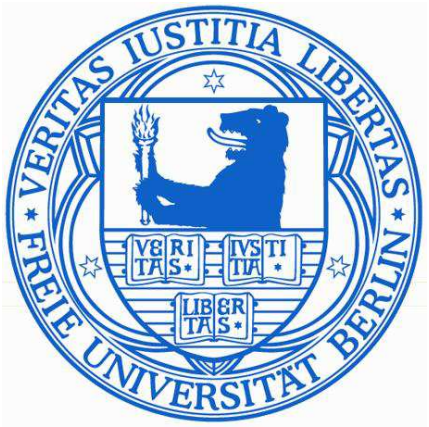

Erwan Varene

Berlin, den 14. November 2012

This work was done between August 2008 and May 2012
in the group of Prof. Dr. Petra Tegeder at the Physics Department
of the Freie Universität Berlin.

Berlin, 14.11.2012

1st referee: Prof. Dr. Petra Tegeder

2nd referee: Prof. Dr. Katharina J. Franke

Date of defense: 07.01.2013

Abstract

In the framework of this thesis the exciton and polaron dynamics in thin oligo- and polythiophene films have been investigated. Two-photon photoemission (2PPE) has been employed to study the electronic structure as well as the exciton formation, relaxation and decay dynamics in the oligothiophene films and at their interface with Au(111). Performing coverage, photon-energy-dependent and time-resolved experiments on sexithiophene (6T)/Au(111), we found that a photoinduced electron transition between the highest occupied molecular orbital (HOMO) and the lowest unoccupied molecular orbital (LUMO) is essential in order to observe the population of a Frenkel exciton that takes place within 100 femtoseconds (fs). In thin 6T films the exciton exhibits a lifetime of 650 fs. On a timescale of 400 fs an energetic stabilization is observed resulting in the formation of a polaron or electron trapping at defect states. The lifetime of this state is 6 picoseconds (ps). Moreover, beside the intramolecular relaxation channel of the exciton and the polaron/trap, a substrate-mediated relaxation channel exists.

In order to investigate the influence of the adsorption geometry on the excited state dynamics, we have studied an alkyl-substituted 6T, namely α,ω-dihexylsexithiophene (DH6T) on Au(111). The exciton and polaron/trap dynamics is 5-6 times faster in DH6T compared to 6T. We believe that the wall-brick-like adsorption geometry of DH6T is responsible for this behavior. Indeed, the alkyl chains in DH6T act as spacers between the 6T cores of neighboring molecules, thus reducing stabilization effects due to intermolecular interactions.

Furthermore, by means of scanning tunneling microscopy (STM) and surface vibrational spectroscopy we have demonstrated a change in the adsorption geometry of α-octithiophene (8T) on Au(111), from flat-lying in the submonolayer to a tilted geometry with the long axis parallel to the substrate in the monolayer. This tilted configuration leads to a strong electronic decoupling between the Frenkel exciton and the metal substrate, leading to the suppression of the substrate-mediated relaxation channel in 8T/Au(111).

Finally we have applied time-resolved 2PPE to study the hot electron dynamics in poly(3,4-ethylene-dioxythiophene): poly-(styrenesulfonate) (PEDT:PSS) and the excited state dynamics in regioregular poly(3-hexylthiophene) (RR-P3HT). The latter shows a biexponential decay, with the fast component (2.6 ps) assigned to bound polaron pairs which recombine quickly or separate to be added to the slow component (7.6 ps) that is attributed to polarons generated via charge transfer between adjacent polymer chains.

The present study shows that 2PPE is the ideal tool to study the dynamics of excited states in small organic molecules as well as in polymers. Therefore this method promises to provide a link between optical and electron spectroscopy.

Deutsche Kurzfassung

Im Rahmen dieser Arbeit wurden die Exziton- und Polarondynamik in dünnen Oligo- und Polythiophenfilmen untersucht. Dabei wurde mithilfe der Zwei-Photonen Photoemission (2PPE) sowohl die elektronische Struktur, als auch die Bildungs-, Relaxation-, und Zerfallsdynamik von Exzitonen in dünnen Oligothiophenfilmen und an der Grenzfläche mit der Au(111)-Oberfäche untersucht. Bedeckungs- und photonenenergieabhängige Messungen, sowie zeitaufgelöste Experimente an α-Sexithiophen (6T)/Au(111) haben gezeigt, dass ein Übergang vom höchsten besetzen Molekülorbital (HOMO) zum niedrigsten unbesetzten Molekülorbital (LUMO) für die Population eines Frenkel-Exzitons unerlässlich ist. Die Bildung dieses Exzitonzustandes erfolgt auf einer Zeitskala von 100 Femtosekunden (fs), und weist in dünnen Filmen eine Lebensdauer von 600 fs auf. Des Weiteren wurde eine energetische Stabilisierung dieses angeregten Zustandes innerhalb von 400 fs beobachtet, welche von der Bildung eines Polarons oder eines an Defektstellen gebundenen Elektrons herrührt. Dieses Polaron/gebundenes Elektron verfügt über eine Lebensdauer von 6 Picosekunden (ps). Es existiert ein intramolekularer und ein substrat-induzierter Zerfallskanal.

Um den Einfluss der Adsorptionsgeometrie auf die Dynamik der angeregten Zustände zu untersuchen, wurden Experimente mit dem alkylsubsituierten 6T, nämlich α,ω-Dihexylsexithiophen (DH6T) auf Au(111) durchgeführt. Im Vergleich zu 6T zerfallen das Exziton und das Polaron/gebundenes Elektron 5-6 mal schneller. Wir gehen davon aus, dass die Adsorptionsgeometrie von DH6T für diese schnellere Zerfallsdynamik verantwortlich ist. In der Tat vergrössern die Dihexylketten den Abstand zwischen den Thiopheneinheiten benachbarter Moleküle und reduzieren dadurch die stabilisierenden intermolekularen Wechselwirkungen.

Darüberhinaus haben wir im Falle von α-Octithiophene (8T)/Au(111) mittels Rastertunnel Mikroskopie (STM) sowie schwingungsspektroskopisch eine bedeckungsabhängige Änderung der Adsorptionsgeometrie beobachtet. Während die 8T Moleküle im Submonolagenbereich flach auf Au(111) adsorbieren, nehmen sie ab Bedeckungen von einer Monolage eine Adsorptionsgeometrie ein, in der das Molekülrückgrat parallel zur Oberfläche verkippt ist. Diese Konfiguration führt zu einer starken elektronischen Entkopplung des Frenkel-Exzitons von der Metalloberfläche, was zur Unterdrückung des substrat-induzierten Zerfallkanals führt.

Schliesslich haben wir mittels zeitaufgelöster 2PPE die Dynamik heisser Elektronen in Poly(3,4-ethylen-dioxythiophen): Poly-(styrensulfonat) und die Dynamik angeregter Zustände in regioregularen Poly(3-hexylthiophen) (RR-P3HT) untersucht. Letztere weist einen biexponentiellen Zerfall auf. Die schnelle Komponente (2.6 ps) wird gebundenen Polaronpaaren zugeordnet, welche entweder schnell rekombinieren oder sich separieren. Die langsame Komponente (7.6 ps) wird Polaronen zugeordnet, welche durch einen Ladungstransfer zwischen benachbarten Polymerketten entstehen.

Contents

List of Figures

1 Introduction

1.1 Motivation

Nowadays, one of the greatest challenge mankind is facing is the energy production. The global energy needs will increase, and new resources have to be found. Moreover, these new energies should be clean and sustainable in order to prevent for a dramatic climate change. In this context, the sun will clearly have to play an important role.

Solar energy can be used in two different ways. On the one hand solar thermal systems use sunlight to heat water that can be utilized in diverse applications like for water treatment, heating or even electricity production. On the other hand, and this will be the focus of this work, the photovoltaic effect allows for direct conversion of light into electrical power. The photovoltaic effect was first observed in 1839 by Becquerel who, while experimenting with a solid electrode in an electrolyte solution, observed a voltage developing when light shines on the electrode [1]. However, the development of this technology really started in 1954 when Chapin and coworkers reported on a silicon-based p-n-junction device with solar power conversion efficiency of 6% [2]. Strong effort put into the research and development over the last 60 years has permitted constant increase of the solar cell efficiency, reaching 43.5% in 2012 with a device based on indium, gallium and arsenic and phosphore in the active layers [3]. However, other semiconductors are attracting much interest in order to reduce the cost for electricity production. In particular, since the discovery of conductive polymers in 1977 by Shirakawa, MacDiarmid and Heeger [4], organic optoelectronic has subsequently developed into a research field of great importance for chemists as well as physicists. In 1986, Tang fabricated an organic photovoltaic cell with 1% efficiency [5]. Further development of high-purity conjugated polymers and molecules, as well as new device architectures have allowed to increase the efficiency of the

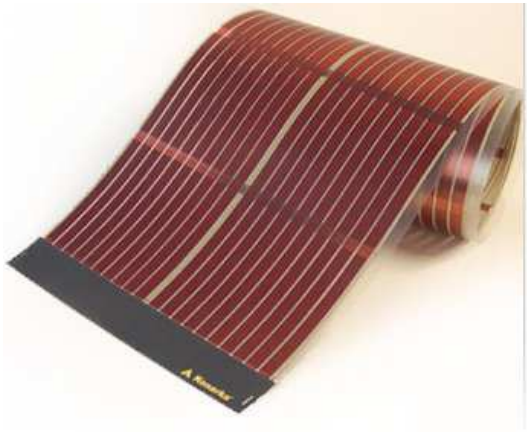

Figure 1.1: Organic photovoltaic cell from the company Konarka [6].

organic photovoltaic cells (OPVCs) up to 10.7% [7]. Although they possess fairly low energy conversion efficiency, OPVCs offer several technological advantages [8] such as their low material costs, ease of processing, possible application on flexible substrates like represented Fig. 1.1 and chemically tunable optoelectronic properties. There are in principle two classes of organic semiconductors available: small organic molecules and polymers. The latter is expected to have higher potential for real low cost production due to the fact that homogenous thin polymer films can be spin casted from solution, while on the other hand small molecules are thermally evaporated onto the substrate under high vacuum conditions and offer the possibility to prepare well-defined ultrathin films with low degree of structural and chemical disorder [9].

1.2 π-conjugated molecules and polymers

Organic π-conjugated molecules and polymers are carbon based compounds showing semiconducting properties. A common structural property of organic semiconductors is the alternation of single and double bounds between carbon atoms. This zigzag backbone (see fig.1.2 (a)) usually adopts a planar conformation. Carbon atoms are sp^2 hybridized. The $2s$ orbital is mixed with only two of the three available $2p$ orbitals, with one p-orbital remaining, commonly denoted as p_z. As seen fig.1.2 (a) p_z orbitals form an electron cloud above and below the molecular plane, and neighboring p_z orbitals can overlap resulting in an extended π-system along the whole molecular chain. Therefore, electrons in this π-orbital do not belong to one atom but to the whole π-system and are spatially delocalized. However, due to the different bond length of the single and double bond, the Peierls instability splits this band into two sub-bands, a completely filled valence band and an empty conduction band, separated by an energy gap. Hence the material is a semiconductor. The highest occupied (HOMO) and the lowest unoccupied (LUMO) molecular orbitals are often denoted as π- and π*- orbitals in π-systems, respectively (see fig.1.2 (b)). The energy difference between HOMO and LUMO referred as a band gap, typically values between 1.5 and 3.5 eV [10]. The transport gap corresponds to the gap measured when one electron is missing in the HOMO and one electron more is located in the LUMO.

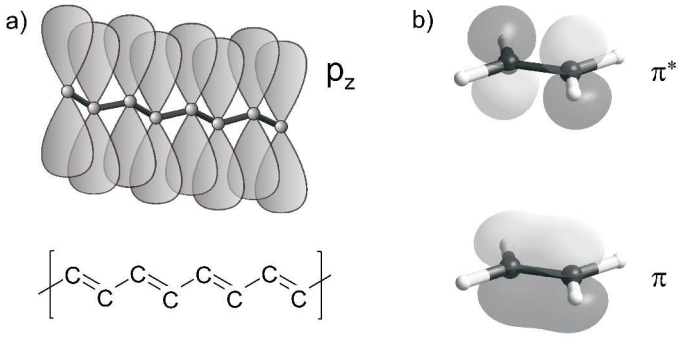

Figure 1.2: a) Schematic representation of p_z orbitals overlap in a conjugated segment of a polymer. b) Bonding π and untibonding π^* orbitals of the primary conjugated molecule - ethylene [11].

By means of doping, a semiconducting compound can be made conductive. For instance, doping of poly(3,4-ethylene- dioxythiophene) (PEDT), which is a thiophene-based semiconducting polymer, with poly(styrene-sulfonate) (PSS), makes the mixture a good conductor. PEDOT:PSS offers many advantages over other conducting polymers because of its simple processing ability, film-forming properties, optical transparency, good mechanical strength, and atmospheric stability [10]. A study of the hot electron dynamics in PEDT:PSS is presented in this work.

1.3 Excitons and polarons: definitions

- **Frenkel excitons**

When a photon of sufficient energy is absorbed by a π-conjugated molecule, an electron undergoes excitation from the π to the π^* orbital, creating a neutrally charged quasi-particle called Frenkel exciton (see fig. 1.3). An exciton is an electron-hole pair bound by Coulomb interaction. The dielectric constant of organic material being small, the Coulomb interaction is strong and therefore Frenkel excitons are relatively small. A momentum-dependent electron energy-loss study of the electronic excitations in α-sexithiophene (6T) [12] has shown a localization of the exciton on one molecule. Moreover, Frenkel excitons have a high binding energy usually between 0.2 and 1.4 eV [13].

- **Mott-Wannier excitons**

In contrast, in inorganic semiconductors, the dielectric constant is generally large. Consequently, electric field screening tends to reduce the Coulomb interaction between electrons and holes. As a result, the Mott-Wannier excitons created in this class of materials have a larger radius, and have a small binding energy typically in the order of 0.01 eV. Therefore they can separate easily at room temperature, because their binding energy is in the order of k_BT (k_B is the Boltzmann constant and T is the temperature) at room temperature (25 meV) [14].

- **Charge-transfer excitons**

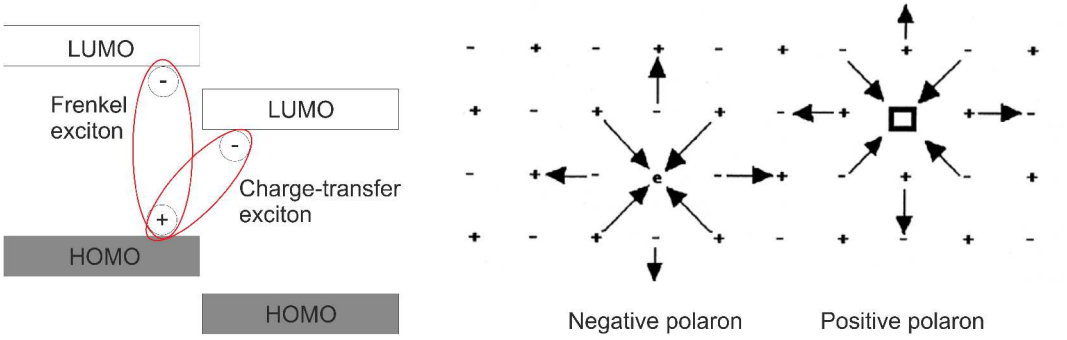

Figure 1.3: Schematic representation of a Frenkel exciton, a charge-transfer exciton as well as negative and positive polarons [15].

When an electron transfer takes place at the donor/acceptor interface (see fig. 1.3), the difference between the LUMO levels generates an energetic driving force to separate the positive and negative charges. However, due to the low dielectric constant, the charges can still interact across the interface, forming a charge-transfer (CT) exciton. Its binding energy can be in the order of a few hundreds meV [16]. It is important to notice that there is not one but a series of CT excitons approaching the conduction band minimum, in the same fashion than the energy levels of a particle in a box [17], see the schematic representation of a CT exciton in Fig. 1.7.

- **Polarons**

A polaron is a quasi-particle composed of a negative (negative polaron) or positive (positive polaron) charge and its polarization field (see fig. 1.3) [18]. Moving through the compound, the charge carries the lattice distortion with it. Polarons have a strong coupling with phonons.

1.4 Organic photovoltaic cells

The energy conversion in OPVCs follows a five-steps mechanism, as schematically shown in fig.1.4:

1. The absorption of photons in the donor material induces an electron excitation from e.g. the highest occupied molecular orbital (HOMO) of the molecule, (respectively the valence band (VB) of the polymer), into the lowest unoccupied molecular orbital (LUMO) (respectively the conduction band (CB)). Thus leaving a hole in the HOMO (or VB).

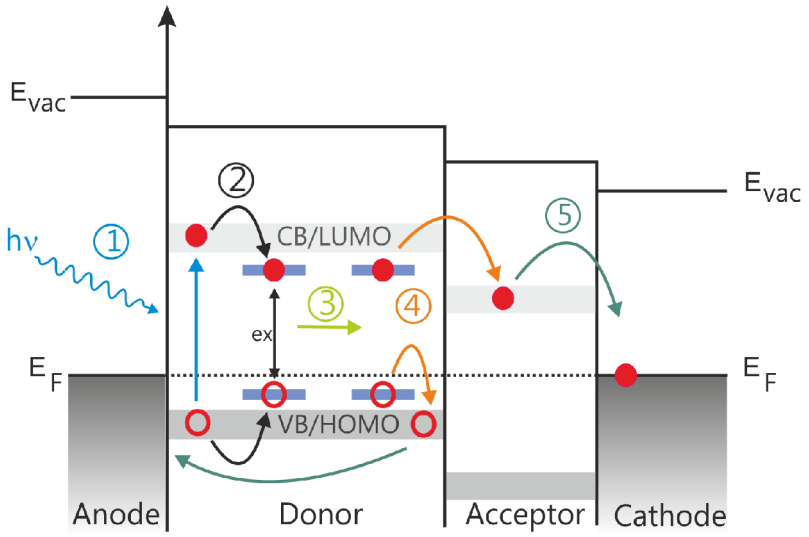

Figure 1.4: Schematic depiction of the processes in a bilayer organic photovoltaic cell. Five-steps mechanism of photogeneration and charge collection in an OPVC: 1) excitation of an electron by light absorption, 2) exciton generation, 3) exciton diffusion, 4) seperation of electron and hole at the donor-acceptor interface and 5) charge extraction. Adopted from [19].

2. Due to the attractive Coulomb force interacting between the electron and the hole, an exciton will be generated. The formation of the exciton after optical excitation in thiophenes will be intensively studied in this thesis.
3. The exciton diffuses towards the donor/acceptor interface.
4. In comparison to excitons produced in inorganic semiconductors, in organic materials their binding energy is typically much higher, therefore an acceptor material is needed to facilitate the separation of the electron and hole at the interface with the donor material.
5. Finally, due to the difference of work function between the anode and the cathode materials, the induced internal electric field will favorize the diffusion of the two charge carriers generated at the interface toward their respective electrode where they will be extracted from the device.

In the following, the electronic and optical processes that take place during the operation of a solar cell will be described in more details.

- **Optical absorption**

As seen above, the first step towards energy conversion in OPVCs is the absorption of light, resulting in bound electron-hole pairs called Frenkel excitons [20]. π-conjugated systems typically provide absorption efficiencies close to 100% in 100 nm thin films [21]. However, in contrast to inorganic semiconductors that can absorb a continuous spectrum of light, organic materials have well-defined electronic transitions that are typically quite narrow. For instance, the major inconvenient of poly(3-hexylthiophene) (P3HT), that is a common electron donor material, is the

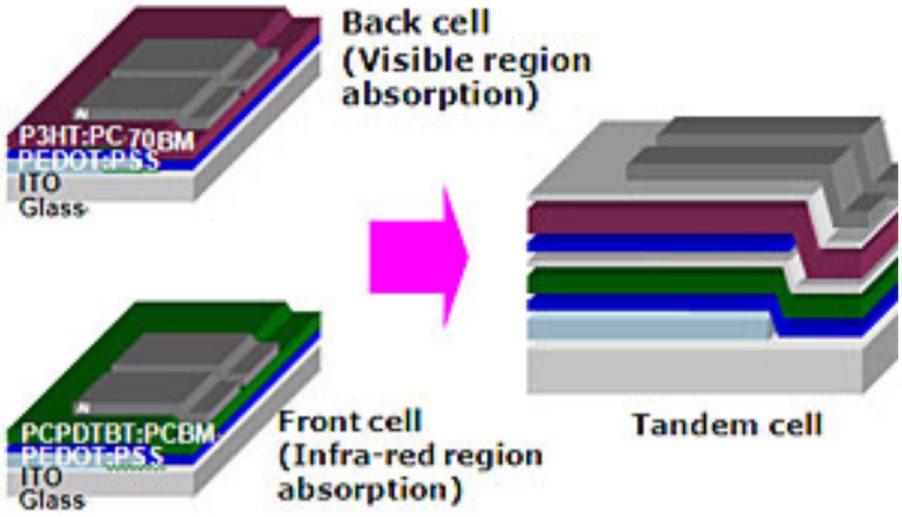

Figure 1.5: Device structure of the all solution processible polymer tandem solar cell. The back cell is a composite of poly(3-hexylthiophene) (P3HT) and [6,6]-phenyl-C71 butyric acid methyl ester (PC70BM). The front cell is a composite of composite of poly[2,6-(4,4-bis-(2-ethylhexyl)-4H-cyclopenta[2,1-b;3,4-b'] dithiophene)-alt-4,7-(2,1,3-benzothiadiazole)] (PCPDTBT) and [6,6]-phenyl-C61 butyric acid methyl ester (PCBM) [23].

poor matching of its absorption spectrum with the solar emission spectrum. The absorption is limited to wavelenghts below 650 nm, and as a consequence it is only able to collect around 20% of the solar photons [22]. Moreover, hot charge carriers created upon photon absorption relax down to the conduction band of the photoactive materials, giving rise to the so-called thermalization [24]. One way to circumvent this effect is the realization of a tandem solar cell. Hence, a combination of various different materials can help to cover more efficiently the emission spectrum of the sun. For instance, the absorption bands of poly[2,6-(4,4-bis-(2-ethylhexyl)-4H-cyclopenta[2,1-b;3,4-b'] dithiophene)-alt-4,7-(2,1,3-benzothiadiazole)] (PCPDTBT) and P3HT complement each other and these two materials cover the spectral region from 400 nm to nearly 900 nm. The maximum efficiency, reported so far, of a cell based on this combination of materials, see fig.1.5, was 6.5% with a 3% efficient back cell and a 4.7% efficient front cell [23].

- **Exciton migration**

Tang *et al.* [5] were the first to use the double-layer photovoltaic (PV) structure to favorize the exciton dissociation at the interface between an electron donor and an electron acceptor material. Later, Sariciftci *et al.* applied this double-layer technique to a conjugated polymer PV cell by evaporating C_{60} on top of a spin-cast poly[2-methoxy-5-(2'-ethylhexyloxy)-p-phenylene vinylene] (MEH-PPV) film [25]. In this cell excitons are photogenerated in the polymer layer upon absorption of the visible light. Subsequently, the excitons migrate in the polymer film by hopping between conjugated segments of the polymer chains. When reaching the polymer/C_{60} heterojunction, an electron is transferred to the high electron affinity C_{60} layer. As a next step, transport of the photogenerated holes and electrons (holes in the polymer and electrons in the fullerene) takes place, followed by charge collection at the electrodes. While the initially reported bilayer device produced 1.2% EQE (external quantum efficiency, electrons collected per incident photon), Halls et *al.* reported 9% EQE with the same materials by optimizing the thickness of the polymer and fullerene layers [26]. These experiments also revealed that the excitons in this device need to be generated near the interface to allow dissociation to occur before recombination. Effectively, the exciton diffusion length in small organic molecules and polymers is in the order of around 3 to 100 nm [21], while >100 nm thick layers are needed to absorb the light efficiently. To circumvent the problem of the limited diffusion length of the exciton, a solution is to blend the donor and acceptor materials as shown fig.1.6 (b). This interpenetrating network allows for an increase of the layer thickness while maintaining a short exciton diffusion path toward the interface. In order

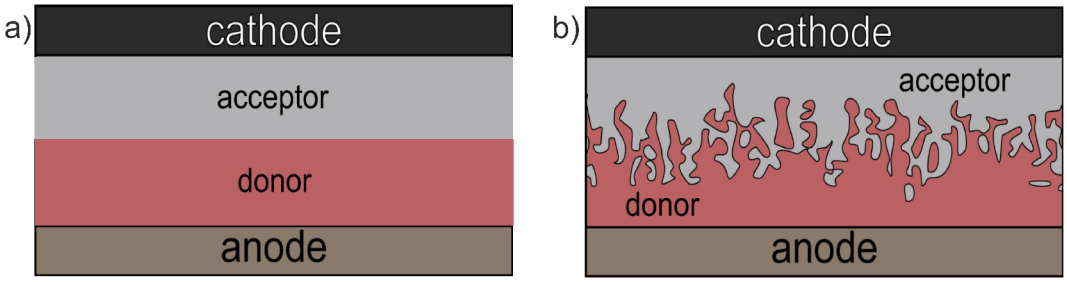

Figure 1.6: Device structure of a) a planar heterojunction and b) a blend heterojunction.

to optimize this structure it is important to control the degree of phase separation in the blend. Codeposition of the two materials generally leads to a high intermixing of the species, followed by a kinetic process of phase separation. Therefore, controlling the kinetic energy given to the system it is possible to increase or decrease the phase separation. For instance, after optimization of the mixing ratio and annealing temperature, a maximum power conversion efficiency of 1.5% was achieved with a solar cell based on a copper phthalocyanine:perylene-3,4,9,10-tetracarboxyl-bis-benzimidazole (CuPc:PTCBI) blend, whereas only 0.013% was obtained in the as-grown bulk heterojunction device [21].

- **Exciton dissociation**

It is commonly accepted that in small organic molecules and polymers photon absorption leads to the formation of Frenkel excitons, which are the primary photoexcitations. At an interface, the exciton is ionized in a process leading to the generation of charge-transfer excitons (CT excitons, see fig. 1.7), and free charge carriers.

Such CT excitons have been observed with two-photon photoemission spectroscopy (2PPE), for instance in pentacene/Bi(111) [17] with binding energy up to 0.5 eV. Thus, the binding energy of a CT exciton is 1 order of magnitude greater than k_BT at room temperature. Therefore the question is: how can the electron-hole pair escape this Coulomb trap in a successful photovoltaic device? Zhu and coworkers [17] have emitted the theory that efficient charge separation at an organic donor/acceptor (D/A) interface must involve hot CT exciton states, as shown schematically in fig. 1.7. The decay of an exciton in the donor into a CT exciton accross the interface is a downhill process. Thus the excess energy involved in this process is favorable to the creation of a hot CT exciton. Then, the thermalization of the hot CT excitons followed by charge-recombination (CR) will compete with the exciton-dissociation (CD). The rate must be maximized while charge-recombination must be suppressed. As an example, a theoretical comparison as been made between the exciton-dissociation and charge-recombination rates in sexithiophene (6T)/C_{60} and in 6T/perylenetetracarboxydiimide (PDI) [27]. By means of quantum chemical methods the electronic couplings, the CR and CD rates have been evaluated for these two system. The results show that, in comparison with the 6T/C_{60} complex, the decay of the lowest CT state to the ground state in the 6T/DPI complex is much faster. Therefore explaining the poorer efficiency in the latter, despite its good electron accepting properties, large exciton diffusion lengths and high electron mobilities [27].

1.5 Outline

In the framework of this thesis, using time- and angle-resolved 2PPE, we have investigated the electronic structure of and the electron dynamics in three π-conjugated thiophene based molecules that are potential candidates as the electron donor materials in OPVC, namely α-sexithiophene (6T), α-octithiophene (8T), α,ω-dihexylsexithiophene (DH6T). Additionally, we have applied our expertise gained on small molecules to two thiophene based polymers, an intrinsic conductive polymer, the poly(3,4-ethylenedioxy- thiophene)-poly(styrenesulfonate) (PEDT:PSS), and a electron donor material for OPVCs, the regioregular poly(3-hexylthiophene) (RR-P3HT). The main

goal of this work was to investigate the impact of the difference in the adsorption geometry of different thiophene based materials on their electronic properties, particularly on the exciton and polaron dynamics.

At first we will introduce the electronic structure of 6T determined experimentally. We will show that the lowest unoccupied molecular orbital (LUMO) is probed through negative ion resonance, meaning that an electron from the metallic substrate is transfered to the LUMO after excitation with the first pulse, and probed with the second pulse, allowing measurement of the transport gap of the molecule, being 2.9 eV. Moreover we have recorded the full lifecyle of the Frenkel exciton from its population following a HOMO-LUMO transition upon its separation into a polaron or a trap or decay through two, an intrinsic and a substrate-mediated coverage dependent, relaxation channels. The binding energy of the Frenkel exciton is 0.9 eV and the lifetimes of the exciton and the polaron/trap in the bulk are 600 ± 60 fs and 6 ± 0.6 ps, respectively.

After investigation of the exciton dynamics in 6T we have chosen to comparatively study DH6T, that is a 6T molecule with an hexyl chain at both ends, inducing a spatial separation between the neighbor 6T units. We will show that the exciton dynamics is by a factor 5 to 6 faster in DH6T than in 6T. Based on STM measurements performed on thin DH6T films, we assign this faster dynamics to the different adsorption geometry. In DH6T the brick-wall-like structure minimizes the overlap between thiophene units of neighboring molecules, and therefore the stabilization by polarization of adjacent molecules, and maximizes the space between molecules promoting more efficient quenching by the metallic substrate.

Further on we have studied 8T. It is known that it is possible to tune the electrical properties of oligothiophene by varying the chain length. It has already been experimentally shown by means of a high resolution electron energy loss spectroscopy (HREELS) [28] that the band gap of oligothiophenes decreases when increasing the chain length. 8T is so far the longest unsubstituted oligothiophene synthesized. Despite its geometrical and electronic similarity with 6T, we will show that the exciton

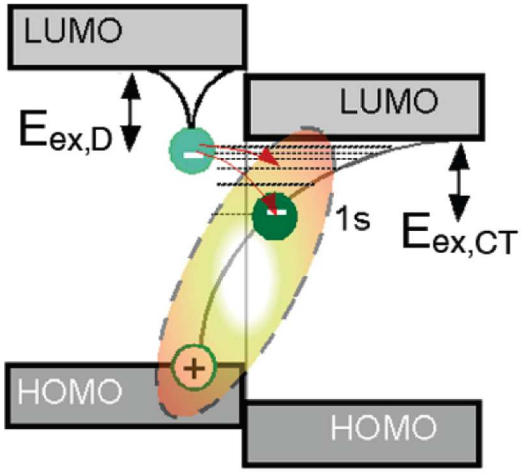

Figure 1.7: Dissociation of a Frenkel exciton in the donor to form the 1s or hot CT excitons across the donor/acceptor interface [17].

dynamics in 8T differs strongly compared to the one of 6T. We found that in 8T the lifetime of the Frenkel exciton is independent on the film thickness, in contrast to 6T in which the exciton lives longer when created further away from the metal substrate. Combining surface vibrational spectroscopy, scanning tunneling microscopy (STM) and 2PPE we will show that in contrast to the flat lying 6T molecules, 8T molecules adopt a tilted configuration on Au(111), with the long axis parallel to the surface in the first monolayer allowing for $\pi - \pi$ interaction. Therefore, due to the tilted adsorption geometry the exciton, that has been shown to localize on one single molecule [29]), can not relax into the metallic substrate. The binding energy of the Frenkel exciton is 0.9 eV and the lifetimes of the exciton and the polaron/trap in the bulk are 300 ± 30 fs and 3.5 ± 0.5 ps, respectively.

As indicated above, there is a second class of organic materials that offers high potential for true low cost devices: the polymers. Transparent electrodes are needed for OPVC applications and PEDT:PSS is until now the most promising material to be used as the electrode in organic optoelectronic devices [30]. Therefore we will present a study on the electron dynamics after photoexcitation of PEDT:PSS and compare it with gold. We will show that the lifetime measured for excitations greater than 1.5 eV above the Fermi level are comparable.

Finally we will present a study of a photoexcited state observed in P3HT, a polymer used in the solar cells offering the best ECE until now [31], and show that we could monitor the creation of a bound polaron with a lifetime of 3 ± 0.5 ps and its separation into two polarons of opposite sign localized on two adjacent polymer chains and living 8 ± 1 ps.

In conclusion, in this work we will demonstrate that 2PPE is a powerful tool to determine important parameters for OPVCs. The work function of the different layers as well as their electronic structure, including the HOMO, the LUMO and the exciton energetic position and dynamics, can be measured. The knowledge about these parameters is needed for better understanding of the different elementary processes in OPVCs and their optimization.

2 Experimental Details

In the framework of this thesis we have investigated the exciton formation and decay dynamics in several organic molecules and polymers by means of time-resolved two-photon photoemission spectroscopy (TR-2PPE). Therefore, the laser system used for this study, the energy dependent measurements allowing for assignment of a feature to occupied or unoccupied state, as well as the treatment of the time-resolved measurements will be shortly introduced in this section.

2.1 Laser System

The laser system (fig.2.1) used for the 2PPE and ultraviolet photoemission spectroscopy (UPS) experiments contains mainly commercially available components from *Coherent*, such as the *Verdi V18* pump laser, the *MIRA 900B* seed oscillator, the regenerative amplifier *RegA 9050* and the optical parametric amplifier (OPA) *vis-OPA 9450*.

Both the *MIRA 900B* seed oscillator and the *RegA 9050* are pumped at 533 nm by the *Verdi V18*. The *MIRA* seed oscillator contains a Ti:sapphire (titan doped corundum, $Ti^{3+} : Al_2O_3$) crystal and provides ultrashort laser pulses with a pulse length of 40 fs at a repetition rate of 80 MHz and a pulse energy of 2 - 3 nJ. Its central wavelength, which is tunable between 770 and 830 nm, is usually set to 800 nm.

Before amplification in the *RegA*, the pulses are stretched in order to minimize their high peak power that could damage the optics of the *RegA*, in which they are amplified at a repetition rate of 300 kHz to pulse energies of 6 - 7 μJ and subsequently guided back into the stretcher/compressor unit where they are compressed again to approximately 50 fs. High focus and short pulses are crucial in the following for the generation of the different photon energy needed for this study and involving several non-linear processes.

The pulses generated that way can be frequency doubled, once (3 eV) or twice (6 eV), or be used as the input of the OPA generating pulse in the visible range between 1.7 and 2.6 eV that can be frequency doubled to access UV range between 3.4 and 5.2 eV. Therefore, tuning the wavelength to access the state of interest is possible.

The laser system has been described in details in the PhD thesis from S. Hagen [32].

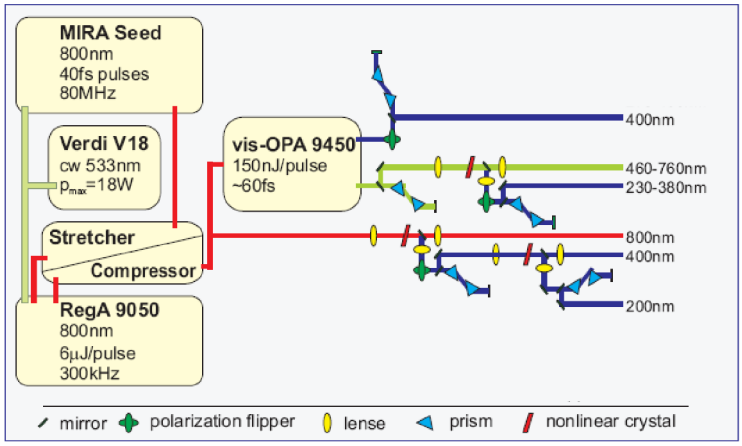

Figure 2.1: Schematic set-up of the laser system adapted from [32].

2.2 Photon energy dependent measurements

A very important advantage of two-photon photoemission (2PPE) spectroscopy over direct photoemission is the possibility to investigate occupied as well as unoccupied electronic states. In 2PPE the first photon excites an electron into a real or virtual intermediate state located between the Fermi level E_F and the vacuum level E_{vac} of the investigated system, which is subsequently ejected over E_{vac} with the second photon. The kinetic energy of the emitted electron will be measured, and depending on the photoexcitation scheme we will be able to assign its origin to an initial, an intermediate or a final state (see fig.2.2) as explained in the following. In order to simplify the explanation, we give examples for one-color 2PPE in which the first and the second photon possesses the same energy. However, in order to address the states of interest it is often useful to use two photons of different energies, but the results can be easily extrapolated from the given method.

In the case of an **occupied initial state**, the energy of two photons will be transfered to a bound electron located in the occupied region of the system, allowing it to overcome the work function. In order to model this process theoretically an intermediate virtual state of infinitesimal lifetime has to be introduced. Varying the photon energy used to probe this state, the electron possessing the same initial state energy, the signal scales with twice the photon energy difference $\Delta E = 2\Delta h\nu$ like seen fig.2.2 (a).

Moreover, as mentioned above, 2PPE gives the possibility to observe **intermediate states** located between E_F and E_{vac}. In this case the first photon excites an electron directly (b) or indirectly (d) into an unoccupied intrinsic state of the investigate system. In the latter an intermediate state of higher energy is excited directly and decays through scattering events into the investigated state before the second photon ejects the electron above E_{vac}. In both cases the energy of the emitted electron is independent of the energy of the first photon and scales only with the energy difference of the second photon, therefore $\Delta E = \Delta h\nu$.

Finally, electronic states located above E_{vac}, so-called **final states**, can be excited directly or indirectly as well. The electron is emitted through auto-detachment

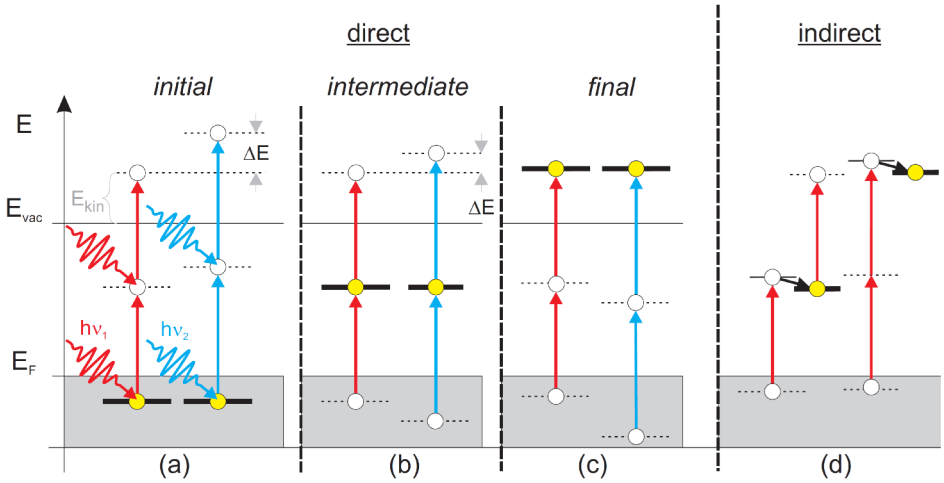

Figure 2.2: Excitation schemes in 2-photon photoemission with yellow circles marking the corresponding probed states. Their distinct photon energy dependencies can be used to analyze the experimentally obtained spectra. Therefore the sample is probed with at least two different photon energies ($h\nu_1$ and $h\nu_2$). According to the kinetic energy shift (ΔE) of the peaks observed in the spectra those can be assigned to either initial, intermediate or final states. For details see text adopted from [32].

processes and is therefore independent of the photon energy used to excite the system, therefore $\Delta E = 0$

2.3 Time-resolved experiments

The title of this thesis already puts the focus of this work on the population and decay dynamics of an exciton created in the molecules. Therefore it is necessary to explain here to the reader how the results of the time-resolved experiments have been treated. In order to study the lifetime of populated intermediate states the femtosecond pump and probe pulses can be delayed with respect to each other by changing the optical path length of one of the beams. Several measurements are performed with constantly increasing the time delay between the two laser pulses yielding so-called 2D-plots seen in the results section p. 22, and allowing us to observe the decay of population of intermediate states, for instance the decay of the excitons investigated in this work.

The population decay of an intermediate state can be described by a set of classical, coupled rate equations, employed to describe this optically coupled 3-level system (see fig.2.3 (a)):

$$\dot{n}_i = -\left|V_{ik}(t,\tau)\right|^2 n_i + \Gamma_1 n_k \tag{2.1}$$

$$\dot{n}_k = \left|V_{ik}(t,\tau)\right|^2 n_i - \left|V_{kf}(t,\tau)\right|^2 n_k - \Gamma_1 n_k \tag{2.2}$$

$$\dot{n}_f = -\left|V_{kf}(t,\tau)\right|^2 n_k \tag{2.3}$$

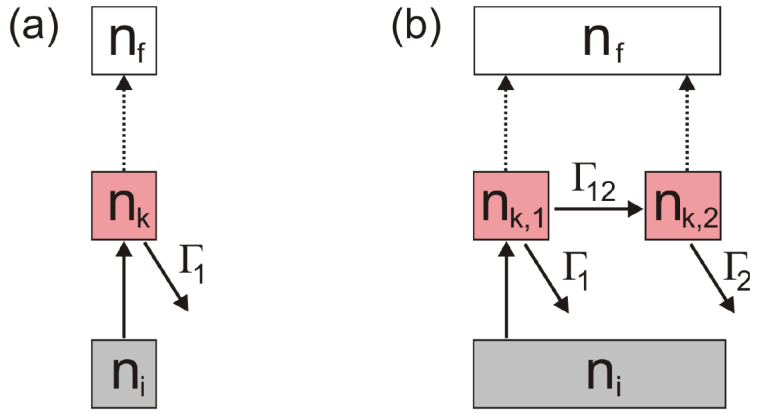

Figure 2.3: Schema of a 3- and a 4-level system with initial, intermediate and final states, after [19]. (a) Decay scheme of a 3-level system. (b) Decay scheme of a 4-level system: the population $n_{k,1}$ fills the population $n_{k,2}$ with a rate Γ_{12}, while both states are probed and decay with Γ_1 and Γ_2 into the ground state.

See PhD thesis of P. Kirchmann [33] for a complete description of the integration of the Bloch equations leading to these rate equations.

The population densities of the initial state i, the intermediate state k and the final state f are denoted by n_x. The probability for the transition $x \rightarrow y$ in the presence of the optical field is given by $|V_{xy}|^2$ and the pump-probe delay by τ. Γ_1 is the decay rate from the intermediate to the ground state, $k \rightarrow i$.

When the excitation density is small (typically the case for excitation densities that don't create damage during 2PPE experiments) n_i is considered constant and $|V_{kf}|^2$ is neglected.

The 2PPE intensity for the intermediate state k is:

$$I_k^{2PPE}(\tau) \propto \int dt\ F_{XC}(t-\tau)R_k(t) \tag{2.4}$$

with F_{XC} representing the envelope of the two laser pulses. Experimentally F_{XC} is determined by measuring the time evolution of the signal arising from a state with infinitesimal lifetime where $R_k(t) = \delta(t)$. Thus, for a 3-level system with a finite lifetime of the intermediate state the response function is given by:

$$R_1(t) = \Theta(t)\ n_1^{(0)} e^{-\Gamma_1 t} \text{with } \Gamma_1 = \frac{1}{\tau_1} \tag{2.5}$$

which describes the exponential decay of the initial population density $n_1^{(0)} = n_1(t = 0)$ of the intermediate state k with a lifetime of τ_1. $\Theta(t)$ denotes the Heaviside function. Later in this thesis, this function is used to determine the decay rate of the hot electrons in PEDT:PSS.

However, as we will see later, the exciton can separate into a polaron. Therefore the 3-level model is not correct in this case and we have to introduce an additional level. Neglecting the optical coupling of k_1 and k_2 by the laser field, the rate equations for the population densities are:

$$\dot{n}_1(t) = -(\Gamma_{12} + \Gamma_1)n_1(t) \tag{2.6}$$

$$\dot{n}_2(t) = -\Gamma_2 n_2(t) + \Gamma_{12} n_1(t) \tag{2.7}$$

The populations in the two coupled intermediate states k_1 and k_2 decay with rates $\Gamma_1$and Γ_2 into the ground state and additionally k_2 is coupled with a rate Γ_{12} to k_1. Moreover, due to the fact that the two states are very close energetically from each other, we will not be able to probe k_1 and k_2 separately but only the sum of k_1 + k_2. Therefore:

$$\dot{n}_1(t) + \dot{n}_2(t) = -\Gamma_1 n_1(t) - \Gamma_2 n_2(t) = -\frac{1}{\tau_1} n_1(t) - \frac{1}{\tau_2} n_2(t) \tag{2.8}$$

and the response function of the investigate states is:

$$R_{(1+2)}(t) = \Theta(t) \left[n_1^{(0)} e^{-\Gamma_1 t} + n_2^{(0)} e^{-\Gamma_2 t} \right] \tag{2.9}$$

3 Results and Discussion

3.1 Oligothiophenes

3.1.1 α-sexithiophene on Au(111)

3.1.1.1 Electronic structure and exciton dynamics

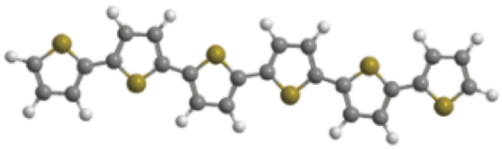

Figure 3.1: Chemical structure of α-sexithiophene (6T)

In this section we present the results of a study in which we have utilized two-photon photoemission spectroscopy (2PPE), which has be proven to be an ideal method to investigate both occupied and unoccupied molecular electronic states. We have determined the electronic structure of α-sexithiophene (6T, see fig.3.1) on Au(111). Moreover a Frenkel exciton has been identified and monitored with fs time-resolved 2PPE allowing us to elucidate its population, relaxation and decay dynamics.

Several surface science studies focusing on the adsorption behavior of 6T on noble metal surfaces exist, for example, on Au(110) [34], Au(111) [35], Ag(100) [36], and Cu(110) [38]. In the monolayer regime, 6T deposited on Au(111) at room temperature forms well-ordered domains of flat-lying molecules, which are arranged in molecular rows [39]. In addition, the occupied band structures and accordingly the hole injection barriers of 6T adsorbed on various noble metals have been determined using mainly UPS [40, 41, 42, 43]. In contrast, studies on the 6T/Au(111) interfacial electronic properties, that is, 6T in the monolayer (ML) regime, are not known so far. A combined ultraviolet photoemission spectroscopy (UPS) and inverse photoelectron spectroscopy (IPES) study on thick (50-100 Å) 6T films on Au determined a HOMO-LUMO gap of 4.2 $\pm$ 0.2 eV [44]. In contrast to time-resolved measurements ranging from femtoseconds to milliseconds to elucidate the decay dynamics of excitons in 6T films (thickness about 50-350 nm) [34, 35, 36], investigations on the exciton formation, relaxation and decay at the 6T/Au(111) interfaces and within thin films are not known so far. A recent 2PPE study investigated the charge transport properties

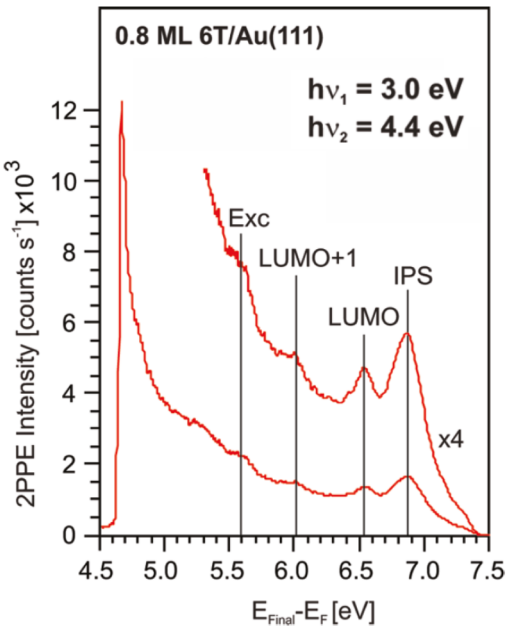

Figure 3.2: Two-color 2PPE spectrum of 0.8 ML 6T/Au(111) recorded with 3.0 and 4.4 eV photons. The spectrum is displayed as a function of final-state energy above the Fermi level, $E_{Final} - E_F = E_{kin} + \Phi$ (with Φ the work function) [37].

of 6T and the dihexyl-substituted 6T (DH6T) adsorbed on Ag(111), respectively, and found a charge localization in DH6T within 230 fs while in 6T no localization was observed. The charge localization has been attributed to the hydrocarbon side chains [45]. The exciton decay dynamics at organic molecule/metal interfaces has been observed so far only for C_{60} films epitaxially grown on Au(111) and Cu(111) using 2PPE [46]. Additionally 2PPE has been used to probe charge transfer excitons on a surface of organic semiconductors, namely pentacene and tetracene, respectively [47, 48].

Fig.3.2 shows an exemplary 2PPE spectrum of 0.8 ML 6T/Au(111) recorded with photon energies $h\nu_1 = 3.0$ eV and $h\nu_2 = 4.4$ eV. Several peaks can be observed and on basis of photon energy dependent experiments (see section experimental section) they can be related to photoemission from unoccupied intermediate states. The peak at 6.9 eV is probed with $h\nu_1 = 3.0$ eV and is therefore located at 3.9 eV with respect to E_F and arises from the n = 1 image potential state (IPS). The peaks at 6.5 and 5.6 eV are probed with $h\nu_2 = 4.4$ eV and therefore located at 2.1 and 1.2 eV above E_F, respectively. We assign the peak at 2.1 eV to the lowest unoccupied molecular orbital (LUMO) and the one at 1.2 eV to a Frenkel exciton. Arguments for assignment of the latter to an exciton will be given below. The feature located at 6.0 eV and probed with $h\nu_1 = 3$ eV has accordingly an energetic position of 3.0 eV with respect to E_F, and is assigned to the LUMO+1. Additionally, not shown here,

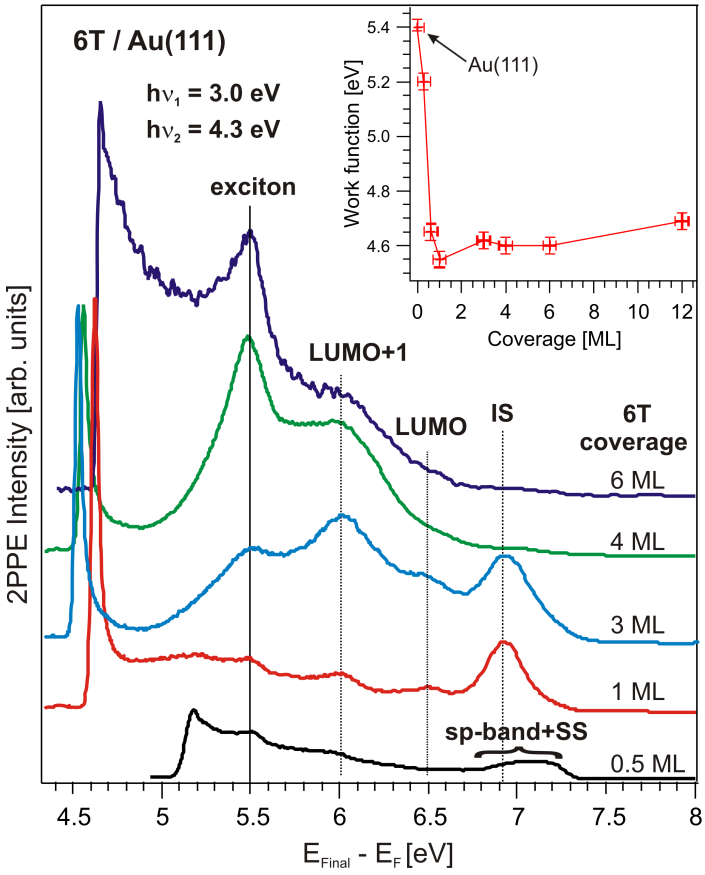

Figure 3.3: Two-color 2PPE spectra recorded at photon energies of 3.0 and 4.3 eV of various 6T coverages. At low 6T coverage, the Au(111) surface state (SS) and the sp-band is observed. The inset shows the work function (Φ) of 6T adsorbed on Au(111) as a function of 6T coverage [37].

the highest occupied molecular orbital (HOMO) and HOMO-1 have been found 0.8 eV and 1.5 eV below E_F, respectively.

Fig.3.3 displays a set of 2PPE spectra taken at different 6T coverages on Au(111). The inset shows Φ as a function of layer thickness. From 5.4 eV for the pure Au(111) the value constantly decreases down to 4.55 eV at 1 ML. The Φ drop is the result of the creation of an interface dipole due to the adsorption of molecules.

Population of an intermediate unoccupied molecular states (e.g. LUMO) can dominantly occur through an intramolecular excitation or a photoinduced substrate to molecule electron transfer. In order to determine if the population of these states results of a process taking place within the film or at the interface with the metallic substrate, we look at the 2PPE intensity of the features as a function of the coverage. We believe that in our experiments the LUMO and LUMO+1 of 6T are populated with electrons photoexcited in the substrate. 2PPE is a very surface sensitive tech-

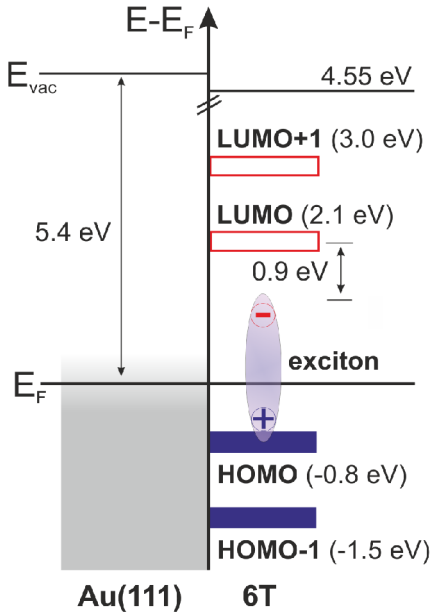

Figure 3.4: Energetic position of 6T-derived photoemission spectral features at a coverage of 1 ML 6T/Au(111). The Fermi level of Au(111) serves as reference. The exciton binding energy is 0.9 eV and the HOMO-LUMO gap is 2.9 eV [49].

nique, therefore the electronic states observed in the spectra are probed at the surface of the molecular film. At low coverages, the LUMO and the LUMO+1 can be efficiently populated via an electron transfer from the metal to the molecule. However, when we increase the coverage, an electron excited in the substrate will have a lower probability of reaching the LUMO or LUMO+1 of a molecule located at the surface of the film and therefore the photoemission intensity of the LUMO and LUMO+1 decreases. A similar behavior has already been observed for C_{60} adsorbed on Cu(111) and Au(111) [46]. On the other hand, most striking is the pronounced photoemission intensity increase from the excitonic state with increasing film thickness. That shows that the exciton formation is the result of an intramolecular excitation, the photoemission intensity increasing with increasing number of molecules (and we will show later that the lifetime of the exciton increases with increasing coverage, inducing as well an increase of the photoemission intensity). Moreover, using photon energies in the range between 2.0 and 2.4 eV, this feature does not appear in the spectrum. Only using photon energies larger than the HOMO-LUMO gap (2.9 eV), allowed us to observe the photoemission feature. This is a clear indication that the exciton is generated via a photoinduced electron transfer from the HOMO to the LUMO of 6T followed by relaxation process due to coulomb interaction between the electron excited into the LUMO and the hole left in the HOMO. More details about the population processes will be given by time-resolved experiments (see below).

Fig.3.4 summarizes the energetic position and assignment of the different electronic

states that we have observed at a coverage of 1 ML 6T on Au(111). The position of the HOMO-1, HOMO and LUMO are in very good agreement with previous scanning tunneling spectroscopy (STS) measurements [39]. We find a HOMO-LUMO gap of 2.9 eV that corresponds to the transport gap because in our study the LUMO is populated with an electron from the metallic substrate. The binding energy of the exciton is 0.9 eV. Although the exciton is not a single particle state, but a quasi-particle formed by a correlated electron and hole bound through Coulomb interaction, in 2PPE the final state being an electron and an ionized molecule, it is often simpler to assign the binding energy to the electron.

Knowing the electronic structure of 6T/Au(111) it is then very interesting to investigate the evolution of the intermediate excited states, in particular the exciton, in order to learn more about the processes involved in their population, relaxation and decay dynamics. There exist different techniques allowing the observe excitons. For instance, excitonic feature commonly appear in optical absorption and emission of semiconductors. Koch *et al.* [50] have discussed recently the importance of choosing the appropriate method in order to study the exciton dynamics. For instance, they insisted on the fact that in absorption and luminescence experiments the exciton signature is not a fingerprint for real exciton population:"*we want to stress the fact that the absorption, transmission and reflection of a classical electromagnetic field are completely determined by the complex-valued optical semiconductor polarization. Especially in the linear regime, there are no populations of electrons, holes or excitons at all, that is, the system is unexcited, and a probe beam merely tests the transition possibilities of the system*". Hereby we present our contribution to this topic, in this work we will show that 2PPE is a powerful tool allowing to monitor the population, relaxation and decay dynamics of the exciton in thin organic films. In accordance with a real exciton population process, we have already pointed out that only exciting the system with photon energies enabling a HOMO-LUMO transition has resulted in the observation of the excitonic state. In the following we will show that our method allows for measurement of the real population, relaxation and decay of the exciton.

In the low coverage regime (1-2 monolayers) in which LUMO and LUMO+1 can be populated with electron from the substrate, the lifetime of the electrons in those two transiently excited states was below our time resolution ($t < 10$ fs), indicating a strong electronic coupling between 6T and Au(111) allowing fast back transfer of the electrons to the metal. Such short lifetimes have already been found in previous studies on several adsorbates [46, 51, 52, 53]. In contrast, the excitonic state exhibits a pronounced lifetime as it is seen Fig.3.5 (a) in the spectrum recorded with photon energies $h\nu_1 = 3.0$ eV and $h\nu_2 = 4.3$ eV on a 30 ML 6T film on Au(111). This false-color 2D plot represents the 2PPE intensity as a function of the intermediate

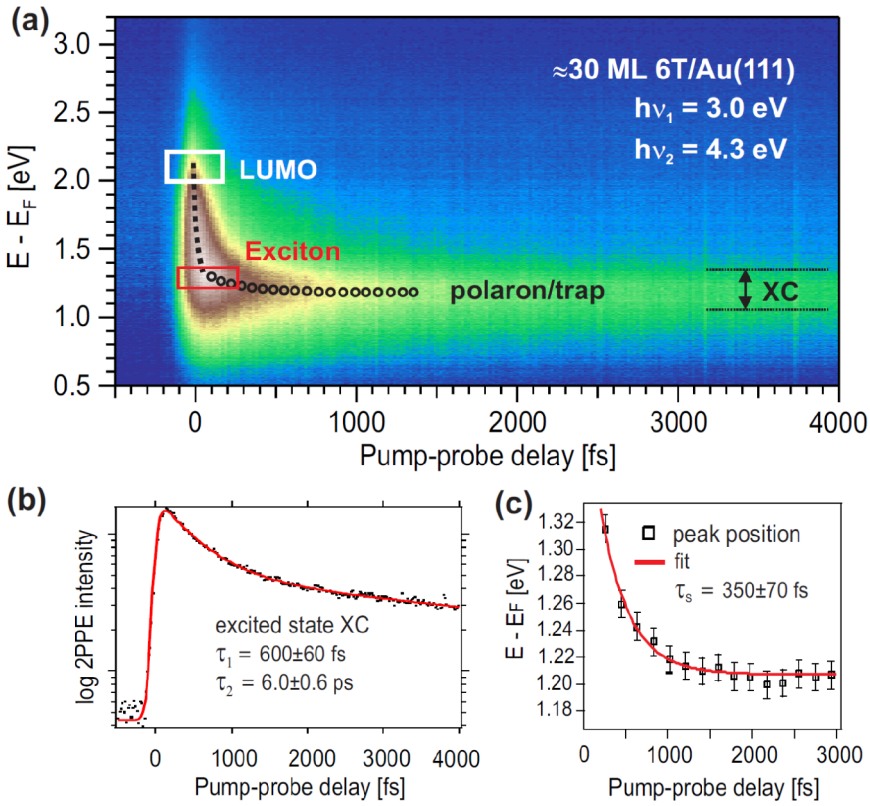

Figure 3.5: Two-dimensional spectrum of time-resolved 2PPE measurements recorded with $h\nu_1 = 3.0$ eV and $h\nu_2 = 4.3$ eV. The dashed line in (a) indicates the energetic stabilization of electrons leading to the formation of the exciton and the dotted line represents the energetic stabilization of electrons caused by the formation of polarons or at defect sites trapped electrons (see text). (b) Cross-correlation traces of the 2PPE intensity integrated over the exciton peak intensities with bi-exponential fit which gives the indicated lifetime. (c) Maximum peak intensity of the exciton state as a function of pump-probe delay which yields the indicated energy stabilization time due to polaron formation or localization at defect sites [49].

unoccupied state energy relative to E_F (vertical axis) and the pump-probe pulse delay (horizontal axis). The pump pulse photoinduces a HOMO-LUMO transition with $h\nu_1 = 3.0$ eV, a very fast energetic stabilization indicated by the dashed line occurs within 100 fs leading to the formation of the exciton due to the coulomb interaction between the photoexcited electron and the hole left in the HOMO. The transition of the electron from a bonding (the HOMO) to an anti-bonding state (the LUMO) is a very efficient source for the stimulation of molecular vibrations, therefore the exciton binding energy of 0.9 eV dissipates to molecular vibrations on a time scale of the inverse of a vibrational quantum ($\approx$ 100 fs, for instance the C-S-C

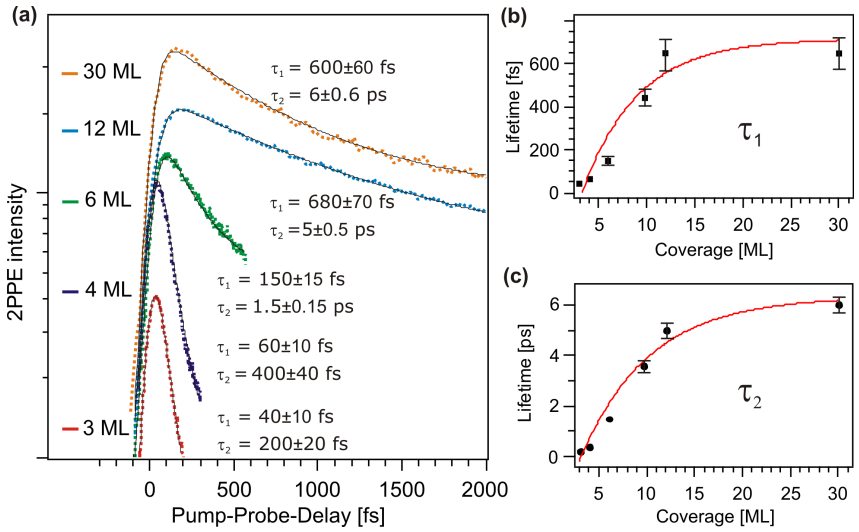

Figure 3.6: (a) Cross-correlation traces of the 2PPE intensity integrated over the exciton peak intensities as a function of 6T coverage on a logarithmic intensity axis. The line represent fits for the bi-exponential decay, which yields the indicated lifetimes. The dependence on film thickness of the transient lifetime (b) τ_1 and (c) τ_2 [49].

ring deformation mode at 700 cm^{-1} [54], which corresponds to a period of 48 fs).

The photoemission intensity of the exciton is plotted as a function of the pump-probe delay. The result, referred as cross correlation (XC) is shown fig.3.5 (b). The fit used to extract the decay rates of this XC includes a convolution of a $sech^2$ function, representing the envelope of the two laser pulses, with a biexponential response function of the system after photoexcitation. The decay constants measured that way are $\tau_1 = 600 \pm 60$ fs, and $\tau_2 = 6 \pm 0.6$ ps and result from the decay of two different states. As explained above, we assigned the first state to an exciton. Its formation take place at an ultrafast time scale due to coupling to molecular vibrations and decays with a rate $\tau_1 = 600 \pm 60$ fs. Moreover, coupling to molecular vibrations can lead to the generation of a polaron. This process may be responsible for the observed energetic stabilization of around 0.1 eV, which proceeds on a time scale of 350 ± 70 fs (see fig.3.5 (c)). Charge localization by defects, also called traps, has also been shown to take place within the same time scale in particular systems [55] and could also lead to an energetic stabilization of the same order.

In order to gain further insight into to the exciton decay we have investigated the dynamics as a function of the 6T-coverage. The resulting XC curves are shown fig.3.6 (a), and the lifetime of the exciton (fig.3.6 (b)) and polaron/trap (fig.3.6 (c)) are plotted versus the layer thickness. Both decays exhibit a significant coverage dependence. A similar behavior has already been observed and discussed for the mono-exponential

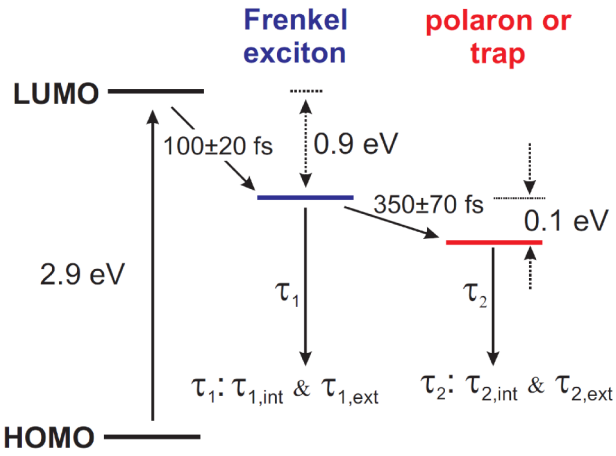

Figure 3.7: Formation, relaxation and decay processes of a Frenkel exciton in sexithiophene adsorbed on Au(111) [49].

decay of excitons in C_{60} on Au(111) and Cu(111) [46]. The two states possess an intrinsic and a distance dependent relaxation channel. Intramolecular exciton recombination is expected to be coverage independent, however, quenching by the metal substrate will be much more efficient at low coverage when the 6T molecule are more electronically coupled to the surface. Therefore, quenching will dominate the dynamics at low coverage, while the asymptotic values $\tau_1 = 600 \pm 60$ fs for the exciton and $\tau_2 = 6 \pm 0.6$ ps for the polaron/trap correspond to the decay in the bulk.

Fig.3.7 summarizes the exciton population, relaxation and decay processes that we have observed in the present study. After photoexcitation of an electron from the HOMO to the LUMO, the creation of a Frenkel exciton with 0.9 eV binding energy takes place within 100 ± 20 fs. The exciton can stabilize into a trap or separate and lead to the creation of two polarons of opposite signs (however, with 2PPE, we can only probe the negative polaron). Both the exciton and the polaron/trap have a coverage dependent lifetime involving an interfacial and a bulk relaxation channel. Thus we have shown that 2PPE is a powerful tool to monitor the whole lifecycle of the Frenkel exciton from its population to its decay. In the following, we will address the influence of the adsorption geometry of the molecules on the excited state dynamics. Therefore we have investigated an alkyl-substituted 6T, namely α,ω-dihexylsexithiophene on Au(111). The hexyl chains inducing a spatial separation between the neighbor 6T units.

3.1.1.2 Comparison with α,ω-dihexylsexithiophene

Although several studies have been published on α-sexithiophene (6T) adsorbed on various metal surfaces [56, 57, 38, 34, 58, 59], little is known about the alkyl-

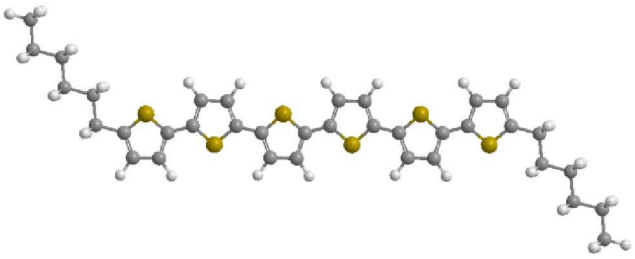

Figure 3.8: Chemical structure of α,ω-dihexylsexithiophene (DH6T).

substituted DH6T [60, 61, 62] despite very promising utilization in organic field-effect transistors (OFETs). Yassar *et al.* [63] have shown that the electronic and optical properties of oligothiophenes (e.g. 6T and DH6T) are largely determined by the structural organization of the molecules in the film. We will apply 2PPE to determine the changes induced in the exciton dynamics by the alkyl-substitution of 6T.

In this section we will present the results of our time-resolved 2PPE study in thin DH6T films on Au(111) (see fig.3.11). Based on STM measurements we will show that the adsorption geometry of DH6T maximizing the distance between neighboring

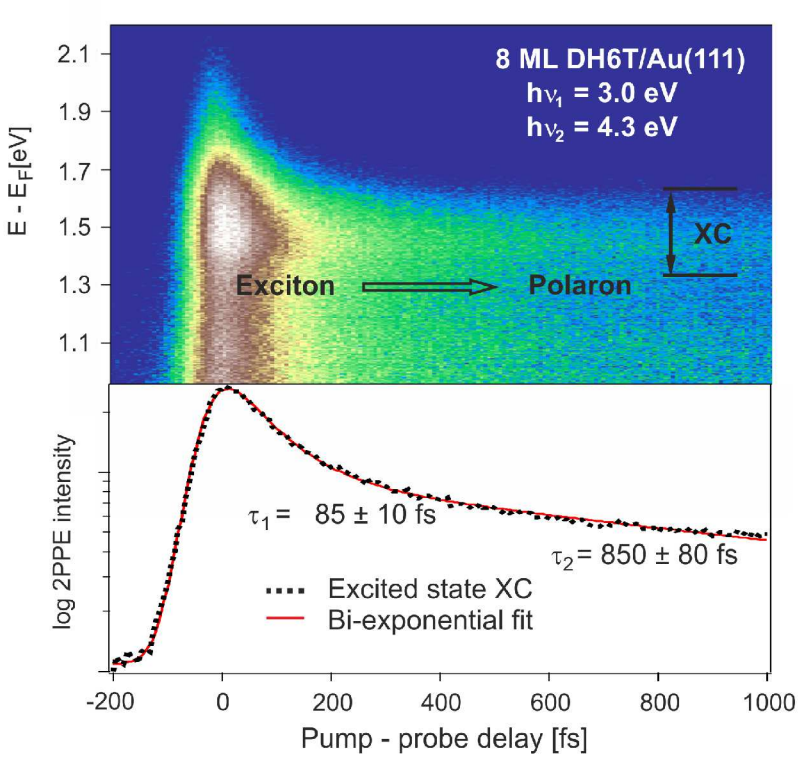

Figure 3.9: Two-dimensional spectrum of time-resolved 2PPE recorded with $h\nu_1 = 3.0$ eV and $h\nu_2 = 4.3$ eV at a coverage of 8 ML.

π-conjugated cores leads to a much faster exciton decay dynamics compared to 6T films. The feature exhibiting a clear lifetime is located at $E - E_F = 1.5$ eV. With UPS, the HOMO has been observed 0.6 eV below E_F. Thus the energetic separation between the HOMO and this state is 2.1 eV (as in 6T). In analogy to 6T we assign this feature to a Frenkel exciton.

Fitting the XC of the exciton, a biexponential decay is observed, as for 6T. This results in the decay rates τ_1 corresponding to the lifetime of the exciton, and τ_2 the decay rate of the polaron/trap that can be created when the exciton breaks, for instance due to coupling to molecular vibrations. Fig.3.10 shows the decay rates measured at several DH6T coverages. Similar to 6T, both the exciton and the polaron/trap created in DH6T exhibit a coverage dependent lifetime indicating the existence of two relaxation channels. As discussed in the case of 6T, one channel is intrinsic to the molecule, whereas the second depends on the distance to the substrate. At low coverage the external relaxation path due to quenching by the metal substrate is responsible for the fast dynamics. On the other hand, at higher coverages the states probed with 2PPE being located on the topmost layers, the substrate-mediated relaxation channel is reduced, and mostly the intrinsic channel subsists, corresponding to the decay in the bulk material, the recombination of the exciton.

Interestingly, as it is seen fig.3.10, despite their similar π-conjugated core, the exciton dynamics in DH6T is 5-6 times faster than in 6T. A similar behavior has been observed on Ag(111) [64], and has been attributed to a stronger lattice interaction with DH6T as compared to 6T. Furthermore, complete localization of the electron was observed within the first 220 fs. However, due to the fact that the photoemission of the electron breaks the exciton, 2PPE does not allow to measure its localization.

In order to understand the faster dynamics in DH6T compared to 6T, we have studied the adsorption geometry of DH6T on Au(111). Fig.3.11 displays a typical

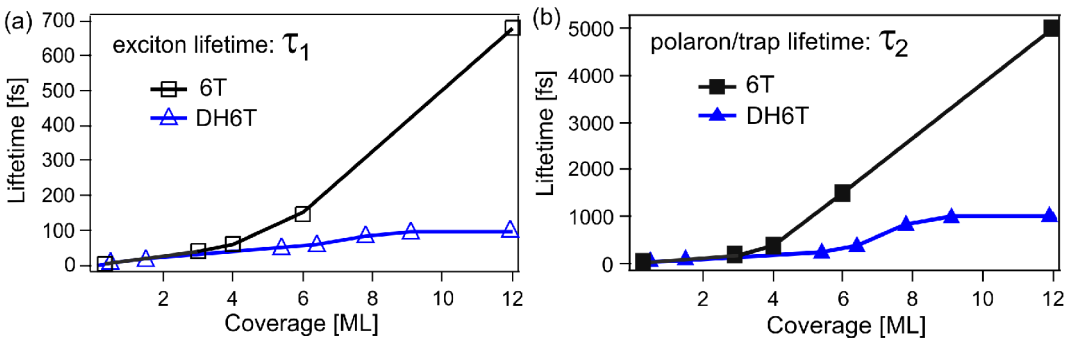

Figure 3.10: Comparison between the lifetime of a) the exciton and b) the polaron/trap state, in 6T and DH6T on Au(111).

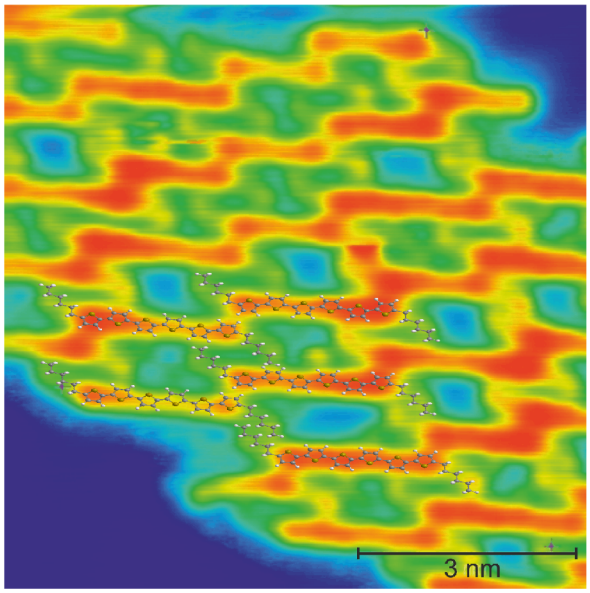

Figure 3.11: STM image of a submonolayer DH6T/Au(111) (V_s = 0.5 V; I_t = 50 pA) at which molecules form islands with a brick-wall-like structure.

STM image recorded at a submonolayer coverage. We can see the typical brick-wall-like structure [65] adopted by the DH6T molecules in small island or in the monolayer. In contrast to 6T forming rows of molecules parallel to each other with an optimal proximity between neighboring molecules, neighboring DH6T molecules are parallel as well, however they are shifted relative to each other along their long axis maximizing the distance between thiophene units of neighboring molecules, therefore intermolecular interactions, for instance stabilization effect due to polarization of neighboring molecules, are reduced, and may result in a faster dynamics in DH6T than in 6T.

Finally, combining 2PPE and STM we could show that the alkyl-substitution of 6T induces a change in the adsorption geometry of the molecule.We believe that because it reduces the intermolecular interactions, the brick-wall like structure of DH6T is responsible for the faster exciton decay dynamics.

3.1.2 α-octithiophene on Au(111)

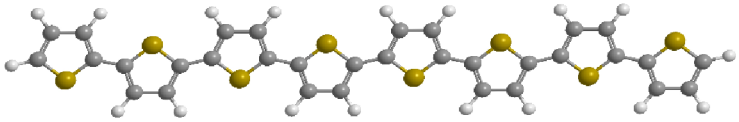

Figure 3.12: Chemical structure of α-octithiophene.

In the previous part we have shown that the alkyl-substitution of 6T, has changed the film structure, leading to a faster exciton dynamics. In this study on α-octithiophene (8T) on Au(111), combining 2PPE, high resolution electron energy loss spectroscopy (HREELS) and STM, we will show that the tilted adsorption of 8T/Au(111), in contrast to the flat-lying 6T/Au(111), strongly affects the exciton dynamics. Indeed, while the exciton lifetime in 6T depends on the film thickness, it is coverage-independent in 8T.

As previously mentioned, small organic molecules are very promising candidates for applications in organic electronic. Due to their semiconducting properties, oligothiophenes have attracted lot of interest in the last years. Moreover, a HREELS [28] study has shown that it is possible to tune the optical and electronic properties of oligothiophenes simply by varying their chain length. So far, due to the low solubility of thiophenes, 8T is the longest unsubstituted synthesized oligothiophene.

The adsorption geometry is already known to have a high influence on the device performance. In particular, it has been shown that the orientation of oligothiophenes with respect to the substrate has a crucial impact on the electronic as well as on the light absorption/emission properties of the molecules [66]. The adsorption properties of 6T has been intensively studied on different substrates [34, 58, 59, 65]. 6T has been found to form well-ordered films of flat-lying molecules on Au while tilted by about 70° with respect to the surface plan on Ag and Cu films. In contrast, little is known about the formation of 8T thin films on metallic substrates. So far only the adsorption of 8T on Cu(111) [67] has been studied.

Combining STM and HREELS, we have demonstrated that the adsorption geometry of 8T/Au(111) changes from flat-lying molecules in the submonolayer, to molecules tilted relative to the substrate with the long molecular axis parallel to the surface in the monolayer like shown Fig. 3.13 (see [68]).

In this section, using STS, and 1PPE we have determined the electronic structure of 8T at the interface with Au(111) and within the films. Moreover, with time-resolved 2PPE, we have measured the exciton dynamics as a function of the 8T coverages.

Figure 3.13: Change in the adsorption geometry from flat-lying in the submonolayer to tilted in the monolayer.

Fig.3.14 (a) displays UPS spectra recorded at 0.05 and 1.00 ML 8T coverages with 6 eV photons. While appearing as a very sharp feature located at -0.48 eV binding energy at 0.05 ML, the surface state (SS) is quenched at higher coverages and shifts toward lower binding energy down to around -0.3 eV and is labeled SS´. Its binding energy and dispersion are consistent with results obtained from other adsorbate-covered Au surfaces [53]. Two molecular features can be seen at -0.8 and -1.1 eV and are assigned to the HOMO and HOMO-1, respectively.

Fig.3.14 (b) shows dI/dV spectra taken at monolayer and bilayer coverages. The same double peak structure is seen at 1 ML and 2 ML. The features located at 2.0 and 2.4 V are assigned to the LUMO and LUMO+1 of 8T, respectively. No shift of the LUMO and LUMO+1 are observed when increasing the coverage from the mono- to the bilayer, indicating a weak electronic coupling between the molecules and the substrate. The separation of 0.4 eV between the two peaks is in very good agreement with the energy difference determined on a thin 8T film using electronic HREELS [28].

Fig.3.14 (c) summarizes the electronic structure measured with STS, UPS and 2PPE. The transport gap is 2.8 eV, that is 0.1 eV smaller than in 6T. A smaller gap is expected because of the longer backbone of 8T (*e.g.* particle in a box). The binding

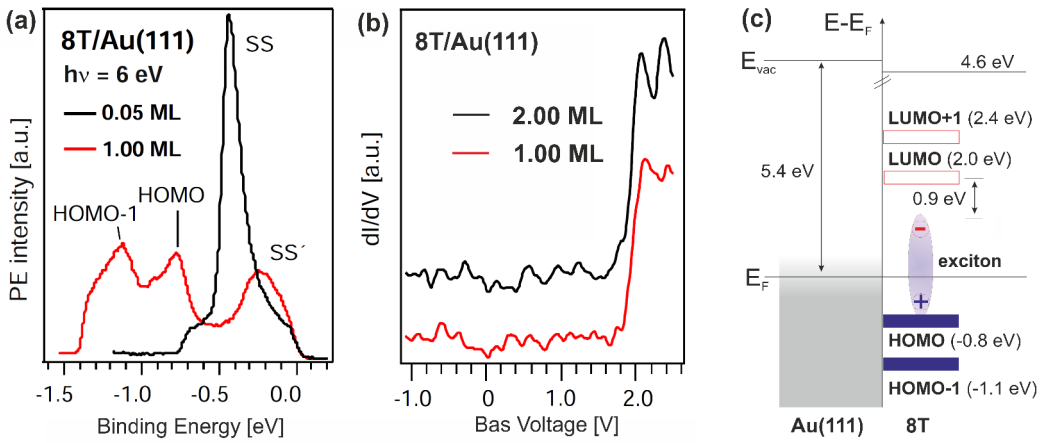

Figure 3.14: (a) Direct photoemission spectra recorded with a photon energy of 6 eV at 0.05 and 1.00 ML 8T coverages. (b) dI/dV spectroscopic data taken at a monolayer and bilayer coverages of 8T/Au(111) [69].

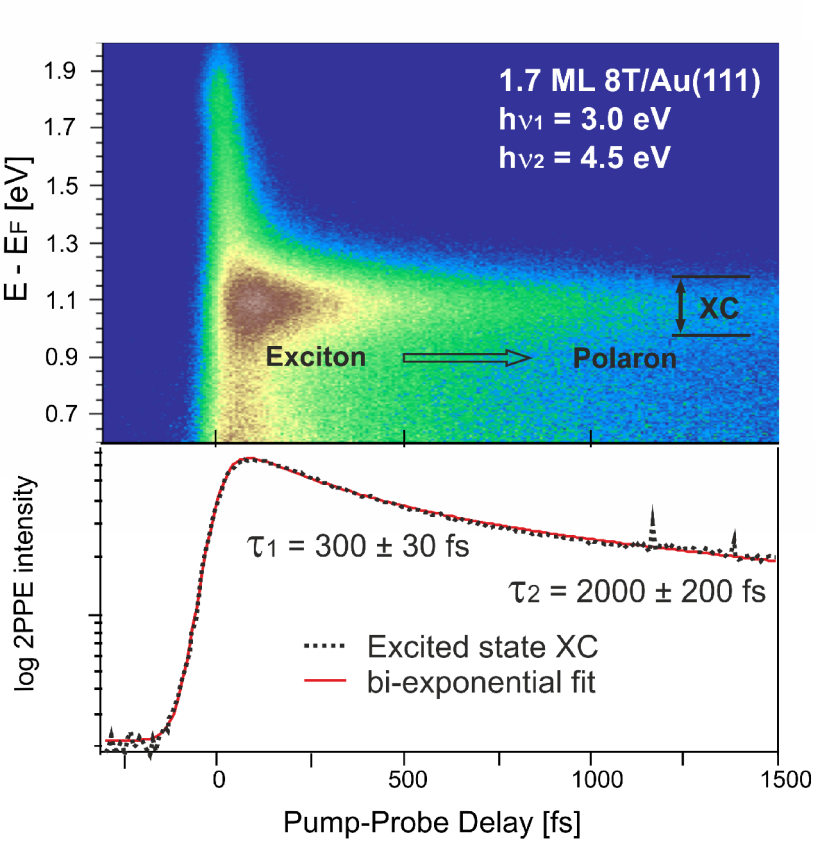

Figure 3.15: Two-dimensional spectrum of time-resolved 2PPE measurements recorded with $h\nu_1 = 3.0$ eV and $h\nu_2 = 4.5$ eV. The 2PPE intensity is plotted versus the intermediate state energy on the vertical axis and the pump-probe delay on the horizontal axis. Below is the cross-correlation (XC) trace of the 2PPE intensity integrated over the exciton peak intensity with bi-exponential fit which gives the indicated lifetimes.

energy of the exciton is 0.9 eV and is the same as for 6T.

Having determined the electronic structure of 8T, we focus on the coverage dependent exciton dynamics. The top panel of fig.3.15 shows a time-resolved 2PPE measurement recorded at 1.7 ML 8T/Au(111) with photon energies $h\nu_1 = 3.0$ eV and $h\nu_2 = 4.5$ eV. At positive delays, $h\nu_1 = 3.0$ eV photons excite electrons and $h\nu_2 = 4.5$ eV photons lift electrons above the vacuum level. Most striking is the feature at 1.1 eV exhibiting a lifetime toward positive delays. In analogy with 6T, we assign this feature to a Frenkel exciton created after a HOMO-LUMO transition induced by the absorption of a $h\nu_1 = 3.0$ eV photon, and possessing a binding energy of 0.9 eV.

The fit used to extract the lifetime of the exciton is the same than for 6T. In this case as well, a bi-exponential decay was best fitting the experimental data. Thus, in

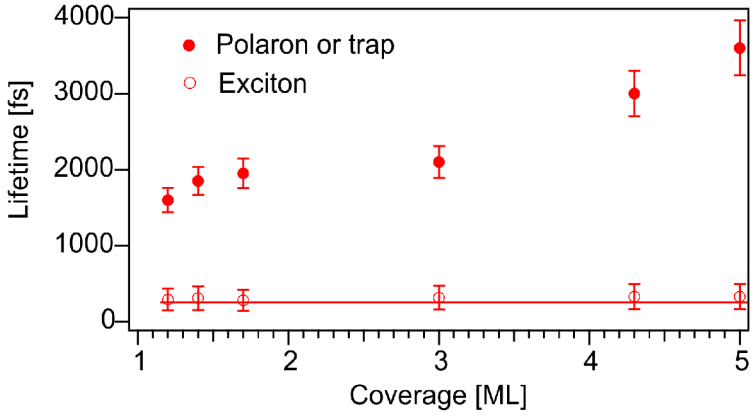

Figure 3.16: Lifetime of the exciton and the polaron/trap as a function of the 8T-coverage.

analogy with 6T, we interpret this as follow: first the 3.0 eV photon induces a HOMO-LUMO transition, due to the Coulomb attraction between the created electron and hole a Frenkel exciton with a binding energy of 0.9 eV is created. The 0.9 eV involved in the stabilization of the electron-hole pair is given to the environment by excitation of molecular vibration modes. The Frenkel exciton can then either recombine with a decay rate τ_1 or relax to form a polaron or trap state showing a lifetime of τ_2.

In order to learn more about possible relaxation channels of both excited states investigated here, we have performed coverage-dependent time-resolved experiments. The extracted lifetimes of the exciton and the polaron/trap are plotted versus the coverage in fig.3.16. As observed in 6T, the polaron exhibits a coverage-dependent lifetime . However, most striking here is the constant, coverage-independent, lifetime $\tau_1 = 300 \pm 30$ fs of the exciton, indicating a strong electronic decoupling between the molecules and the substrate. Due to the fact that 8T is electronically and structurally very similar to 6T, this pronounce difference in the exciton dynamics is surprising. However, in the previous section we have shown that 8T adopts a tilted adsorption geometry with the long axis parallel to Au(111), in contrast to the flat lying 6T molecules on the surface. Moreover a momentum-dependent electron energy-loss study on 6T [12] has shown that the extension of the electron-hole pairs along the molecules is comparable to the length of the molecules. We believe that, due to the adsorption of 8T in a tilted configuration, the exciton is localized in the molecular plane located parallel to the substrate, and therefore the electronic coupling between the exciton and the metal is very weak, even in the first layer, leading to the observed coverage-independent lifetime. However, a theoretical study on the spatial extension of the exciton would be valuable in order to confirm this hypothesis.

3.2 Polymers

3.2.1 poly(3,4-ethylene-dioxythiophene): poly-(styrenesulfonate)

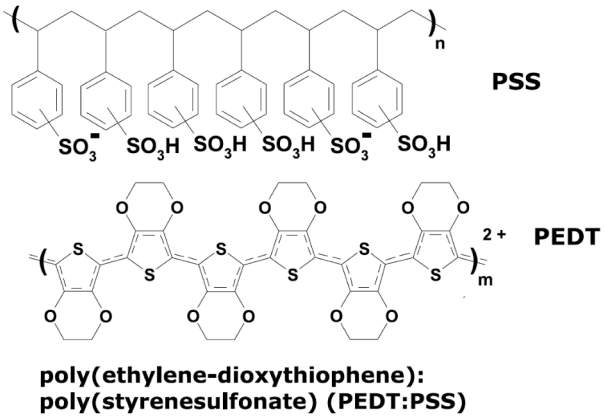

Figure 3.17: Chemical structure of PEDT:PSS

In the introduction we have pointed out that beside small molecules, another class of material has shown a high potential for organic optoelectronic, namely polymers. In order to successfully build devices based on organic compounds only, intrinsic conductive polymers (ICPs) will play a very important role as electrode material or a hole injection layer. PEDT:PSS is one of the prototypical ICP and has already been implemented in organic light emitting diodes (OLEDs) [70, 71] as well as in fiel-effect transistors (FETs) [72, 73] for instance. In PEDT, unhybridized p_z-orbitals of neighboring carbon atoms overlap to form π-bonds in which electrons are relatively delocalized. Single and double bounds of different length alternating along the chain, the band splits into a filled valence band and an empty conductive band. Therefore PEDT is a semiconductor. However, doped with PSS, the polymer becomes conductive. It is already known that charge carriers created in the polymer are polarons [74] that exhibit a strong electron-phonon (e-p) coupling, giving rise to new states in the band-gap. Therefore the polymer absorbs in the infrared region and is transparent [75]. The high work funciton of PEDT:PSS ranging between 5.0 and 5.6 eV depending of the amount of residual water in thin films [76] leads to a low hole injection barrier, and is comparable to atomically clean gold surface (e.g. $\Phi(\mathrm{Au}(111)) = 5.4$ eV [37]).

The dynamics of photoexcited charge carriers in the polymer plays an important role in optoelectronic applications, and has until now only been investigated with infrared-induced transient absorption in the sub-picosecond range. In this section we will introduce our investigation on the charge carrier dynamics in PEDT:PSS using femtosecond time-resolved 2PPE. This technique has already been intensively utilized

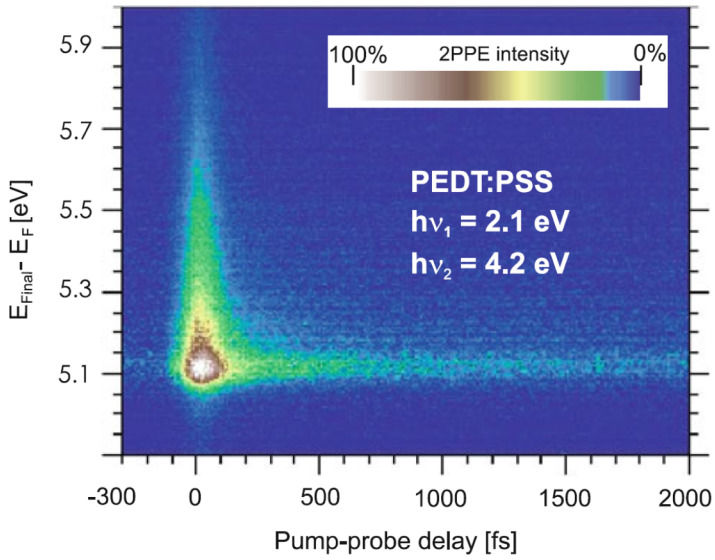

Figure 3.18: 2PPE intensity (color map) as a function of pump-probe delay (horizontal axis) and final state energy above the Fermi level (EF) (vertical axis) from PEDT:PSS recorded with photon energies of $h\nu_1 = 2.1eV$ for the visible and $h\nu_2 = 4.2eV$ for the UV laser pulses. The excited electron distribution is probed with $h\nu_1$ at negative delays, while at positive delays it is probed with $h\nu_2$ [81].

to study electron thermalization in various metals and semiconductors [77, 78, 79], but so far not in polymers. In polymers the cross section for light absorption is not very high in comparison to metals in which the penetration depth is typically around 10-20 nm. Moreover, another important difference between these two classes of materials is the charge carrier density that is in the order of $10^{20}cm^{-3}$ in PEDT:PSS [80] while around $10^{22}cm^{-3}$ in metals.

Fig.3.18 shows a time-resolved 2PPE measurement on PEDT:PSS. At positive delays where a lifetime can be clearly observed, the electrons are excited above E_F with $h\nu_1$ and probed with $h\nu_2$. In order to gain informations about the dynamics of the photoexcited charge carriers, we integrate the photoemission yield over a small energy range centered on the final state energy of interest and plot it in function of the time, resulting in the so-called cross correlation (XC) providing us the temporal evolution of the hot electrons population. Fits of these XC recorded at energies $E-E_F$ between 0.9 eV and 1.8 eV (XC in the range between 1.1 and 1.7 eV shown in fig.3.19 (a)) with a model including a convolution of a $sech^2$ function, representing the temporal width of the pulse, with a mono-exponential decay, result in the relaxation times shown fig.3.19 (b) with relaxation times measured on gold for comparison. The model utilized here fits the data well for $E - E_F \geq 1.5eV$, at lower excitation energies the dynamics is more and more dominated by the generation of secondary electrons.

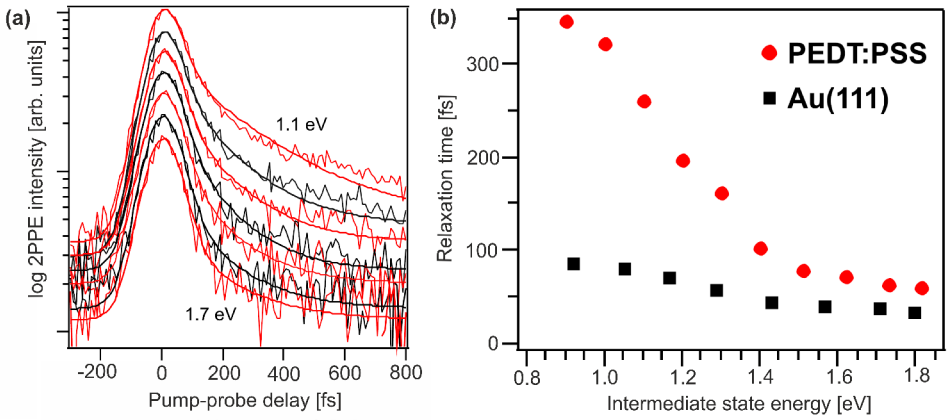

Figure 3.19: (a) Cross correlation curves for PEDT:PSS recorded at intermediate state energies $E - E_F$ between 1.1 and 1.7 eV. (b) Relaxation times of the photoexcited electron distribution for PEDT:PSS and Au(111) [81].

Most striking is the strong energy-dependent lifetime which is due to the availability of more phase space at higher energies. Moreover, at $E_{Final} - E_F \geq 1.5eV$ the relaxation times for PEDT:PSS and Au are very similar. On one hand, the high charge carrier density in the metal allows for a more reduced electron-electron interaction by screening, which reduces Coulomb interactions. On the other hand, the polaronic nature of the charge carriers in PEDT:PSS strongly favorites electron-phonon interaction in the polymer, leading to comparable lifetimes in the two materials. However at $E_{Final} - E_F \leq 1.5eV$ the charge carrier dynamics in PEDT:PSS is much slower than in Au, we attribute this to refilling effects due to Auger processes (creation of secondary electrons by decay of electrons and holes). Moreover, polarons tend to stabilize on weakly localized states on the polymer chain, thus reducing the probability of recombination by meeting polarons of opposite sign at low carrier excitation densities.

3.2.2 Regioregular poly(3-hexylthiophene)

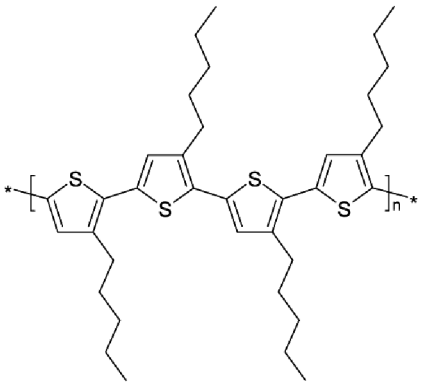

Figure 3.20: Chemical structure of P3HT.

In the introduction we have mentioned that polymers are promising candidates for all-organic devices. In particular, best performances for OPVCs are obtained using regioregular poly(3-hexylthiophene) (RR-P3HT, see fig.3.20) as donor material, and the previously investigated PEDT:PSS as an electrode. In P3HT, electrons are usually delocalized on the π-conjugated backbone, resulting in conductivity as high as 1000 S/cm. Despite of their high relevance for OPVCs, investigations on the dynamics of photoexcited charge carriers at polymer/polymer interfaces are limited to only a few 2PPE studies using nanosecond laser pulses on conjugated polymer films on metal substrates [82, 83, 84, 85, 86, 87, 88, 89].

In this study we have carried out time-resolved 2PPE experiments on thin RR-P3HT films spin casted on PEDT:PSS shown Fig.3.21. A broad photoemission feature labeled A can be observed at $E - E_F = 4.9eV$ and shows a clear lifetime toward positive time delays. Therefore this unoccupied intermediate state is populated by electrons excited by the $h\nu_1 = 2.1$ eV photons and then probed by the $h\nu_2 = 4.2$ eV photons. Thus the state A is located 0.7 eV above E_F. By mean of UPS, the valence band (VB) edge of P3HT has been measured 0.2 eV below the Fermi level of PEDT:PSS [90] and the commonly accepted band gap of P3HT is 1.9 - 2.1 eV [91]. Therefore the state A is located 1.0-1.2 eV below the conduction band edge (CB, see fig.3.22). Fitting the XC of the state shown in the bottom panel of fig.3.21 with a biexponential response function results in a fast component (2.6 ps) and a slow component (7.6 ps).

As we have shown in the case of the oligothiophenes, the adsorption of a photon of energy greater than the band gap can generate an exciton. For P3HT, the binding energy and the lifetime of the exciton have already been reported to be 0.7 eV [93] and 100 fs [94], respectively. If an exciton is created close to a dissociation center,

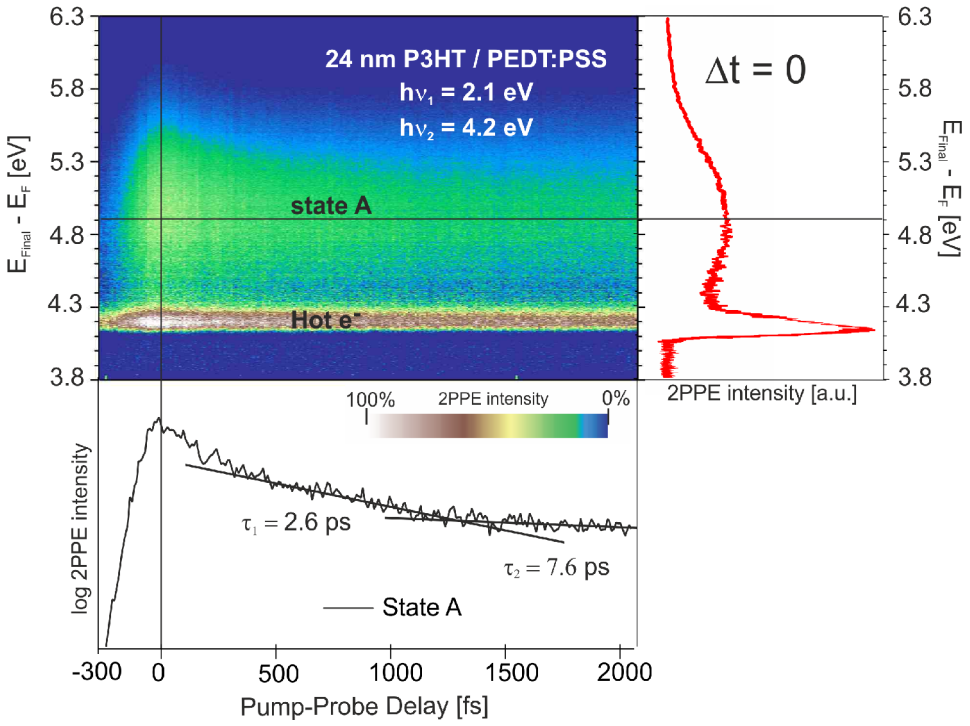

Figure 3.21: 2D-plot of 2PPE spectra as a function of pump-probe delay of a 24 nm P3HT film on PEDOT:PSS. For positive delays, the VIS pulse ($h\nu_1 = 2.1$ eV) arrives at the surface before the UV pulse ($h\nu_2 = 4.2$ eV), therefore the unoccupied intermediate state labeled as state A is VIS-pumped and UV-probed. The spectrum on the right corresponds to a cut at zero time delay. The bottom panel shows cross correlation trace for the energy region of state A [92].

for instance another polymer chain, it can undergo charge transfer and produce a bond polaron pair with positive and negative polaron on adjacent chain. This bound polaron pair can recombine, be trapped by a defect state, or dissociate into two charge carriers. Moreover it is known from the literature that two delocalized polaron bands located at 0.1 eV and 1.85 eV, as well as two localized polaron bands at 0.35 eV and 1.25 eV, respectively, are existent in RR-P3HT [30], viz. in the energy regime where we find the broad 2PPE feature. Therefore we assign the fast component (2.6 ps) to bound polaron pairs, in which positive and negative polarons are bound to each other on adjacent chains by Coulomb interaction. The bound polaron can recombine quickly or separate and be added to the slow component (7.6 ps) assigned to polarons generated by charge transfer between adjacent polymer chains. In order to confirm our assignment, a comparison between RR-P3HT that form a lamellae structure with non-negligible interchain interaction and regio-random (RRa)-P3HT that keeps a chainlike morphology would be necessary.

However, our study shows that time-resolved 2PPE is a powerful tool to investigate

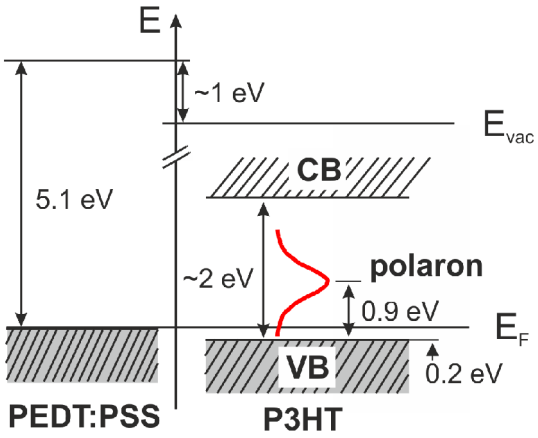

Figure 3.22: Energetic position of the polaron in P3HT observed in the present study. The Fermi level of PEDT:PSS serves as reference [92].

the excited state dynamics in polymer films as well.

3.3 Summary

In the framework of this thesis, we have used time-resolved two-photon photoemission (2PPE) in order to investigate the electronic structure and excited states dynamics upon photoexcitation in oligothiophenes and polymers relevant for optoelectronic applications.

In **α-sexithiophene (6T)** we were able to follow the full lifecycle of Frenkel excitons, from its population following a photoinduced HOMO-LUMO transition, to its decay or separation into a polaron or trap state. Coverage-dependent measurements have shown that two relaxation channels exist for the exciton as well as for the polaron. A substrate-mediated decay can occur at the interface and has a coverage dependent rate, moreover an intramolecular relaxation channel exits, the recombination of the Frenkel exciton.

In comparison to 6T, the Frenkel exciton relaxes faster in **α,ω-dihexylsexithiophene (DH6T)**. By means of STM measurement we have shown that the wall-brick-like adsorption configuration of the DH6T molecules increases the space between the conjugated cores of neighboring molecules, thus reducing the intermolecular interaction, for instance the stabilization due to polarization of adjacent molecules, thus leading to a faster decay dynamics.

In contrast, the dynamics of the exciton in **α-octithiophene (8T)** differs significantly from that in 6T, and possesses in that case a coverage-independent lifetime. We have shown a change in the adsoption geometry of 8T/Au(111), from flat-lying in the submonolayer to a tilted configuration with the molecular backbone parallel to the surface in the ML-regime, leading to electronic decoupling from the metal of the excitonic state localized on 8T.

We have measured the dynamics of the non-equilibrium electron distribution in the conducting polymer poly(3,4-ethylene-dioxythiophene): poly- (styrenesulfonate) (**PEDT:PSS**) and found out that the energetic relaxation of electrons excited at intermediate states $\geq$ 1.5 eV above E_F takes place on a similar time scale as for gold.

Finally we have applied our expertise gained on small organic molecules to the study of an excited state dynamics in a thin regioregular poly(3-hexylthiophene) (**RR-P3HT**). We have observed a bound polaron pair that can decay or separate and lead to the formation of two polarons of opposite sign on two adjacent polymer chains. The lifetimes of the bound polaron pair and the polaron are 2.6 ps and 7.6 ps, respectively.

In conclusion, we have shown that 2PPE is a very powerful tool to investigate the electronic structure, *e.g.* determination of the HOMO and LUMO positions, the transport gap and the interface dipole. Moreover time-resolved measurements allow for the study of excitation and decay of excited states in organic semiconductors, i.e. in small molecules as well as in polymers. Therefore this method promises to provide a link between optical and electron spectroscopy. This can be useful for better understanding of the elementary processes in organic photovoltaics and optimization of organic optoelectronic devices.

In this work we have focused on a few materials for the anode/donor interface, however other substituted oligothiophenes used in solar cells are available and should be further studied. Moreover, in the future, it will be interesting to investigate the donor/acceptor interface, in particular the exciton dissociation at these interfaces plays an important role in the cell efficiency, and acceptor/cathode interfaces in order to gain a complete picture of the processes in OPVCs, from the light absorption to the charge carriers extraction.

4 Publications

- **Optically induced inter- and intrafacial electron transfer probed by two-photon photoemission: electronic states of sexithiophene on Au(111)**
  Erwan Varene, Isabel Martin, and Petra Tegeder
  J. Phys. Chem. Lett., **2** (2011) 252-256.

- **Assembly and electronic structure of octithiophene on Au(111)**
  Erwan Varene, Yan Pennec, and Petra Tegeder
  Chem. Phys. Lett., **515** (2011) 141-145.

- **Coverage-dependent adsorption geometry of octithiophene on Au(111)**
  Erwan Varene, Lea Bogner, Stephan Meyer, Yan Pennec, and Petra Tegeder
  Phys. Chem. Chem. Phys., **14** (2012) 691-696.

- **Dynamics of optically excited electrons in the conducting polymer PEDT:PSS**
  Erwan Varene and Petra Tegeder
  Appl. Phys. A, **106** (2012) 803-806.

- **Polaron dynamics in thin polythiophene films studied with time-resolved photoemission**
  Erwan Varene and Petra Tegeder
  Appl. Phys. A, **107** (2012) 13-16 (Rapid Communication).

- **Ultrafast exciton population, relaxation and decay dynamics in thin oligothiophene films**
  Erwan Varene, Lea Bogner, Christopher Bronner and Petra Tegeder
  Phys. Rev. Lett., **109** (2012) 207601.

- **Influence of the adsorption geometry on the exciton dynamics in oligothiophenes**
  Erwan Varene, Lea Bogner, and Petra Tegeder
  In preparation

- **Exciton dynamics in α,ω-dihexylsexithiophene and sexithiophene: structure-property relationship**
  Erwan Varene and Petra Tegeder
  In preparation

THE JOURNAL OF PHYSICAL CHEMISTRY Letters

pubs.acs.org/JPCL

Optically Induced Inter- and Intrafacial Electron Transfer Probed by Two-Photon Photoemission: Electronic States of Sexithiophene on Au(111)

Erwan Varene, Isabel Martin, and Petra Tegeder*

Freie Universität Berlin, Fachbereich Physik, Arnimallee 14, D-14195 Berlin, Germany

ABSTRACT Using two-photon photoemission spectroscopy, we investigated the electronic structure of the organic semiconductor α-sexithiophene (6T) adsorbed on Au(111). Beside the quantitative determination of the energetic position of electronic states originating from the highest occupied molecular orbitals (HOMO and HOMO-1) and the lowest unoccupied molecular orbitals (LUMO and LUMO+1), a localized exciton state that possesses a binding energy of 0.9 eV has been identified. Whereas the creation of the exciton is the result of an intramolecular excitation involving a HOMO−LUMO transition, the transient population of the LUMO and LUMO+1 follow from an optically induced charge transfer from the metallic substrate to the molecule. The present study provides important parameters such as the energetic position of the transport level and the exciton binding energy, which are needed to understand the physics in organic-molecules-based optoelectronic devices.

SECTION Surfaces, Interfaces, Catalysis

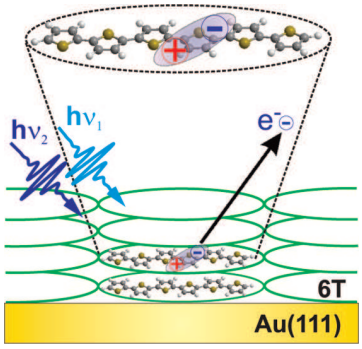

Semiconducting materials based on organic molecules or polymers are promising candidates for applications in electronic devices such as organic photovoltaic cells, light-emitting diodes, and thin film transistors.[1−4] The electronic structure at interfaces between organic or polymeric semiconductors and inorganic substrates is the most fundamental issue to understand the functionalities of organic films. Measuring the alignment of molecular orbitals (or bands) with respect to the Fermi level of the (metallic) substrate yields quantitative information on the barriers for electron (hole) injection at the molecule−metal interface. Whereas the energy level alignment of bands due to the highest occupied molecular orbital (HOMO) has been widely studied by means of ultraviolet photoemission spectroscopy (UPS), spectroscopic information on unoccupied molecular states, for example, the lowest unoccupied molecular orbital (LUMO), are rather limited. Additionally, in organic semiconductors, excitonic states play an important role; in particular, their binding energy is one of the key parameters that governs the physics of optoelectronic devices. For instance, in photovoltaics, the created exciton has to be separated to generate free charge carriers that can diffuse to the corresponding electrodes.[5]

In the present study, we utilized two-photon photoemission (2PPE) spectroscopy, which has been proven to be an ideal tool to investigate both occupied and unoccupied molecular electronic states,[6,7] to determine the electronic structure of α-sexithiophene (6T, Figure 1) on Au(111) at the interface and within the film. The oligothiophene 6T, a π-conjugated chain-like planar molecule, has been widely investigated because it serves as a model system for the structural less controllable polythiophene. Furthermore, it is used in organic field effect transistors[8,9] and in bulk heterojunction photovoltaic cells.[10] Several surface science studies focusing on the adsorption behavior of 6T on noble metal surfaces exist, for example, on Au(110),[11] Au(111),[12] Ag(100),[13] and Cu(110).[14] In the monolayer regime, 6T deposited on Au(111) at room temperature forms well-ordered domains of flat-lying molecules, which are arranged in molecular rows.[12] In addition, the occupied band structures and accordingly the hole injection barriers of 6T adsorbed on various noble metals have been determined using mainly UPS.[15−19] In contrast, studies on the 6T/Au(111) interface electronic properties, that is, 6T in the monolayer (ML) regime, are not known so far. A combined UPS and inverse photoelectron spectroscopy (IPES) study on thick (50−100 Å) 6T films on Au determined a HOMO−LUMO gap of 4.2 ± 0.2 eV.[20]

An exemplary two-color 2PPE spectrum of 0.8 ML 6T recorded at $h\nu_1 = 3.0$ eV and $h\nu_2 = 4.4$ eV is shown in Figure 1. Several peaks are observed, and on the basis of photon-energy-dependent measurements,[21] they can be related to photoemission from unoccupied intermediate states. The peak at 6.88 eV arises from the $n = 1$ image potential state (IPS), which exhibits an energetic position of 3.88 eV with respect to E_F (corresponding to ∼0.7 eV below the vacuum level, E_{vac}). For comparison, the $n = 1$ IPS on clean Au(111) possesses a binding energy of 0.8 eV with respect to E_{vac},

Received Date: December 1, 2010
Accepted Date: January 13, 2011
Published on Web Date: January 20, 2011

DOI: 10.1021/jz1016203 | J. Phys. Chem. Lett. 2011, 2, 252–256

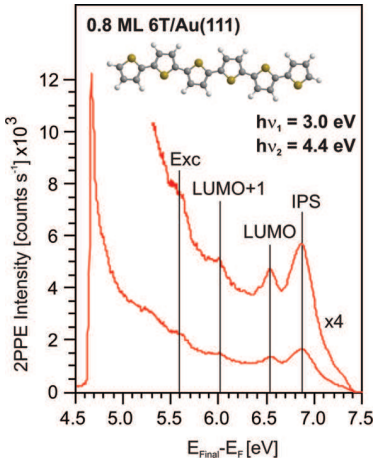

Figure 1. Two-color 2PPE spectrum of 0.8 ML 6T/Au(111) recorded with 3.0 and 4.4 eV photons. The spectrum is displayed as a function of final-state energy above the Fermi level, $E_{Final} - E_F = E_{kin} + \Phi$ (with Φ the work function).

whereas on the *n*-heptane (1 ML)-covered surface, it is located at 0.6 eV.[22] The peaks at 6.52 and 5.6 eV in the 2PPE spectrum originate both from states, which are probed by the 4.4 eV photons, and thus they are located at 2.12 and 1.2 eV above E_F, respectively. We assign the peak at 2.1 eV to the LUMO and the one at 1.2 eV to an exciton (Exc) state. Arguments for the latter assignment will be given below. The feature seen at 6.01 eV is probed by the 3 eV photons; accordingly, it possesses an energetic position of 3.0 eV with respect to E_F and is attributed to the LUMO+1 state. Additionally, in a one-color 2PPE experiment using 4.3 eV photons at a coverage of 2 ML, also 6T-derived occupied initial states are obtained. (See the Supporting Information.) Photoemission from the HOMO and HOMO-1 are found at −0.8 and −1.5 eV with respect to E_F, respectively. UPS studies on thick 6T films observed the HOMO level between −1.2 and −1.0 eV.[17,20]

Figure 2 displays a set of two-color 2PPE spectra taken at photon energies of 3.0 and 4.3 eV at various 6T coverages. Most striking is the pronounced photoemission intensity increase from the excitonic state with increasing coverage; at 4 ML, the spectrum is dominated by this peak. In contrast, the intensities of the peaks attributed to the LUMO and LUMO+1 as well as the IPS drop with rising coverage. To understand this behavior, one has to consider the excitation mechanisms possible in 2PPE. The transient population of unoccupied molecular electronic states dominantly occurs either via a photoinduced substrate to molecule electron transfer or through intramolecular excitation, for example, HOMO−LUMO transition. We believe that the LUMO and LUMO+1 level is transiently populated by an optically induced interfacial electron transfer from the gold substrate to the molecules. This interpretation is consistent with the observed intensity decrease in the LUMO and LUMO+1 peaks with increasing 6T coverage. With increasing film thickness, the electronic coupling between the 6T molecules and the metal surface is expected to decrease and accordingly the transition dipole moment for electron transfer excitation from the substrate to the adsorbate. The proposed excitonic state is

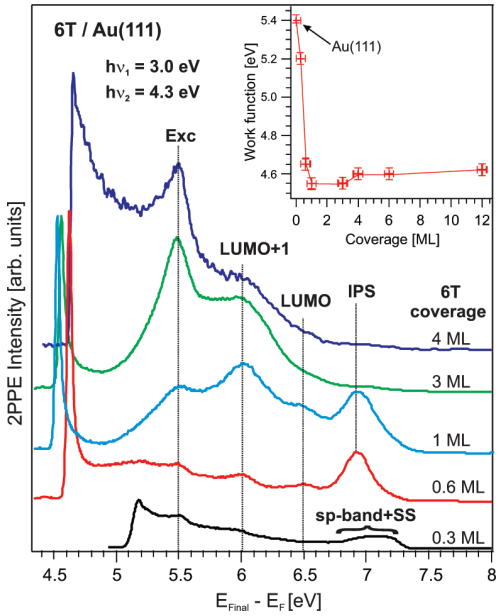

Figure 2. Two-color 2PPE spectra recorded at photon energies of 3.0 and 4.3 eV of various 6T coverages. At low 6T coverage, the Au(111) surface state (SS) and the sp band is observed. The inset shows the work function (Φ) of 6T adsorbed on Au(111) as a function of 6T coverage.

visible at any film thickness because of the intramolecular excitation process. In the first layer, quenching may occur to a certain extent by the stronger interaction with the metallic substrate. However, an intramolecular excitation channel for, for example, the LUMO (HOMO−LUMO transition), may be operative, although on the basis of a detectable photoemission signal, we found no clear indication (see below). A similar behavior of 2PPE peak intensities resulting from molecular electronic and exciton states as a function of film thickness has been observed for C_{60} adsorbed on Cu(111)[23] and Au(111).[24] Note that shifting of energetic positions of the electronic states as a function of coverage (at least up to 3 ML), as known for other organic/electrode interfaces,[23−25] is not found.

As the photoemission peaks originating from the LUMO and LUMO+1, the peak intensity of the first IPS decreases with increasing coverage. It is only visible on thin films (≤∼2 ML), for which an effective matrix element exists, allowing excitation of electrons from metal states to the 2D delocalized IPS (see below). This state is predominantly located near the vacuum interface.[26] In addition, at higher coverages, the surface roughness may increase, leading also to a reduction of the IPS intensity.[27] Another quantity that has closely been monitored is the coverage-dependent work function (Φ, see inset of Figure 2). For the clean Au(111) surface, a value of 5.4 eV is observed, which continuously decreases in an approximately linear fashion by 0.85 eV until a coverage of 1 ML is reached. Here it possesses a value of 4.55 eV. Further coverage increase (> 3 ML) leads to a slight increase in Φ by 0.05 eV. The Φ-drop is the result of the creation of an interface dipole due to the adsorption of 6T molecules in the monolayer regime.

DOI: 10.1021/jz1016203 | J. Phys. Chem. Lett. 2011, 2, 252–256

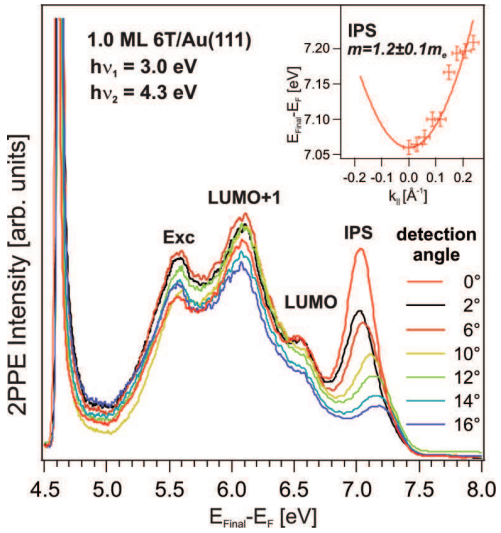

Figure 3. Angular-dependent 2PPE measurements of 1 ML 6T/Au(111) measured with 3.0 and 4.3 eV photons. The inset shows the dispersion of the image potential state (IPS), which exhibits a free electron-like character.

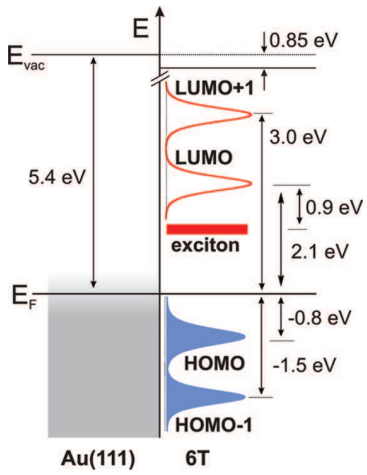

Figure 4. Energetic position and assignment of 6T-derived photoemission spectral features at a coverage of 1 ML 6T adsorbed on Au(111) observed in the present study. The Fermi level of Au(111) serves as reference.

Further evidence that the 2PPE feature at 1.2 eV above E_F results from photoemission of an exciton state is given by photon-energy-dependent measurements in the range between 2.0 and 2.4 eV. Using photon energies in a two-color pump−probe scheme in which the photon energy of the pump laser pulse is below the energetic threshold for the direct photoexcitation (an energy around 2.9 eV is needed to excite an HOMO−LUMO transition) does not lead to the appearance of this peak in the 2PPE spectrum. This is a clear indication that this electronic state originates from an exciton, which is generated via an optically induced intramolecular electron transfer from the HOMO to LUMO level of 6T, followed by a relaxation process due to the attractive Coulomb interaction between the electron and hole. The relaxation of the electron resulting in the formation of the excitonic state occurs most likely on an ultrafast time scale, which is possibly the reason why the photoemission of electrons from the LUMO excited via an intramolecular transition is not observed in the 2PPE experiment.

To gain deeper insight into the properties of the unoccupied electronic states, we performed dispersion measurements using angle-resolved 2PPE, which provides information about the extent of electron delocalization/localization parallel to the surface. Figure 3 shows a series of angular-dependent measurements at a 6T coverage of 1 ML, recorded at photon energies of 3.0 and 4.3 eV. Both unoccupied molecular states, the LUMO and LUMO+1, as well as the exciton state show no dispersion, viz. they are localized in contrast to the IPS. The IPS exhibits a free-electron-like parabolic dispersion parallel to the surface having an effective mass of $1.2 \pm 0.1\ m_e$. (See the inset of Figure 3.)

Figure 4 summarizes the energetic positions and assignments of the 6T-derived electronic states observed at a coverage of 1 ML 6T on Au(111). The Fermi level of the Au(111) surface serves as reference. The work function at the 1 ML coverage is 4.6 eV; that is, a decrease of 0.85 eV compared with the bare Au(111) surface is observed. The LUMO level obtained from 2PPE is at 2.1 eV and thus 0.9 eV lower than that determined by IPES.[20] The HOMO position is higher by 0.2 to 0.4 eV compared with the value (−1.0 to −1.2 eV) found in UPS studies. As a result, the HOMO−LUMO gap (peak-to-peak separation) from 2PPE is 2.9 eV, whereas a gap of 4.2 ± 0.2 eV is obtained from combined UPS/IPES. Note that the gap determined in both the 2PPE and the UPS/IPES corresponds to the transport gap because in the 2PPE, the LUMO is populated via a metal-to-molecule electron transfer (creating a negative ion resonance) and not through an intramolecular charge transfer. Accordingly, both experiments 2PPE and IPS should give similar LUMO positions (transport levels). However, the difference may be attributed to the lower sensitivity (energy resolution) and count rates (intensities) in IPES compared with 2PPE. Therefore, the shoulder around 3 eV observed in IPES[20] may be assigned to the LUMO+1 and not to the LUMO. In 2PPE, we found the energetic position of the exciton state to be at 1.2 eV above E_F, and hence it possesses a binding energy of 0.9 eV. This "measured" binding energy exceeds the one estimated by Hill et al.[20] by 0.5 eV. Angular-dependent 2PPE shows that the exciton state is localized; therefore, we assign it to a Frenkel exciton (singulet). Localized singulet (Frenkel) excitons are common in organic (molecular) semiconductors; however, it has been discussed if a strictly Frenkel-like nature of excitons in condensed organic semiconductors is correct.[5]

In conclusion, the presented results elucidate the electronic structure, that is, sexithiophene (6T)-derived occupied (HOMOs) and unoccupied (LUMOs) molecular electronic and excitonic states at the interface between 6T and Au(111) and within the 6T film. The interfacial excitation mechanism, viz., optically induced electron transfer between the metallic substrate and 6T, and the intrafacial that is the intramolecular HOMO−LUMO transition, have been proposed to be the underlying processes for the population of the electronic states. The transport gap (HOMO−LUMO gap) as well as the binding

DOI: 10.1021/jz1016203 | J. Phys. Chem. Lett. 2011, 2, 252–256

energy of a localized Frenkel exciton have been determined. Further experiments, including femtosecond time-resolved 2PPE measurements to determine the inter- and intrafacial charge carrier and exciton dynamics, are in progress.

EXPERIMENTAL METHODS

For the 2PPE measurements, an ultra-high vacuum chamber (base pressure of 1×10^{-10}mbar) for photoemission spectroscopy and surface science techniques in combination with a tunable femtosecond (fs) laser system was used. The Au(111) crystal was cleaned by a standard procedure of Ar^+ sputtering and annealing. 6T molecules were dosed onto the Au(111) crystal (held at 289 K) using a home-built effusion cell held at 500 K. To determine the 6T coverage, thermal desorption spectroscopy was employed. (See the Supporting Information.) The fs-laser system consists of a Ti/sapphire oscillator in combination with a 300 kHz regenerative amplifier. It supplies pulses with a central wavelength ranging from 800 to 830 nm. The output is used to pump an optical parametrical amplifier (OPA), which yields photons with a tunable energy in the range from 1.7 to 2.7 eV and additionally a fixed 3 eV output. Through frequency doubling in a β-barium borate crystal, the photon energy range from 3.4 to 5.4 eV is achieved. After thorough temporal compression, pulses with a duration of ~60 fs are obtained. These are focused onto the sample under an angle of 45° with respect to the surface normal. Photoelectrons are detected in a custom-built time-of-flight (TOF) spectrometer and are analyzed with respect to their kinetic energy (E_{kin}). (For details, see ref 21.) The energy resolution of the TOF spectrometer depends on the kinetic energy of the electrons; ~20 meV at $E_{kin} \approx 1$ eV.

SUPPORTING INFORMATION AVAILABLE Additional 2PPE data of 6T/Au(111) and a description of the preparation of 6T films. This material is available free of charge via the Internet at http://pubs.acs.org/.

AUTHOR INFORMATION

Corresponding Author:

*To whom correspondence should be addressed. E-mail: petra.tegeder@physik.fu-berlin.de. Phone: +49 (0)30 83856234. Fax: +49 (0)30 83856059.

ACKNOWLEDGMENT Funding by the Deutsche Forschungsgemeinschaft (DFG) through the priority program SPP 1355 and collaborative research center SFB 658 is gratefully acknowledge.

REFERENCES

(1) Katz, H. E.; Huang, J. Thin-Film Organic Electronic Devices. *Annu. Rev. Mater. Res.* **2009,** *39*, 71–92.
(2) Koch, N. Organic Electronic Devices and Their Functional Interfaces. *ChemPhysChem* **2007,** *8*, 1438–1455.
(3) Günes, S.; Neugebauer, H.; Serdar Sariciftci, N. Conjugated Polymer-Based Organic Solar Cells. *Chem. Rev.* **2007,** *107*, 1324–1338.
(4) Walzer, K.; Maennig, B.; Pfeiffer, M; Leo, L. Highly Efficient Organic Devices Based on Electrically Doped Transport Layers. *Chem. Rev.* **2007,** *107*, 1233–1271.
(5) Krause, S.; Casu, M. B.; Schöll, A.; Umbach, E. Determination of Transport Levels of Organic Semiconductors by UPS and IPS. *New J. Phys.* **2008,** *10*, 085001–16.
(6) Zhu, X.-Y. Electronic Structure and Electron Dynamics at Molecule/Metal Interfaces: Implications for Molecule-Based Electronics. *Surf. Sci. Rep.* **2004,** *56*, 1–83.
(7) Lindstrom, C. D.; Zhu, X.-Y. Photoinduced Electron Transfer at Molecule-Metal Interfaces. *Chem. Rev.* **2006,** *106*, 4281–4300.
(8) Katz, H. E. Organic Molecular Solids as Thin Film Transistor Semiconductors. *J. Mater. Chem.* **1997,** *7*, 369–376.
(9) D. Fichou, D. Structural Order in Conjugated Oligothiophenes and its Implications on Opto-Electronic Devices. *J. Mater. Chem.* **2000,** *10*, 571–588.
(10) Sakai, J.; Taima, T.; Saito, K. Efficient Oligothiophene: Fullerene Bulk Heterojunction Organic Photovoltaic Cells. *Org. Electron.* **2008,** *9*, 582–590.
(11) Prato, S.; Floreano, L.; Cvetko, D; De Renzi, V.; Morgante, A.; Modesti, S.; Biscarini, F.; Tamboni, R.; Taliani, C. Anisotropic Ordered Planar Growth of α-Sexithienyl Thin Films. *J. Chem. Phys. B* **1999,** *103*, 7788–7795.
(12) Kiel, M.; Duncker, K.; Hagendorf, C.; Widdra, W. Molecular Structure and Chiral Separation in α-Sexithiophene Ultrathin Films on Au(111): Low-Energy Electron Diffraction and Scanning Tunneling Microscopy. *Phys. Rev. B* **2008,** *75*, 195439–1−8.
(13) Duncker, K.; Kiel, M.; Höfer, A.; Widdra, W. Commensurate Surface Structures and Concerted *cis-trans*-Isomerization within Ordered Monolayers of α-Sexithiophene on Ag(001). *Phys. Rev. B* **2008,** *77*, 155423−1-8.
(14) Kiguchi, M.; Entani, S.; Saiki, K.; Yoshikawa, G. One-Dimensional Ordered Structure of α-Sexithienyl on Cu(110). *Appl. Phys. Lett.* **2004,** *84*, 3444–3446.
(15) Chandekar, A.; Whitten, J. E. Ultraviolet Photoemission and Electron Energy Loss Spectroscopy of Oligothiophene Films. *Synth. Met.* **2005,** *150*, 259–264.
(16) Koch, N.; Heimel, G.; Wu, J.; Zojer, E.; Johnson, R. L.; Brédas, J.-L.; Müllen, K.; Rabe, J. P. Influence of Molecular Conformation on Organic/Metal Interface Energetics. *Chem. Phys. Lett.* **2005,** *431*, 390–395.
(17) Knupfer, M.; Liu, X. Interface Electronic Properties of Oligothiophenes: The Effect of Chain Length and Chemical Substituents. *Surf. Sci.* **2006,** *600*, 3978–2981.
(18) Grobosch, M.; Knupfer, M. Charge-Injection Barriers at Realistic Metal/Organic Interfaces: Metals Become Faceless. *Adv. Mater.* **2007,** *19*, 754–756.
(19) Ivanco, J.; Netzer, F. P.; Ramsey, M. G. On Validity of the Schottky-Mott Rule in Organic Semiconductors: Sexithiophene on Various Substrates. *J. Appl. Phys.* **2007,** *101*, 103712–1−6.
(20) Hill, I. G.; Kahn, A.; Soos, Z. G.; Pascal, R. A., Jr. Charge-Separation Energy in Films of π-Conjugated Organic Molecules. *Chem. Phys. Lett.* **2000,** *327*, 181–188.
(21) Hagen, S.; Lou, Y.; Haag, R.; Wolf, M.; Tegeder, P. Electronic Structure and Electron Dynamics at an Organic Molecule/Metal Interface: Interface States of Tetra-*tert*-butyl-Imine/Au(111). *New. J. Phys.* **2010,** *12*, 125022.
(22) Lindstrom, C. D.; Quinn, D.; Zhu, X.-Y. Using Image Resonances to Probe Molecular Conduction at the *n*-Heptane/Au(111) Interface. *J. Chem. Phys.* **2005,** *122*, 124714–1−10.
(23) Dutton, G.; Zhu, X.-Y. Unoccupied States in C_{60} Thin Films Probed by Two-Photon Photoemission. *J. Phys. Chem. B* **2002,** *106*, 5975–6981.

DOI: 10.1021/jz1016203 | *J. Phys. Chem. Lett.* **2011**, *2*, 252–256

(24) Dutton, G.; Quinn, D. P.; Lindstrom, C. D.; Zhu, X.-Y. Exciton Dynamics at Molecule-Metal Interfaces: C_{60}/Au(111). *Phys. Rev. B* **2005,** *72*, 045441−1−11.
(25) Blumenfeld, M. L.; Steele, M. P.; Monti, O. L. A. Near- and Far-Field Effects on Molecular Energy Level Alignment at an Organic/Electrode Interface. *J. Phys. Chem. Lett.* **2010,** *1*, 145–148.
(26) Güdde, J.; Berthold, W.; Höfer, U. Dynamics of Electronic Transfer Processes at Metal/Insulator Interfaces. *Chem. Rev.* **2006,** *106*, 4261–4280.
(27) Hagen, S.; F. Leyssner, F.; D. Nandi, D.; M. Wolf, M.; Tegeder, P. Reversible Switching of Tetra-*tert*-butyl-azobenzene on a Au(111) Surface Induced by Light and Thermal Activation. *Chem. Phys. Lett.* **2007,** *444*, 85–90.

DOI: 10.1021/jz1016203 | *J. Phys. Chem. Lett.* **2011**, *2*, 252–256

Chemical Physics Letters 515 (2011) 141–145

Contents lists available at SciVerse ScienceDirect

Chemical Physics Letters

journal homepage: www.elsevier.com/locate/cplett

Assembly and electronic structure of octithiophene on Au(1 1 1)

Erwan Varene [a], Yan Pennec [b], Petra Tegeder [a,*]

[a] Freie Universität Berlin, Fachbereich Physik, Arnimallee 14, 14195 Berlin, Germany
[b] Department of Chemistry and Physics and Astronomy, University of British Columbia, Vancouver, BC, Canada V6T 1Z4

ARTICLE INFO

Article history:
Received 13 May 2011
In final form 2 September 2011
Available online 7 September 2011

ABSTRACT

Scanning tunneling microscopy and spectroscopy as well as photoemission spectroscopy have been employed to study the adsorption behavior and electronic structure of α-octithiophene (8T) on Au(1 1 1). At a monolayer (ML) and bilayer coverage well-ordered molecular rows forming closely packed films are found, with 8T molecules tilted with respect to the surface plane allowing for intermolecular π–π-interactions. Two unoccupied electronic states are observed, which possess the same energetic position for 1 and 2 ML, indicating a low electronic coupling strength between 8T and the metallic substrate. This study shows that 8T grow on Au(1 1 1) in an ordered way generating a defined interface which is a basic requirement for future applications of 8T in (opto) electronic devices.

1. Introduction

The electronic properties of interfaces formed between functional organic materials and metal electrodes have a major impact on the performance of (opto) electronic devices. Thereby the energetic alignment of molecular electronic states with respect to the Fermi level is crucial since it determines the charge (electrons and holes) injection barriers. The interaction strength between the molecules and the surface competes with intermolecular interactions to govern self-assembly of molecules into regular patterns on the substrate. Well-ordered and defect-free films with defined interfaces are needed to improve electronic devices based on organic molecules. The growth of such films is dominated by the adsorption structure of the first molecular layer, i.e., the molecules in direct contact with the substrate. Therefore, investigations of adsorbed molecules at the atomic level is required in order to gain insights into the growth mode and the influence of the molecular layer structure on the electronic structure, which is decisive for the optimization of the devices. This has driven studies on the adsorption, growth and electronic structure of thin films of various organic molecules on different noble metal surfaces [1].

Organic macromolecules with a π-conjugated backbone have been widely investigated because of their promising physical properties which open prospects for technological applications in molecular (opto) electronics [2–4]. In particular, oligothiophenes, like α-sexithiophene (6T) which has been used as an active layer in one of the first field-effect transistor [5], have attracted much attention due to their optical and electronic properties. Indeed, high charge mobilities as well as absorption and emission in the visible spectral range [6–8] make them very good candidates for organic light-emitting diodes [9] and solar cells [10].

In contrast to 6T for which several surface science studies exist focusing on the adsorption behavior on noble metal surfaces, e.g., on Au(110) [11], Au(1 1 1) [12–14], Ag(1 0 0) [15], Ag(1 1 0) [16,17], and Cu(1 1 0) [18], little is known for α-octithiophene (8T, see Figure 1b). So far, on metal surfaces only a conformational analysis of *N*-silyl substituted 8T adsorbed on Cu(1 0 0) using scanning tunneling microscopy (STM) is available [19]. Although the physical properties and accordingly the performance of oligothiophenes based devices may be turned by the number of thiophene rings (cf. particle in a box). For instance, high resolution electron energy loss (HREELS) and UV–Vis spectroscopic investigations on α-oligothiophene thin films have demonstrated that the gap between the highest occupied molecular orbital (HOMO) and the lowest unoccupied molecular orbital (LUMO) decreases (linearly) with increasing number of thiophene rings [20]. This has been reproduced by a Hückel molecular orbital model [20] and density functional theory [21]. Furthermore, in a hybrid solar cell based on 8T and GaAs(1 1 1) the highest hole mobility in the oligothiophene series has been observed [22]. Up to know 8T is the unsubstituted oligothiophene with the longest chain length which has been synthesised which is due to the pure solubility.

In the present study we utilized low-temperature (15 K) STM, scanning tunneling spectroscopy (STS) and photoemission spectroscopy (PES) in order to determine the coverage dependent absorption properties and electronic structure of 8T on Au(1 1 1), respectively. In the sub-monolayer regime no nucleation or island formation of 8T molecules is found. In contrast, at a monolayer (ML) as well as at a bilayer coverage 8T form well-ordered rows and densely packed film. Thereby the self-assembly is most likely driven by the π–π-interaction between the tilted molecules. From the STS data we determined the LUMO and LUMO + 1 levels to be

* Corresponding author.
E-mail address: petra.tegeder@physik.fu-berlin.de (P. Tegeder).
URL: http://physik.fu-berlin.de/einrichtungen/ag/ag-tegeder (P. Tegeder).

0009-2614/$ - see front matter © 2011 Elsevier B.V. All rights reserved.
doi:10.1016/j.cplett.2011.09.010

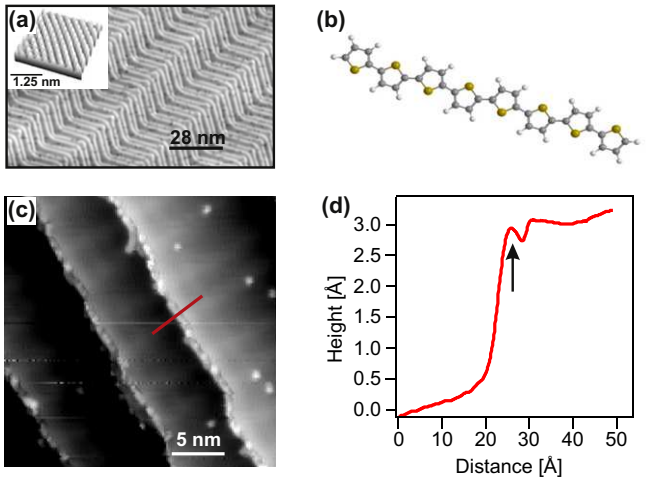

Figure 1. (a) Low-temperature (15 K) STM image of the Au(1 1 1) surface ($V_s = -1$ V, $I_t = 100$ pA) showing a large terrace with high purity. The image is revealing the "herringbone" reconstruction. Inset: STM image with atomic resolution of the Au(1 1 1) surface ($V_s = 0.9$ V, $I_t = 55$ pA) showing the hexagonal lattice of the surface atoms. (b) Balls and stick model of α-octithiophene (8T) investigated in the present study. (c) STM image of low-coverage 8T/Au(1 1 1) ($V_s = 0.5$ V, $I_t = 51$ pA); 8T was deposited on the substrate held at $T_{sub} = 300$ K. (d) Corresponding line profile as marked by the red line in (c). Black arrow marks the position of the molecules, which is the bottom of the step edge. The step edge height is ≈3 Å. (For interpretation of the references to colour in this figure legend, the reader is referred to the web version of this article.).

located at 2.0 and 2.4 eV, respectively, with respect to the Fermi level at a 8T coverage of 1 ML. The electronic states do not shift in energy with increasing coverage (2 ML), indicating that the adsorbate/substrate-interaction is comparatively weak. From PES the HOMO and HOMO-1 could be identified, which possess a binding energy of −0.8 and −1.1 eV with respect to E_F.

2. Experimental

STM and STS experiments: All STM and STS experiments were performed at University of British Columbia with a custom-designed ultrahigh vacuum (UHV) apparatus (base pressure 10^{-10} mbar) comprising a commercial low-temperature scanning tunneling microscope (Createc; based on the design described in Ref. [23]). The STM was operated typically at 15 K to obtain high-resolution topographic and spectroscopic data. The STM tip is made out of an etched tungsten wire and was prepared by Ar^+ - bombardment in UHV. Topographic data were acquired in the constant current mode, with typical tunneling resistances in the range of 10–104 MΩ. Tunneling spectroscopy data were recorded with a lock-in technique (with a typical modulation amplitude and frequency of 20 mV and 1 kHz, respectively).

For photoemission measurements an ultra-high vacuum chamber (base pressure of 10^{-10} mbar) in combination with a tunable femtosecond (fs) laser system was used. The fs-laser system consists of a Ti/sapphire oscillator in combination with a 300 kHz regenerative amplifier. It supplies pulses with a central wavelength of 830 nm. Through frequency doubling in a β-barium borate crystal performed twice, pulses with photon energy of 6 eV are achieved. These are focused onto the sample under an angle of 45° with respect to the surface normal. Photoelectrons are detected in a time-of-flight (TOF) spectrometer and are analyzed with respect to their kinetic energy (E_{kin}) (for details see Ref. [24]). During photoemission measurements the sample was kept at liquid nitrogen temperature.

The Au(1 1 1) surface was prepared by repeated cycles of argon sputtering (1.5 keV,5μA/cm^2) followed by annealing at 750 K. 8T molecules (Advanced Technology and Industrial Co., Ltd.) were first out-gassed in vacuum for several hours and then evaporated from an organic molecular beam effusion cell held at 510 K at a substrate temperature of 300 K.

3. Results and discussion

3.1. Sub-monolayer regime of α-octithiophene on Au(1 1 1)

STM images of the bare and α-octithiophene (8T) covered Au(1 1 1) surface are shown in Figure 1. The Au(1 1 1) surface is compressed in the direction due to the breaking of symmetry, resulting in the formation of a zigzag pattern well-known as "herringbone" reconstruction, which is clearly visible in Figure 1a [25]. Fcc and hcp packing region are separated by corrugation lines. Between two closer corrugation lines (separation ≈2.4 nm) hcp packing exists, whereas the wider distance area (≈3.9 nm) comprise fcc packing. After deposition of 8T at a substrate temperature of 300 K the molecules tend to diffuse toward the gold step edges and form closed molecular chains along the edges as can be seen in Figure 1c. From the line profile (Figure 1d) we infer that 8T molecules stabilize at the lower edge of the steps. A similar behavior has been observed for 6T/Au(1 1 1) [12,14]. Note that 8T deposition on the cold sample (80 K) also lead to localization of the molecules at the step edges, indicating a high mobility of 8T on the terraces.

Generally, steps (like other surface defects) act as preferential adsorption sites, as they represent perturbations in the surface periodicity and electronic structure. This can lead to positive or negative changes in the local adsorption energy. However, electronic effects such as the Smoluchowski effect [26] or local-density-of states (LDOS) modulation at steps [27–29] can also generate preferential adsorption at step edge. Thereby the LDOS is affected by perturbations due to adsorbates and by surface state electron scattering (Friedel oscillations). In the case 6T/Au(1 1 1) a weak chemical interaction (no charge transfer) between 6T and Au(1 1 1) has been assumed on the basis of photoelectron spectroscopy and quantum chemical calculation. It has been proposed that the preferential adsorption of 6T at the bottom of the edge is caused by changes in the LDOS [12]. For 8T on Au(1 1 1) we suppose similar effects due to the akin electronic and geometrical structure.

A second effect relevant in this context is the so-called Ehrlich-Schwöbel barrier, which is the energy required for an atom or molecule to descend a monolayer-height step edge in addition to that of the conventional (two-dimensional (2D)) surface diffusion barrier [30]. Large barriers suppress the downward flux of particles between the layers preventing a layer-by-layer growth (2D growth), and instead promoting (unwanted) three-dimensional growth. It turned out that this concept is very efficient in order to describe inorganic thin film growth; however in organic systems the situation is much more complex. In organic molecules the intrinsic anisotropy and internal degrees of freedom evoke a series of activation barriers for crossing steps that depend on the molecular conformation and on the orientation of the diffusing molecules [31–34]. In addition a layer-dependent step-edge barrier has been observed [35]. For instance the rodlike para-sexiphenyl which adsorbs on mica in an upright geometry an Ehrlich-Schwbel barrier of 0.67 eV has been determined [33]. However, in spite of a possible high barrier, it will be shown later in the contribution that a layer-by-layer growth occur at least up to the bilayer regime.

At higher coverage, as shown in Figure 2a, we find adsorption of 8T on top of the molecules previously trapped at the lower step edge; this behavior is corroborated by the line profile displayed in Figure 2b. Thereby the adsorption of 8T on top of the molecules is only observed until the bottoms of the steps are completely filled. At this coverage, we did not obtain any domains, ordered

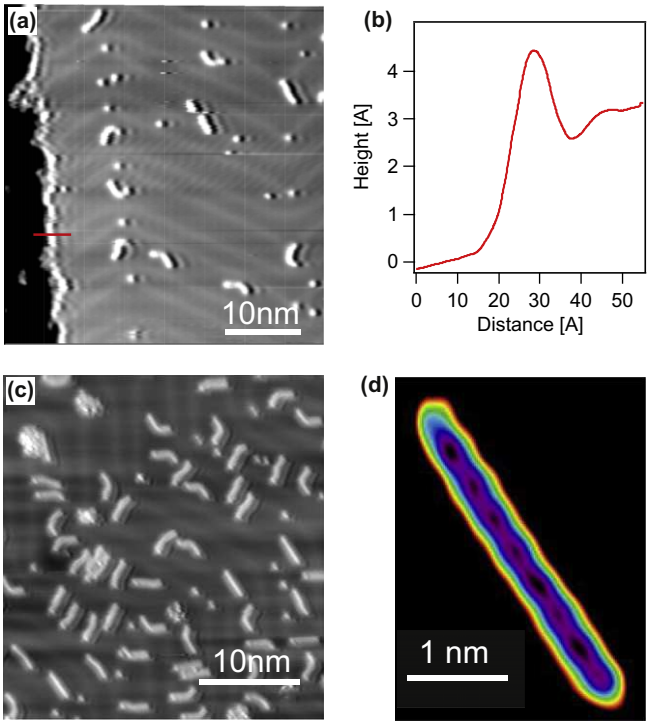

Figure 2. (a) Sub-monolayer 8T/Au(1 1 1) (V_s = 0.5 V; I_t = 51 pA), at which 8T adsorb on top of the molecules previously trapped at the lower step edge. In addition, molecules absorb mostly in bent configuration and stick only on fcc packing area. (b) Corresponding line profile as marked by the red line in (a). (c) Higher 8T-coverage in comparison to (a). Molecules tend to absorb more often in a straight configuration and a beginning of alignment can be seen. (d) Sub-molecular resolution STM image of a single molecule exhibiting eight features corresponding to the 8 thiophene rings within the molecule. (For interpretation of the references to colour in this figure legend, the reader is referred to the web version of this article.).

molecular clusters or even first fruits of self-organization on substrate terraces, but single molecules absorbed randomly in straight or bent configuration. In the linear 8T the thiophene repeating units are arranged in an all-trans-configuration. In the bended molecule, some thiophene rings are forced to rotate, i.e., a cis-configuration must be present in the folded chain. A similar bended molecular conformation has been observed for 6T/Au(1 1 1) [14]. From all images examined it was not possible to deduce any preferential absorption form. 8T molecules are dominantly localized at the fcc packing area of the Au(1 1 1) surface and tend to settle at kinks formed by the corrugation lines. Note that the smaller features seen in the STM-images are most probably thiophenes rings resulting either from an uncompleted purification of the 8T powder or from decomposition of the molecules during evaporation.

At a slightly higher coverage (Figure 2c), 8T molecules still absorb preferentially on the fcc packing area, however, due to a lack of space, they begin to also localize at hcp regions. Furthermore the molecules are predominantly found in a straight conformation but again no nucleation or island formation is observed. In contrast, repulsive intermolecular interactions seem to be operative preventing nucleation. Long-range substrate mediated interaction mechanisms between adsorbates due to (i) elastic deformation of the substrate [36], (ii) the oscillatory potential between molecules and metal surfaces associated with the Friedel oscillations of surface-state electrons [37] and (iii) Coulomb repulsion among localized charges built up at the molecule-surface interface by charge redistribution occurring upon chemisorption [38] have been proposed in order to explain the self-assembly of molecules and atoms on metal substrates. The 8T molecules adsorb on Au(1 1 1) surface without a long-range ordering, however the preferential linear arrangement of the conjugated chains may arise from a balance between a weak 8T/substrate interaction and a weak intermolecular repulsion. Further coverage and substrate-temperature dependent measurements are needed in order to elucidate the origin of the adsorption behavior of 8T on Au(1 1 1) in the low-coverage regime.

The 8T molecule in its straight conformation exhibits an average length of 30 ± 1 Å. This compares well with the previously reported dimension of 8T based on crystallographic data of single crystals [39] and STM measurements of 6T on Au(1 1 1) [12,13]. A closer approach to the molecule allows sub-molecular resolution of an 8T molecule (see Figure 2d) showing that the individual molecule exhibits a structure with 8 maxima which are related to the 8 thiophene rings within the molecule. We interpret the appearance of the regular 8 dark depressions in the center with a planar adsorption geometry in which 8T adsorbs on the Au(1 1 1) surface through the π-conjugated system.

3.2. Mono- and bilayer α-octithiophene on Au(1 1 1)

In the following we investigate the adsorption structure of 8T on Au(1 1 1) in the first and second monolayer (ML) which is important for the performance of electronic devices based on organic molecules. Figure 3a displays a representative STM image of 8T deposited at room temperature on Au(1 1 1) at an incomplete bilayer coverage. In both the mono- and the bilayer the molecules adsorb in a well-ordered structure in contrast to the submonolayer regime. The monolayer and the bilayer exhibit the same arrangement, in which the molecules align parallel to their long axis, forming arranged rows extending over a long distance on the gold terraces. Analyzing various STM images we conclude that the

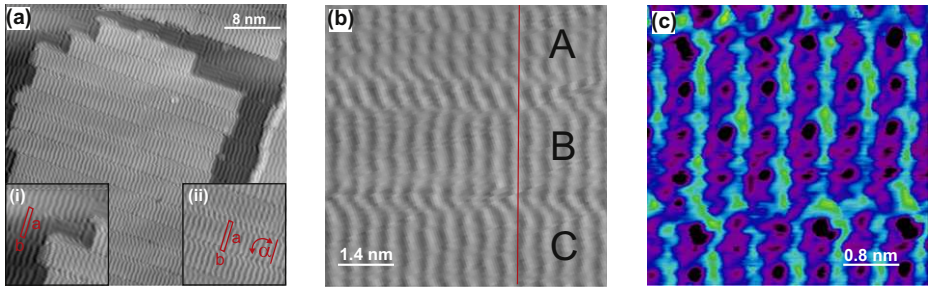

Figure 3. (a) STM image of a mono-and bilayer 8T/Au(1 1 1) (V_s = − 0.6 V, I_t = 50 pA) showing nicely aligned molecular rows. The herringbone reconstruction of the Au(1 1 1) surface is still slightly visible through the 8T bilayer. Inset: The cell parameters of the (i) monolayer and (ii) the bilayer calculated in averaging on 11 rows and 30 lines are the same for both coverages, namely a = 30.5 ± 0.5 Å, b = 5.8 ± 0.1 Å and α = 90°. (b) Row assembly: Rows A and B are in phase, while B and C are anti-phase. The red line is a guide to the eyes (V_s = − 0.6 V, I_t = 50 pA). (c) High resolution STM image of a monolayer 8T/Au(1 1 1) (V_s = 2 V, I_t = 200 pA). Bright features can be observed on the molecules, which are assigned to the sulfur and the appearance of only four of them confirms the tilted absorption of the molecules in the monolayer. Note that mono-and bilayer show the same structure. (For interpretation of the references to colour in this figure legend, the reader is referred to the web version of this article.).

alignment of the molecules between two rows is random (see Figure 3b) even though the STM image in Figure 3c suggests an antiphase alignment between adjacent rows. The cell parameters calculated by averaging 11 rows and 30 lines are $a = 30.5 \pm 0.5$ Å, $b = 5.8 \pm 0.1$ Å and $\alpha = 90°$ (see inset of Figure 3a) are the same for both coverages. The formation of well-ordered, densely packed rows with increasing 8T coverage indicates that at higher coverage attractive intermolecular interactions prevail in comparison to the sub-monolayer regime (see above). The rise of attractive forces may be associated with a molecular rearrangement from a flat to tilted adsorption geometry. This geometry allows for intermolecular π–π-interaction (π-stacking). By comparison, in the case of thiophene on Au(1 1 1) as well as on Ag(1 1 1) and Cu(1 1 1) it has been shown that the angle between the molecular plane and the surface increases with rising coverage, which has been attributed to intermolecular π–π-interaction [40]. Figure 3b shows an image of 8T in the monolayer measured with submolecular resolution. In spite of the fact that single 8T molecules exhibit 8 dark depressions in the center (see Figure 2d) only 4 are observed on the molecules in the monolayer. This reinforces the assumption of tilted molecules in the film.

Since the electronic properties of interfaces, *viz.* charge injection barriers have a huge impact on the performance of molecular based devices we studied the electronic structure of 8T in the mono- and bilayer regime using STS. Figure 4a shows STS data of the 8T/Au(1 1 1) recorded at a coverage of 1 and 2 ML, respectively. The dI/dV-spectrum of 1 ML taken at the center of 8T molecules shows double peak structure at positive sample bias with maxima at 2.0 and 2.4 V. We attribute these features to be arise from the 8T derived LUMO and LUMO + 1, respectively. At 2 ML 8T on Au(1 1 1) the energetic position of the unoccupied molecular electronic states with respect to the Fermi level are the same as for 1 ML, but the LUMO and LUMO + 1 peaks are nicely resolved. The separation of 0.4 eV between the two peaks fits well to the energy difference determined on a thin 8T film by using electronic HREELS [20]. At both 1 ML and 2 ML the narrow peaks and the constant energetic positions, i.e., surprisingly no decoupling effect due to the presents of the first molecular layer is found, observed in the STS data reveal that the adsorbate/substrate interaction and accordingly the electronic coupling between the 8T molecules and the metal surface is comparatively weak. The dI/dV spectrum of 1 ML does not exhibit any clear peak structure up to -1.0 V, a region where we would expect to observe the HOMO of 8T. However it is known that STS of occupied electronic states of small molecules adsorbed on a metal surface can be affected by the high LDOS of the metal at E_F. When applying a negative bias voltage between the sample and the STM-tip it is normally most likely to fill the empty states of the tip with electrons coming from occupied electronic states at E_F of the metal than from molecular orbitals (e.g., the HOMO) due to the large difference in LDOS.

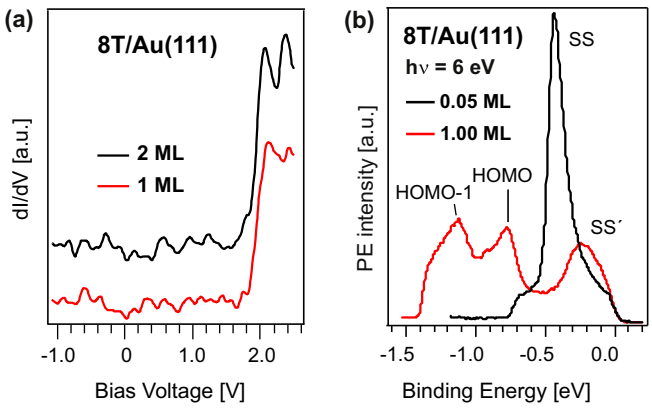

Figure 4. (a) dI/dV spectroscopic data taken at a monolayer and bilayer coverage of 8T on Au(1 1 1). (b) Photoemission data taken with 6 eV photons at a coverage of 0.05 and 1 ML 8T on Au(1 1 1).

Thus, in order to gain information about occupied electronic states of 8T on Au(1 1 1), we performed photoemission experiments using 6 eV photons. Figure 4b shows photoemission data of the 8T/Au(1 1 1) recorded at a coverage of 0.05 and 1.00 ML, respectively. The spectrum at 0.05 ML shows a sharp feature labeled as SS at a binding energy of −0.48 eV with respect to E_F, which is associated with the Shockley surface state [24]. At a coverage of 1 ML 8T/Au(1 1 1) the surface state is quenched and new features appear. The peak labeled SS' at a binding energy of −0.3 eV is the surface state of the adsorbate-covered Au(1 1 1) surface. Its binding energy and dispersion (not shown here) is consistent with results obtained from other adsorbate-covered Au surfaces [43,24]. In addition two peaks are observed at binding energies of −0.8 and −1.1 eV which we attribute to photoemission from the HOMO and HOMO-1, respectively. At a bilayer coverage we observe a slight shift of approximately 30 meV in the energetic positions of both occupied electronic states. Note that the adsorption of 8T molecules leads to a reduction of the work function as can be directly witnessed in the broadening of the spectra when going from 0.05 to 1 ML. Thereby it is possible to probe deeper below the Fermi level. With the LUMO located at 2.0 eV above E_F and the HOMO level at −0.8 eV with respect to E_F a HOMO–LUMO gap of 2.8 eV is obtained.

Comparing the electronic structure of 8T/Au(1 1 1) and 6T/Au(1 1 1), in both 6T and 8T the HOMO is located at −0.8 eV with respect to E_F. STS measurements on single 6T molecules [41] show the LUMO level at 2.0 V as for 8T/Au(1 1 1). This is surprising, since one would accept that the energy of the LUMO level should decrease with respect to the Fermi level with increasing chain length [20,21]. However the STS measurements on 6T/Au(1 1 1) were done on single molecules, in a molecular film the intermolecular interaction may lead to shifts in the energetic position of the molecular states, for instance a site-specific polarization of molecules has been demonstrated for tetracene adsorbed on Ag(1 1 1) [42]. Indeed, two-photon photoemission measurements revealed an energetic position of the LUMO at a coverage of 1 ML 6T of 2.1 eV above E_F [44]. Hence, at 1 ML coverage 6T/Au(1 1 1) and 8T/Au(1 1 1) possess a HOMO–LUMO gap of 2.9 and 2.8 eV, respectively, *viz.* the gap in 8T is smaller than in 6T, which is in agreement with the prediction [20,21].

4. Conclusion

In summary, scanning tunneling microscopy (STM) and spectroscopy (STS) as well as photoemission spectroscopy (PES), have been utilized in order to study the adsorption behavior and the electronic structure of α-octithiophene (8T) on Au(1 1 1) as a function of 8T coverage. At a submonolayer coverage 8T adsorbs preferentially at the step edges of the Au(1 1 1) surface. With increasing coverage 8T are also found on the terraces in a bended or linear configuration. Due to repulsive forces no nucleation or island formation are observed in this low-coverage regime. In contrast, for a monolayer (ML) well-ordered rows forming a closely packed film are found. The molecules are arranged in a tilted geometry with respect to the surface plane, which permits an intermolecular π–π-interaction. In the second layer the molecules adopt the same adsorption geometry as in the first layer. From STS measurements the energetic position of the lowest unoccupied molecular orbital (LUMO) and the LUMO + 1 have been determined. They are located at 2.0 and 2.4 eV with respect to the Fermi level of the Au(1 1 1) surface at a coverage of 1 ML. The energetic

positions of the electronic molecular states are the same in the second (decoupled) layer indicating that the adsorbate/substrate interaction and accordingly the electronic coupling are not strong. PES allowed to determine the energetic position of the highest occupied molecular orbital (HOMO) and HOMO-1, which are located at −0.8 and −1.1 eV with respect to the Fermi level, respectively. Thus a HOMO–LUMO gap of 2.8 eV is obtained.

Since 8T on Au(1 1 1) forms well-ordered, closed packed films with a defined interface further experiments, concerning the charge carrier and exciton dynamics, energetics and localization/delocalization at the interface between 8T and the Au(1 1 1) surface as well as within the 8T film using time- and angle-resolved two-photon photoemission spectroscopy, are in progress. These experiments gain important insights into elementary processes relevant for the performance of molecule-based optoelectronic devices.

Acknowledgments

Funding by the Deutsche Forschungsgemeinschaft (DFG) through the priority program SPP 1355 "Elementary Processes in Organic Photovoltaics" is gratefully acknowledged. We thank J.I. Pascual (Freie Universität Berlin) for very fruitful discussions and for providing us the Au(1 1 1) crystal.

References

[1] E. Umbach, M. Sokolowski, R. Fink, Appl. Phys. A: Mater. Sci. Process. 63 (1996) 565;
G. Witte, C. Wöll, J. Mater. Res. 19 (2004) 1889;
P. Leclere et al., Chem. Mater. 16 (2004) 4452;
J.R. Heath, Annu. Rev. Mater. Res. 39 (2009) 1.
[2] R.H. Friend et al., Nature 397 (1999) 121.
[3] C.D. Dimitrakopoulos, P.R.L. Malenfant, Adv. Mater. 14 (2002) 99.
[4] P. Peumans, S. Uchida, S.R. Forrest, Nature 425 (2003) 158.
[5] G. Horowitz, D. Fichou, X.Z. Peng, Z.G. Xu, F. Garnier, Solid State Commun. 72 (1989) 381.
[6] L. Torsi, A. Dodabalapur, L.J. Rothberg, A.W.P. Fung, H.E. Katz, Science 272 (1996) 1462.
[7] F. Garnier et al., J. Am. Chem. Soc 115 (1993) 8716.
[8] D.V. Lap, D. Grebner, S. Rentsch, J. Phys. Chem. A 101 (1997) 107.
[9] G. Gigli, O. Inganas, M. Anni, M. De Vittorio, R. Cingolani, G. Barbarella, L. Favaretto, Appl. Phys. Lett. 78 (2001) 1493.
[10] P. Liu, X. Wang, Y. Zhang, X. Zhou, W. Deng, Synth. Met. 155 (2005) 565.
[11] S. Prato et al., J. Chem. Phys. B 103 (1999) 7788.
[12] A.J. Mäkinen, J.P. Long, N.J. Watkins, Z.H. Kafafi, J. Phys. Chem. B 109 (2005) 5790.
[13] M. Kiel, K. Duncker, C. Hagendorf, W. Widdra, Phys. Rev. B 75 (2007) 195439.
[14] H. Glowatzki, S. Duhm, K.F. Braun, J.P. Rabe, N. Koch, Phys. Rev. B 76 (2007) 125425.
[15] K. Duncker, M. Kiel, A. Höfer, W. Widdra, Phys. Rev. B 77 (2008) 155423.
[16] G. Yoshikawa, M. Kigushi, S. Ikeda, K. Saiki, Surf. Sci. 559 (2004) 77.
[17] H. Inoue, G. Yoshikawa, K. Saiki, Jpn. J. Appl. Phys. 3A (2006) 1794.
[18] M. Kiguchi, S. Entani, K. Saiki, G. Yoshikawa, Appl. Phys. Lett. 84 (2004) 3444;
M. Kiguchi, G. Yoshikawa, S. Ikeda, K. Saiki, Surf. Sci. 603 (2004) 566.
[19] T. Yokoyama, S. Kurata, S. Tanaka, J. Phys. Chem. B 110 (2006) 18130.
[20] H.J. Egelhaaf, D. Oelkrug, D. Oeter, Ch. Ziegler, W. Göpel, J. Mol. Struc. 348 (1995) 405;
D. Oeter, H.J. Egelhaaf, Ch. Ziegler, D. Oelkrug, W. Göpel, J. Chem. Phys. 101 (1994) 6344.
[21] S.S. Zade, M. Bendikov, Org. Lett. 8 (2006) 5243.
[22] J. Ackermann, C. Videlot, A.E. Kassmi, R. Guglielmetti, F. Fages, Adv. Funct. Mater. 15 (2005) 810.
[23] G. Meyer, Rev. Sci. Instrum. 67 (1996) 2960.
[24] S. Hagen, Y. Luo, R. Haag, M. Wolf, P. Tegeder, New. J. Phys. 12 (2010) 125022.
[25] J.V. Barth, H. Brune, G. Ertl, R.J. Behm, Phys. Rev. B 42 (1990) 9307.
[26] R. Smoluchowski, Phys. Rev. 60 (1941) 661.
[27] E.C.H. Sykes, P. Han, S.A. Kandel, K.F. Kelly, G.S. Mccarty, P.S. Weiss, Acc. Chem. Res. 36 (2003) 945.
[28] M.F. Crommie, C.P. Lutz, D.M. Eigler, Nature 363 (1993) 524.
[29] Ph. Avouris, I.-W. Lyo, P. Molinas-Mata, Chem. Phys. Lett. 240 (1995) 423;
Ph. Avouris, I.-W. Lyo, Science 264 (1994) 942.
[30] R.L. Schwöbel, E.J. Shipsey, J. Appl. Phys. 37 (1966) 3682;
G. Ehrlich, F.G. Hudda, J. Chem. Phys. 44 (1966) 1039.
[31] F.- J. Meyer zu Heringdorf, M.C. Reuter, R.M. Tromp, Nature 412 (2001) 517;
L. Kilian, E. Umbach, M. Sokolowski, Surf. Sci. 573 (2004) 359.
[32] M. Fendrich, J. Krug, Phys. Rev. B 76 (2007) 121302. R.
[33] G. Hlawacek, P. Puschnig, P. Frank, A. Winkler, C. Ambrosch-Draxel, C. Teichert, Science 321 (2008) 108.
[34] J.E. Goose, E.L. First, P. Clency, Phys. Rev. B 81 (2010) 205310.
[35] X.N. Zhang, E. Barrena, D. Goswami, D.G. de Oteyza, C. Weis, H. Dosch, Phys. Rev. Lett. 103 (2009) 136101.
[36] H. Brune, M. Giovannini, K. Bromann, K. Kern, Nature 394 (1998) 451;
K. Pohl, M.C. Bartelt, J. de la Figuera, N.C. Bartelt, J. Hrbek, R.Q. Hwang, Nature 397 (1999) 238.
[37] S. Lukas, G. Witte, Ch. Wöll, Phys. Rev. Lett. 88 (2002) 028301.
[38] I. Fernandez-Torrente, S. Monturet, K.J. Franke, J. Fraxedas, N. Lorente, J.I. Pascual, Phys. Rev. Lett. 99 (2007) 176103.
[39] D. Fichou, B. Bachet, F. Demanze, I. Billy, G. Horowitz, F. Garnier, Adv. Mater. 8 (1996) 500.
[40] A. Nambu, H. Kondoh, I. Nakai, A. Kmemiya, T. Ohta, Surf. Sci. 530 (2003) 101;
P.K. Milligan, B. Murphy, D. Lennon, B.C.C. Cowie, M. Kadodwala, . J. Phys. Chem. B 105 (2001) 140;
J. Nara, S. Higai, Y. Morikawa, T. Ohno, Appl. Surf. Sci. 237 (2004) 433;
T. Matsuura, Y. Shimoyama, Eur. Phys. 7 (2002) 233;
X. Chen, E.R. Frank, R.J.J. Hamers, Vac. Sci. Technol. B 14 (1996) 1136;
G.J. Su, H.M. Zhang, L.J. Wan, C.L. Bai, Surf. Sci. 531 (2003) L363.
[41] F. Jäckel, U.G.E. Perera, V. Iancu, K.-F. Braun, N. Koch, J.P. Rabe, S.W. Hla, Phys. Rev. Lett. 100 (2006) 126102.
[42] S. Soubatch, C. Weiss, R. Temirov, F.S. Tautz, Phys. Rev. Lett. 102 (2009) 177405.
[43] F. Forster, A. Bendounan, F. Reinert, V.G. Grigoryan, M. Springborg, Surf. Sci. 601 (2007) 5595.
[44] E. Varene, I. Martin, P. Tegeder, J. Phys. Chem. Lett. 2 (2011) 252.

PCCP

View Online / Journal Homepage / Table of Contents for this issue
Dynamic Article Links

Cite this: *Phys. Chem. Chem. Phys.*, 2012, **14**, 691–696

www.rsc.org/pccp

PAPER

Coverage-dependent adsorption geometry of octithiophene on Au(111)

Erwan Varene,[a] Lea Bogner,[a] Stephan Meyer,[a] Yan Pennec[b] and Petra Tegeder*[a]

Received 9th September 2011, Accepted 26th October 2011
DOI: 10.1039/c1cp22875g

The adsorption behavior of α-octithiophene (8T) on the Au(111) surface as a function of 8T coverage has been studied with low-temperature scanning tunneling microscopy, high resolution electron energy loss spectroscopy as well as with angle-resolved two-photon photoemission and ultraviolet photoemission spectroscopy. In the sub-monolayer regime 8T adopts a flat-lying adsorption geometry. Upon reaching the monolayer coverage the orientation of 8T molecules changes towards a tilted configuration, with the long molecular axis parallel to the surface plane, facilitating attractive intermolecular π–π-interactions. The photoemission intensity from the highest occupied molecular orbitals (HOMO and HOMO − 1) possesses a strong dependence on the adsorption geometry due to the direction of the involved transition dipole moment for the respective photoemission process. The change in molecular orientation as a function of coverage in the first molecular layer mirrors the delicate balance between intermolecular and molecule/substrate interactions. Fine tuning of these interactions opens up the possibility to control the molecular structure and accordingly the desirable functionality.

1 Introduction

Organic molecules are promising candidates for applications in optoelectronic devices, for example in organic photovoltaic cells (OPVC),[1,2] organic light-emitting diodes (OLEDs)[1,3] or organic field effect transistors (OFETs).[3–5] Due to their semiconducting properties, oligothiophenes show a high potential for the above-mentioned applications. The variation of the chain length of these π-conjugated compounds allows us to tune their optical and electronic properties.[6–10] For instance, it has been shown by high resolution electron energy loss spectroscopy (HREELS) that the size of the gap between the highest occupied molecular orbital (HOMO) and the lowest unoccupied molecular orbital (LUMO) can be tuned by the number of thiophene rings.[11] So far, the longest unsubstituted α-oligothiophene that has been synthesized is the α-octithiophene (8T). It possesses the highest carrier mobility in the class of unsubstituted oligothiophenes.[12,13]

It is well-known that the properties of interfaces between active layers are crucial for the performance of optoelectronic devices. For oligothiophenes it has been shown that the orientation of the molecules is of particular importance[14] especially for the light emission/absorption and charge transport properties. Intermolecular interaction competes with molecule/substrate interaction both defining the adsorption geometry and the arrangement of the molecular film and accordingly the electronic structure of the system. For instance, α-sexithiophene (6T) has been found to form well-ordered films with molecules flat-lying on Au films while tilted by about 70° with respect to the surface plane on Ag and Cu films, respectively.[15] Since the quality and the properties of these interfaces are substantially dominated by the adsorption of the first molecular layer, it is important to gain detailed information on its geometry. Although the adsorption behavior of 6T on different metal surfaces has been intensively studied,[16–25] so far only two recent scanning tunneling microscopy (STM) studies investigated the adsorption of 8T on Cu(111)[26] and Au(111).[27] In the latter we analyzed the adsorption behavior ranging from single molecules to the first two layers of 8T on Au(111). Thereby, we proposed that the molecular adsorption geometry is changing from flat-lying 8T in the sub-monolayer regime to a tilted geometry in the first monolayer. However, no conclusive proof on the adsorption geometry of 8T/Au(111) on the basis of the STM results could be given.

In the present contribution we utilized complementary experimental techniques, namely STM, HREELS, as well as two-photon photoemission (2PPE) and ultraviolet photoemission spectroscopy (UPS) in order to obtain a comprehensive picture on the adsorption behavior of 8T on Au(111) as a function of 8T-coverage. We found that 8T adopts a planar (flat-lying) adsorption geometry in the low-coverage regime ($\ll$1 monolayer, ML), whereas for higher coverage ($\sim$1 ML) the molecules realign to a tilted configuration, with the long molecular axis parallel to the surface. This variation in geometry is accompanied by a change in the photoemission intensity from the HOMO and HOMO − 1 due to the modification in the direction of the transition dipole moment for photoionization.

[a] *Freie Universität Berlin, Fachbereich Physik, Arnimallee 14, 14195 Berlin, Germany. E-mail: petra.tegeder@physik.fu-berlin.de*
[b] *Department of Chemistry and Physics and Astronomy, University of British Columbia, Vancouver, B.C. V6T 1Z4, Canada*

2 Experimental section

All experiments were performed under ultrahigh vacuum (UHV) conditions (base pressure 10^{-10} mbar) using three different setups, each holding one of the complementary experimental techniques used in this experiment: scanning tunneling microscopy (STM), high resolution electron energy loss spectroscopy (HREELS), and two-photon photoemission (2PPE) spectroscopy.

The Au(111) surface was prepared by repeated cycles of Ar^+ sputtering (1.5 keV, 5 μA cm^{-2}) followed by annealing at 800 K. 8T molecules (Advanced Technology and Industrial Co., Ltd.) were first out-gassed in the vacuum for several hours and then evaporated from an organic molecular beam effusion cell held at 510 K at a substrate temperature of 300 K.

The STM (Createc based design) was operated typically at 15 K to obtain high-resolution topographic data. Topographic data were acquired in the constant current mode, with typical tunneling resistances in the range of 10–104 MΩ.

The HREEL spectra were recorded at a sample temperature of 100 K, in both specular ($\theta_i = \theta_r = 60°$) and off-specular ($\theta_i = 53°$; $\theta_r = 60°$) scattering geometries. The energy of the primary electrons was set to 3.5 eV, with an overall resolution around 3.1 meV measured as the full-width at half-maximum of the elastic peak. In specular scattering geometry, the spectral signal contains both dipole- and impact-scattering components. The selection rule for dipole-scattering at metal surfaces is the same as that for infrared reflection absorption spectroscopy. This means that only vibrations with a non-vanishing component of the dipole moment change normal to the metal surface are observable. Thus making HREELS ideal for characterizing the geometrical structure and predominant orientation of adsorbates. To distinguish between dipole- and impact-scattering components, off-specular spectra arising only from impact-scattering were obtained at an incident angle of 53° (corresponding to 7° off-specular), keeping the angle of the reflected beam unchanged.

For the 2PPE measurements a tunable femtosecond (fs) laser system, consisting of a Ti/sapphire oscillator in combination with a 300 kHz regenerative amplifier, was used. It supplies pulses with a central wavelength of 830 nm. Twice performed frequency doubling of the fundamental beam in β-barium borate (BBO) crystals yields pulses with a photon energy of 6 eV. Furthermore the output is used to pump an optical parametrical amplifier (OPA), which yields photons with a tunable energy in the range from 1.7 to 2.7 eV. Through frequency doubling in a BBO crystal, the photon energy range from 3.4 to 5.4 eV is achieved. After thorough temporal compression, pulses with a duration around 60 fs are obtained. These are focused onto the sample under an angle of 45° with respect to the surface normal. Photoelectrons are detected in a custom-built time-of-flight (TOF) spectrometer and are analyzed with respect to their kinetic energy (E_{kin}). The energy resolution of the TOF spectrometer depends on the kinetic energy of the electrons, it is 20 meV at $E_{kin} = 1$ eV (for details see ref. 28 and 29).

3 Results and discussion

We first studied the adsorption behavior of 8T in the sub- and monolayer regime with STM. It has been shown that in the sub-monolayer regime 8T molecules adsorb preferentially at the step edges and the fcc packing regions of the reconstructed Au(111) surface without forming ordered islands or exhibiting any other indication of self-assembly. The sub-molecular resolution STM image of a single molecule, as shown in Fig. 1(a), exhibits 8 regular maxima which are related to the 8 thiophene rings within the molecule.[27] In the monolayer regime 8T possesses a well-ordered and densely packed structure in which the molecules are aligned in rows parallel to each other's backbone as shown in Fig. 1(b). The formation of self-assembled layers with rising coverage implies the development of attractive intermolecular interactions in contrast to the sub-monolayer regime and may be related to a reorientation. The high resolution STM image of 1 ML 8T on Au(111) (Fig. 1(b)) shows only 4 dark depressions per molecule instead of the 8 observed for the single molecules. This observation may be attributed to a change in adsorption geometry from planar, flat-lying molecules in the sub-monolayer regime to a tilted configuration in the monolayer. The latter would allow for attractive intermolecular π–π-interaction (π-stacking). Note that the 8T bilayer exhibits the same structure as the ML.[27]

To gain a deeper insight into the adsorption properties of 8T on Au(111) as a function of coverage we performed angular dependent HREELS measurements (Fig. 2). The HREEL spectra shown in Fig. 2(a) and (b) are recorded in specular and off-specular geometry. For a sub-monolayer coverage (Fig. 2(a)), the specular spectrum is dominated by three very intense features, which can be assigned to out-of-plane vibrations, namely the ring deformation (γ(ring): 441 cm^{-1}) and to C–H deformation modes (γ(C–H): 674 cm^{-1}, 774 cm^{-1}), respectively. The vibrational frequencies and the assignments are listed in Table 1 together with the literature values of vibrational modes of condensed 8T.[30] In off-specular scattering geometry these features become very weak indicating that their intensities are predominantly originating from dipole-scattering. In-plane modes of 8T located in the energy range between 1000–1500 cm^{-1} in the infrared spectrum of condensed 8T[30] are not observed in HREELS, whereas the out-of-plane modes are strong. This leads to the clear indication that 8T adopts a planar geometry in the low-coverage regime.

When increasing the coverage towards one monolayer, the number of vibrational modes visible in the spectrum rises significantly, pointing towards a change in the molecular

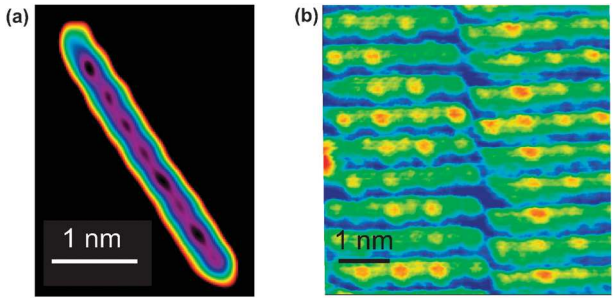

Fig. 1 (a) Sub-molecular resolution STM image of a single molecule exhibiting 8 features corresponding to the 8 thiophene rings within the molecule. (b) High resolution STM image of a monolayer 8T/Au(111) ($V_s = 2$ V, $I_t = 200$ pA). Four bright features can be observed on the molecules, which are assigned to the sulfur atoms (see text for details).

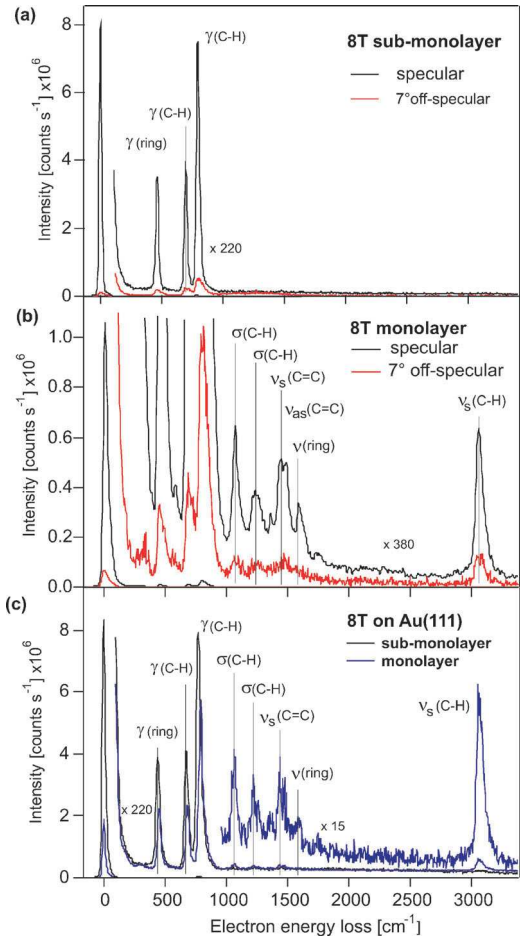

Fig. 2 HREEL spectra recorded with a primary electron energy of 3.5 eV of 8T/Au(111) as a function of coverage: (a) sub-monolayer and (b) monolayer 8T measured in specular and 7° off-specular scattering geometry. (c) Comparison between HREEL spectra for a sub-ML and 1 ML 8T recorded in specular scattering geometry.

Table 1 Vibrational frequencies (in cm^{-1}) and assignments for sub-ML and ML 8T adsorbed on Au(111), and for condensed 8T, respectively [ν: stretching; σ: in-plane bending; γ: out-of-plane bending; da indicates a strong dipole activity]

Assignment	Sub-ML	ML	Solid[30]
γ (ring)	441 (da)	449	455
γ (C–H)	674 (da)	682	687
γ (C–H)	774 (da)	794	790
σ (C–H)	—	1065 (da)	1047
σ (C–H)	—	1229 (da)	1222
ν_s (C=C)	—	1441 (da)	1424
ν_{as} (C=C)	—	1482 (da)	1491
ν (ring)	—	1582 (da)	1510
ν_s (C–H)	—	3075 (da)	3050

adsorption geometry (see Fig. 2(b)). In detail, the observation of dipole active in-plane modes in the energy region between 1000–1500 cm^{-1} such as the C=C symmetric and asymmetric stretch modes (ν_s(C=C): 1441 cm^{-1}; ν_{as}(C=C): 1482 cm^{-1}), the C–H bending mode (σ(C–H): 1065 and 1229 cm^{-1}), and the symmetrical stretch vibration of the C–H group (ν_s(C–H): 3057 cm^{-1}), demonstrates that the molecules are tilted with respect to the substrate. Fig. 2(c) represents a comparison between HREEL spectra recorded in specular scattering geometry for a sub-ML and a ML 8T. In addition to the presence of dipole active in-plane modes at a coverage of 1 ML, the out-of-plane modes at 441, 674, and 774 cm^{-1} lose intensity compared to the sub-ML spectrum, which also underline the coverage dependent reorientation. Thus from the vibrational analysis we conclude that 8T molecules change their adsorption geometry from flat-lying in the sub-ML regime to a tilted geometry when reaching a monolayer coverage.

Generally, the molecular adsorption structure is governed by the strength of adsorbate/substrate interaction, *viz.* the electronic coupling strength and adsorbate/adsorbate interaction. The formation of well-ordered, densely packed rows with increasing 8T coverage indicates that at higher coverage attractive intermolecular interactions prevail in comparison to the sub-monolayer regime. The rise of attractive forces is associated with a molecular rearrangement from a flat to a tilted adsorption geometry, allowing for intermolecular π–π-interaction (π-stacking). By comparison, in the case of thiophene on Au(111) as well as on Ag(111) and Cu(111) it has been shown that the angle between the molecular plane and the surface increases with rising coverage, which has been attributed to intermolecular π–π-interaction.[31] In contrast, α-sexithiophene (6T) on Au(111) adopts in both the sub-ML and monolayer regime a planar, flat-lying adsorption geometry.[18,19] The reason for the different adsorption behavior between 8T and 6T on Au(111) is not obvious since at least the electronic structure of both molecules on Au(111) is very similar.[27,32] However, this demonstrates that with fine balance between intermolecular interactions and molecule/substrate interactions the molecular structure can be varied, resulting in desirable functionalities.

The change in adsorption geometry as a function of 8T-coverage can also be observed by two-photon photoemission as will be shown in the following. Fig. 3(a) shows angular-dependent two-color 2PPE measurements recorded with 2.18 eV and 4.36 eV photons at 0.5 ML 8T/Au(111). At this coverage the molecules are still flat-lying. Two dominant features are observed and on the basis of photon energy dependent measurement (data not shown here), we can assign them to occupied or unoccupied electronic states. The broad feature around $E_{Final} - E_F = 6.12$ eV contains contribution of the Shockley surface state (SS) located at −0.42 eV with respect to E_F and the $n = 1$ image potential state (IPS) at 0.6 eV below the vacuum level (corresponding to 3.98 eV above E_F).[28] Note that both states show a dispersion. The peak at $E_{Final} - E_F = 5.78$ eV is an occupied state located at −0.78 eV, which we attribute to photoemission from the HOMO of 8T.[27] When turning the sample toward negative angles (see Fig. 4(a)) the electric field of the incoming p-polarized light becomes more perpendicular to the molecular backbone of the flat-lying 8T, and obviously the photoemission intensity from the HOMO increases. It has been shown that the photoemission yield (I) from a respective state can depend on the angle of incidence of the laser pulses. Thus, I should be proportional to the square of the projection of the electromagnetic field vector $\mathbf{E}_{light}$ onto the transition dipole moment for photoionization μ_{ion}: $I \propto |\mathbf{E}_{light}.\mu_{ion}|^2$.[33] This reveals that the transition dipole moment for the photoemission from the

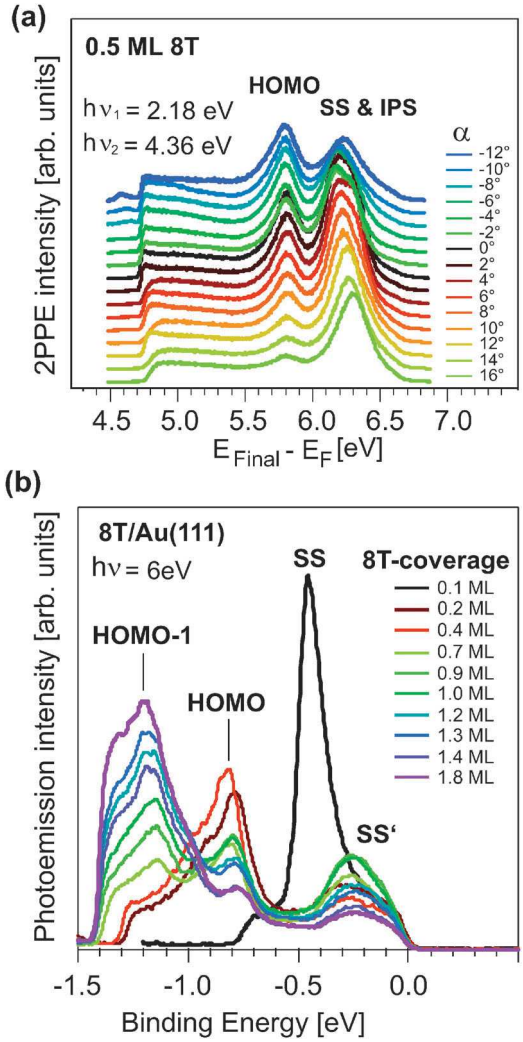

Fig. 3 (a) Angular-dependent two-color 2PPE measurements of 0.5 ML 8T/Au(111) measured with 2.18 eV and 4.36 eV photons. An increase of the photoemission intensity from the HOMO is observed when turning the sample from positive to negative angles (see text). (b) Direct photoemission spectra recorded with a photon energy of 6 eV at various 8T coverages.

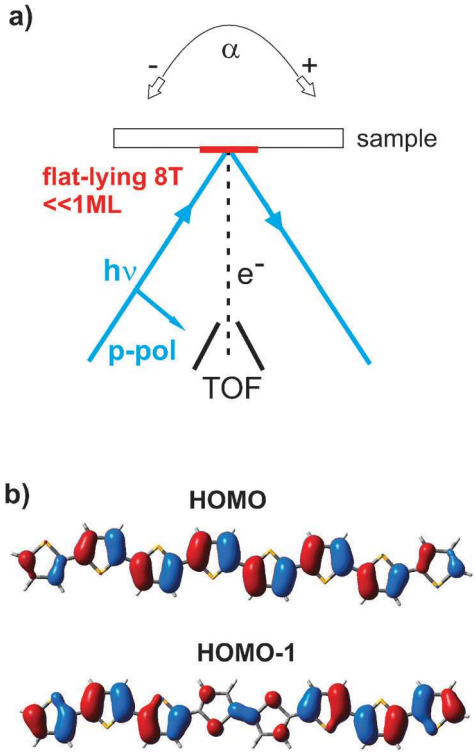

Fig. 4 (a) Scheme of the experimental setup for angle-resolved 2PPE measurements. For coverages below 1 ML 8T adopts a flat-lying adsorption geometry. (b) Calculated HOMO and HOMO − 1 of a free standing 8T molecule using density functional theory (DFT). DFT calculations have been performed utilizing the hybrid functional M06[36] and the Dunning–Huzinaga basis set cc-pVDZ[37] implemented in the Gaussian09[38] program package. For visualization of the MOs GaussView5[39] has been employed.

HOMO is oriented nearly perpendicular to the molecular backbone.

Fig. 4(b) displays a set of UPS spectra taken with 6 eV photons at various 8T coverages. The spectrum at 0.05 ML shows a sharp feature labeled as SS at a binding energy of −0.48 eV with respect to E_F, which is associated with the Shockley surface state.[28] At higher coverages SS is quenched and new features appear. The peak labeled SS′ at a binding energy of −0.3 eV is the surface state of the adsorbate-covered Au(111) surface. Its binding energy and dispersion (not shown here) is consistent with results obtained from other adsorbate-covered Au surfaces.[28] In addition two peaks are observed at binding energies of −0.8 and −1.1 eV which we attribute to photoemission from the HOMO and HOMO − 1, respectively. Most striking is the opposed behavior of the photoemission intensity arising from the HOMO and HOMO − 1 when increasing the amount of molecules. The photoemission intensity from the HOMO decreases while it increases for the HOMO − 1 with rising coverage. As demonstrated above, when increasing the coverage toward the monolayer regime the adsorption geometry of 8T on Au(111) changes from flat-lying to a tilted configuration. Thus, the angle between the incoming p-polarized laser beam and the molecular plane increases and I_{HOMO} decreases. In contrast, the increase of I_{HOMO-1} shows that the photoionization transition dipole moment of the HOMO − 1 lies parallel to the molecular backbone.

To corroborate our interpretation we applied symmetry selection rules (Laporte selection rule (*i.e.* a dipole transition is only allowed when the initial and final state have opposite parity) for planar all-*trans* conjugated 8T with C_{2h} symmetry[34]). The HOMO and HOMO − 1 can be assigned to molecular orbitals with B_g and A_u symmetries, respectively (see Fig. 4(b)). In the low coverage regime where the 8T molecules lie flat on the surface, normal emission is allowed for the HOMO but forbidden for the HOMO − 1, which does support our data. In the case of the higher coverage regime where the molecular plane is now tilted relative to the substrate plane, as well as to the detector, transition from the HOMO − 1 is not forbidden anymore and emission from the HOMO can still occur, however with a lower probability (see Fig. 4(a)). A further increase of the photoemission intensity from the HOMO − 1 for coverages above 1 ML may be attributed to a higher number of molecules present on the surface.

Note that also final state effects influence the photoemission intensities.[35]

Finally, it can be seen in Fig. 3(b) that with increasing coverage the HOMO shifts by 40 meV toward lower binding energies, while the HOMO − 1 shifts by 70 meV to a higher binding energy. To explain these effects we have to look at the Kohn–Sham orbitals shown in Fig. 4(b), which are calculated at the M06/cc-pVDZ level[36,37] using Gaussian09.[38] The HOMO appears to be located along the π-bonds in the plane of the molecule, thus the electronic coupling of this state is stronger in the sub-monolayer regime when the 8T molecules lie flat on the surface and decreases with rising coverage since the 8T molecules change their adsorption geometry. In contrast, the HOMO − 1 is partially located at the sulfur atoms. This leads to a stronger electronic coupling in the tilted molecular configuration due to the thiophilicity of the Au surface.

4 Conclusions

In summary, the adsorption behavior of α-octithiophene (8T) on Au(111) as a function of coverage ranging from the sub-monolayer to monolayer regime has been analyzed with scanning tunneling microscopy (STM) and high resolution electron energy loss spectroscopy (HREELS). At a sub-monolayer coverage 8T molecules adsorb in a flat-lying adsorption geometry. Upon reaching the monolayer (ML) coverage the molecules realign forming a well-ordered film with the molecules tilted with respect to the surface plane. This geometry permits attractive intermolecular π–π-interaction. The change in the adsorption geometry with increasing coverage has also been followed in photoemission experiments, namely ultraviolet photoemission spectroscopy (UPS) and angle-resolved two-photon photoemission (2PPE). The photoemission intensity from the HOMO and HOMO − 1, which are located at −0.8 and −1.1 eV with respect to the Fermi level, exhibited a strong dependence on the adsorption geometry due to the direction of the involved transition dipole moment for the respective photoemission process. In addition the energetic position of both the HOMO and HOMO − 1 shifted as the molecular orientation with respect to the surface changed. This effect has been explained by the different electronic coupling of the particular electronic state with the gold substrate.

Due to the change in the adsorption geometry as a function of 8T coverage, it is very interesting to gain insights into charge carrier dynamics at the interface between 8T and Au(111) as a function of the molecular orientation. The dynamics of charge carriers are of particular relevance for the performance of molecule-based optoelectronic devices.

Acknowledgements

Funding by the Deutsche Forschungsgemeinschaft (DFG) through the priority program SPP 1355 and the collaborative research center SFB 658 is gratefully acknowledged.

References

1 Y. Shirota and H. Kageyama, *Chem. Rev.*, 2007, **107**, 953.
2 P. Peumans, A. Yakimov and S. R. Forrest, *J. Appl. Phys.*, 2003, **93**, 3693.
3 E. Menard, M. A. Meitl, Y. Sun, J. U. Park, D. J. L. Shir, Y. S. Nam, S. Jeon and J. A. Rogers, *Chem. Rev.*, 2007, **107**, 1117.
4 C. D. Dimitrakopoulos and P. R. L. Malefant, *Adv. Mater.*, 2002, **14**, 99.
5 C. Reese and Z. Bao, *Mater. Today (Oxford, UK)*, 2007, **10**, 20.
6 D. Fichou, *J. Mater. Chem.*, 2000, **10**, 571.
7 X. Yang, L. Wang, C. Wang, W. Long and Z. Shuai, *Chem. Mater.*, 2008, **20**, 3205.
8 G. Horowitz, R. Hajlaoui, D. Fichou and A. E. Kassmi, *J. Appl. Phys.*, 1999, **85**, 3202.
9 R. Yamada, H. Kumazawa, T. Noutoshi, S. Tanaka and H. Tada, *Nano Lett.*, 2008, **8**, 1237.
10 B. Q. Xu, X. L. Li, X. Y. Xiao, H. Sakaguchi and N. J. Tao, *Nano Lett.*, 2005, **5**, 1491.
11 H. J. Egelhaaf, D. Oelkrug, D. Oeter, Ch. Ziegler and W. Göpel, *J. Mol. Struct.*, 1995, **348**, 405; D. Oeter, H. J. Egelhaaf, Ch. Ziegler, D. Oelkrug and W. Göpel, *J. Chem. Phys.*, 1994, **101**, 6344.
12 S. Nagamatsu, K. Kaneto, R. Azumi, M. Matsumoto, Y. Yoshida and K. Yase, *J. Phys. Chem. B*, 2005, **109**, 9374.
13 R. Bourguiga, M. Mahdouani, S. Mansouri and G. Horowitz, *Eur. Phys. J.: Appl. Phys.*, 2007, **39**, 7.
14 G. Koller, S. Berkebile, J. Ivanco, F. Netzer and M. Ramsey, *Surf. Sci.*, 2007, **601**, 5683.
15 T. Okajima, S. Narioka, S. Tanimura, K. Hamano, T. Kurata, Y. Uehara, T. Araki, H. Ishii, Y. Ouchi, K. Seki, T. Ogama and H. Koezuka, *J. Electron Spectrosc. Relat. Phenom.*, 1996, **78**, 379.
16 S. Prato, L. Floreano, D. Cvetko, V. De Renzi, A. Morgante, S. Modesti, F. Biscarini, R. Tamboni and C. Taliani, *J. Phys. Chem. B*, 1999, **103**, 7788.
17 A. J. Mäkinen, J. P. Long, N. J. Watkins and Z. H. Kafafi, *J. Phys. Chem. B*, 2005, **109**, 5790.
18 M. Kiel, K. Duncker, C. Hagendorf and W. Widdra, *Phys. Rev. B: Condens. Matter*, 2007, **75**, 195439.
19 H. Glowatzki, S. Duhm, K.-F. Braun, J. P. Rabe and N. Koch, *Phys. Rev. B: Condens. Matter*, 2007, **76**, 125425.
20 K. Duncker, M. Kiel, A. Höfer and W. Widdra, *Phys. Rev. B: Condens. Matter*, 2008, **77**, 155423.
21 G. Yoshikawa, M. Kigushi, S. Ikeda and K. Saiki, *Surf. Sci.*, 2004, **559**, 77.
22 H. Inoue, G. Yoshikawa and K. Saiki, *Jpn. J. Appl. Phys.*, 2006, **3A**, 1794.
23 M. Kiguchi, S. Entani, K. Saiki and G. Yoshikawa, *Appl. Phys. Lett.*, 2004, **84**, 3444; M. Kiguchi, G. Yoshikawa, S. Ikeda and K. Saiki, *Surf. Sci.*, 2004, **566–568**, 603.
24 A. Höfer, K. Duncker, M. Kiel, S. Wedekind and W. Widdra, *Phys. Rev. B: Condens. Matter*, 2011, **83**, 075414.
25 T. Wagner, D. R. Fritz and P. Zeppenfeld, *Synth. Met.*, 2011, **161**, 2006.
26 T. Kakudate, S. Tsukamoto, N. Nakaya and T. Nakayama, *Surf. Sci.*, 2011, **605**, 1021.
27 E. Varene, Y. Pennec and P. Tegeder, *Chem. Phys. Lett.*, 2011, **515**, 141.
28 S. Hagen, Y. Luo, R. Haag, M. Wolf and P. Tegeder, *New J. Phys.*, 2010, **12**, 125022.
29 S. Hagen, P. Kate, M. V. Peters, S. Hecht, M. Wolf and P. Tegeder, *Appl. Phys. A: Mater. Sci. Process.*, 2008, **93**, 253.
30 G. Louarn, J. P. Buisson and S. Lefrant, *J. Phys. Chem.*, 1995, **99**, 11399.
31 A. Nambu, H. Kondoh, I. Nakai, A. Kmemiya and T. Ohta, *Surf. Sci.*, 2003, **530**, 101; P. K. Milligan, B. Murphy, D. Lennon, B. C. C. Cowie and M. Kadodwala, *J. Phys. Chem. B*, 2001, **105**, 140; J. Nara, S. Higai, Y. Morikawa and T. Ohno, *Appl. Surf. Sci.*, 2004, **237**, 433; T. Matsuura and Y. Shimoyama, *Eur. Phys. J.*, 2002, **7**, 233; X. Chen, E. R. Frank and R. J. J. Hamers, *J. Vac. Sci. Technol., B*, 1996, **14**, 1136; G. J. Su, H. M. Zhang, L. J. Wan and C. L. Bai, *Surf. Sci.*, 2003, **531**, L363.
32 E. Varene, I. Martin and P. Tegeder, *J. Phys. Chem. Lett.*, 2011, **2**, 252.
33 L. Gundlach, J. Szarko, L. D. Socaciu-Siebert, A. Neubauer, R. Ernstorfer and F. Willig, *Phys. Rev. B: Condens. Matter*, 2007, **75**, 125320.
34 O. Laporte and W. F. Meggers, *J. Opt. Soc. Am.*, 1925, **11**, 459.
35 R. L. Kurtz, D. A. Browne and G. J. Mankey, *J. Phys.: Condens. Matter*, 2007, **19**, 355001.

36 Y. Zhao and D. G. Truhlar, *Theor. Chem. Acc.*, 2008, **120**, 215.
37 T. H. Dunning Jr., *J. Chem. Phys.*, 1989, **90**, 1007.
38 M. J. Frisch, G. W. Trucks, H. B. Schlegel, G. E. Scuseria, M. A. Robb, J. R. Cheeseman, J. A. Montgomery Jr., T. Vreven, K. N. Kudin, J. C. Burant, J. M. Millam, S. S. Iyengar, J. Tomasi, V. Barone, B. Mennucci, M. Cossi, G. Scalmani, N. Rega, G. A. Petersson, H. Nakatsuji, M. Hada, M. Ehara, K. Toyota, R. Fukuda, J. Hasegawa, M. Ishida, T. Nakajima, Y. Honda, O. Kitao, H. Nakai, M. Klene, X. Li, J. E. Knox, H. P. Hratchian, J. B. Cross, C. Adamo, J. Jaramillo, R. Gomperts, R. E. Stratmann, O. Yazyev, A. J. Austin, R. Cammi, C. Pomelli, J. W. Ochterski, P. Y. Ayala, K. Morokuma, G. A. Voth, P. Salvador, J. J. Dannenberg, V. G. Zakrzewski, S. Dapprich, A. D. Daniels, M. C. Strain, O. Farkas, D. K. Malick, A. D. Rabuck, K. Raghavachari, J. B. Foresman, J. V. Ortiz, Q. Cui, A. G. Baboul, S. Clifford, J. Cioslowski, B. B. Stefanov, G. Liu, A. Liashenko, P. Piskorz, I. Komaromi, R. L. Martin, D. J. Fox, T. Keith, M. A. Al-Laham, C. Y. Peng, A. Nanayakkara, M. Challacombe, P. M. W. Gill, B. Johnson, W. Chen, M. W. Wong, C. Gonzalez and J. A. Pople, *Gaussian 03, revision C.02*, Gaussian, Inc., Wallingford, CT, 2004.
39 R. Dennington and T. K. J. Millam, *GaussView Version 5*, Semichem Inc., Shawnee Mission, KS, 2009.

Appl Phys A (2012) 106:803–806
DOI 10.1007/s00339-012-6766-0

Applied Physics A
Materials Science & Processing

Dynamics of optically excited electrons in the conducting polymer PEDT:PSS

Erwan Varene · Petra Tegeder

Received: 27 September 2011 / Accepted: 2 January 2012 / Published online: 21 January 2012

Abstract Femtosecond time-resolved two-photon photoemission spectroscopy is employed to study the dynamics of the non-equilibrium electron distribution in the conducting polymer poly(3,4-ethylene-dioxythiophene): poly(styrenesulfonate) (PEDT:PSS) film following optical excitation at 2.1 eV. We found that the electron thermalization occurs on a ultrafast timescale of around 60 fs analogous to the relaxation times of optically excited electrons in Au(111).

1 Introduction

π-Conjugated polymers are promising as low-cost and easily processable alternatives to inorganic semiconductors or metals in electronic applications. Utilizing intrinsic conducting polymers (ICP) as electrodes and hole injection layers in optoelectronic devices based on organic materials is thereby a key for a successful implementation of organic electronics. One of the prototypical ICP is poly(3,4-ethylene-dioxythiophene):poly(styrene-sulfonate) (PEDT:PSS; see Fig. 1), which has been used for instance for the fabrication of very efficient organic light emitting diodes (OLED) [1, 2] and field-effect transistors [3, 4]. In PEDT, double bonds are alternating with single bonds along the polymer chain. Thereby the unhybridized p_z-orbital of one carbon atom overlaps with the p_z-orbital of the neighboring carbon atom to form a π-bond, in which the electrons are weakly bound and therefore are relatively delocalized. However, due to the different bond length of the single and double bond, the Peierls instability splits this band into two sub-bands, the completely filled valence band and an empty conduction band, separated by an energy gap. Hence the material is a semiconductor, but through doping with PSS the polymer becomes conductive. It has been shown that charge carriers created after absorption of light in π-conjugated polymer are polarons [5]. The strong electron–phonon coupling of these quasi-particles gives rise to new energy states in the band-gap, thus the polymer absorbs in the IR region and is transparent [6]. Moreover, varying the ratio of PEDT:PSS induces changes in the micromorphology which facilitate adjustment of the overall conductivity of thin films [7]. In OLEDs PEDT:PSS is one of the most frequently used anode material due to its high work function and accordingly the low hole injection barrier. It has been shown that the work function possesses values between 5.0 and 5.6 eV, which was mainly attributed to the amount of residual water in thin films [8]. Thus the work function (Φ) can be much higher than the values known for atomically clean gold surfaces (e.g., $\Phi(\mathrm{Au}(111)) = 5.4$ eV [9]).

It is known that the charge transport in this class of polymers is dominated by disorder leading to charge localization that is dominant at all practical temperatures, i.e. temperatures where no damage of the material occurs. In this material, polarons are formed in less ordered regions of the doped polymers [10]. Interacting with phonons, charge carriers hop from localized sites to another. Upon transport, the charge carriers can either transfer their energy to the lattice by exciting phonons or radiative recombination gives rise to photoluminescence.

The dynamics of electronic excitations in organic molecules or polymers with potential application in optoelectronic devices plays an important rule. Up to now the dynamics of electrons in PEDT:PSS has only been studied by

E. Varene · P. Tegeder (✉)
Fachbereich Physik, Freie Universität Berlin, Arnimallee 14, 14195 Berlin, Germany
e-mail: tegeder@physik.fu-berlin.de
Fax: +49-30-83856059

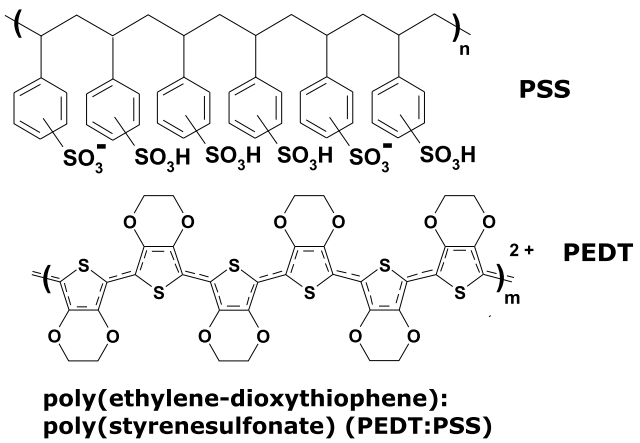

Fig. 1 Chemical structure of the conducting polymer mixture PEDT:PSS

infrared-induced transient adsorption in the sub-picosecond time-domain [11]. Femtosecond (fs) time-resolved two-photon photoemission (2PPE) spectroscopy has been used to study electron thermalization in various metals, metallic films and semiconductors [12–19] but interestingly so far this technique has not been utilized to investigate the dynamic behavior of charge carriers in conducting polymer films. In metals, light is adsorbed near the surface within the optical penetration depth of typically 10–20 nm. This leads to the creation of free charge carriers, which relax predominantly by electron–electron (e–e)-scattering on a femtosecond timescale. Subsequent energy transfer to the lattice by electron–phonon (e–ph)-scattering occurs on a picosecond timescale. In addition, the nascent carrier distribution is also depleted by transport of excited carriers into the bulk. An important difference between metal and polymer films is the penetration depth of light. For the polymer films the cross section for photon absorption is not very high. Moreover, the charge carrier density in PEDT:PSS is in the order of 10^{20} cm^{-3} [20], while in metals it is around 10^{22} cm^{-3}.

In this contribution we investigate the relaxation dynamics of photoexcited electrons in PEDT:PSS and Au(111) in the fs time domain using 2PPE. The comparison of the charge carrier dynamics between these two classes of materials is motivated by the potential use of PEDT:PSS as an electrode material instead of metals in optoelectronic applications. For the polymer we observed electron relaxation times in the order of 60 fs, akin to the timescale determined for Au(111).

2 Experimental

The present experimental setup combines a tunable femtosecond laser system with an ultrahigh vacuum chamber for two-photon photoemission (2PPE) spectroscopy.

For the 2PPE measurements, femtosecond laser pulses are generated by a 300 kHz Ti:Sapphire laser system, which pumps an optical parametric amplifier (OPA). The OPA delivers pulses with a tunable photon energy between 1.7 and 2.7 eV output. These pulses can be frequency-doubled in a BBO crystal to generate ultraviolet pulses (3.4–5.4 eV photon energy). After a thorough temporal compression pulses with a duration of about 60 fs are obtained. The laser pulses are incident on the surface with an angle of 45° with respect to the surface normal. While the pump pulse $h\nu_1$ excites an electron from below the Fermi level (E_F) to intermediate unoccupied states at energies $E - E_F = E_{\mathrm{kin}} + \Phi - h\nu_2$ (with Φ the work function), the probe pulse $h\nu_2$ photoionizes the sample by lifting the excited electron above the vacuum level (E_{vac}). Photoelectrons are detected in a custom-built time-of-flight spectrometer and are analyzed with respect to their kinetic energy (E_{kin}) (for details see [21]).

The commercial PEDT:PSS dispersion with a PEDT:PSS ratio of 1:6 (Baytron® P AI4083) was used. Thin films were prepared by spin casting the dispersion on freshly cleaned and UV/ozone-treated (for 30 min) indium tin oxide (ITO; on glass) substrate in ambient. After heating the sample at approximately 200°C for 5 min it was transferred into the ultrahigh vacuum system for the time-resolved photoemission experiments.

3 Results and discussion

To gain insight into the dynamics of photoexcited hot electrons after excitation of a PEDT:PSS film with short laser pulses, fs time-resolved 2PPE has been used. In Fig. 2, a two-dimensional false color representation of the photoemission intensity of PEDT:PSS recorded with photon energies of $h\nu_1 = 2.1$ eV for the visible and $h\nu_2 = 4.2$ eV for the UV laser pulses represents the electron distribution as a function of both time delay (horizontal axis) and energy (vertical axis). The spectrum is displayed as a function of final state energy above the Fermi level, $E_{\mathrm{Final}} - E_F = E_{\mathrm{kin}} + \Phi$, thus the energy of the secondary edge corresponds to the work function of PEDT:PSS which is 5.1 eV. Depending on the sequence of laser pulses (or formally the sign of the pump-probe delay), the dynamics are probed either near E_F or at higher intermediate state energies. Negative delays correspond to populating intermediate electronic states with UV light pulses ($h\nu_2$), while the visible pulses ($h\nu_1$) subsequently probe the excited electron distribution. On the other hand, for positive delays the electrons are excited to intermediate states close to the Fermi level (hot electrons) with the visible pulses ($h\nu_1$) and are subsequently probed by the UV pulses ($h\nu_2$). Analyzing the two-dimensional data set by extraction of the time-dependent 2PPE photoelectron yield integrated over the energy intervals centered on the state of

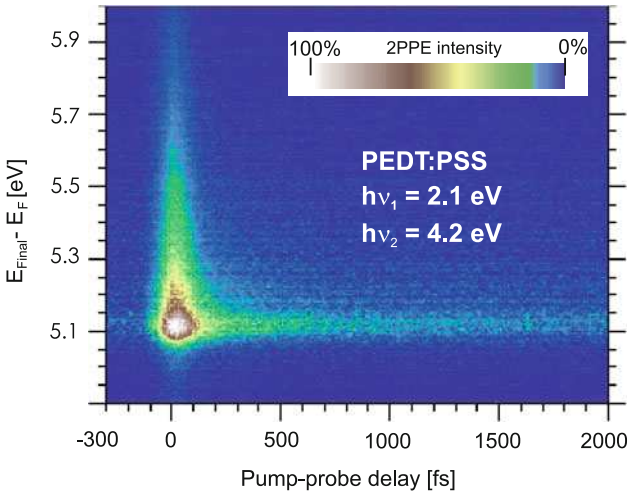

Fig. 2 2PPE intensity (*color map*) as a function of pump-probe delay (*horizontal axis*) and final state energy above the Fermi level (E_F) (*vertical axis*) from PEDT:PSS recorded with photon energies of $h\nu_1 = 2.1$ eV for the visible and $h\nu_1 = 4.2$ eV for the UV laser pulses. The excited electron distribution is probed with $h\nu_1$ at negative delays, while at positive delays it is probed with $h\nu_2$

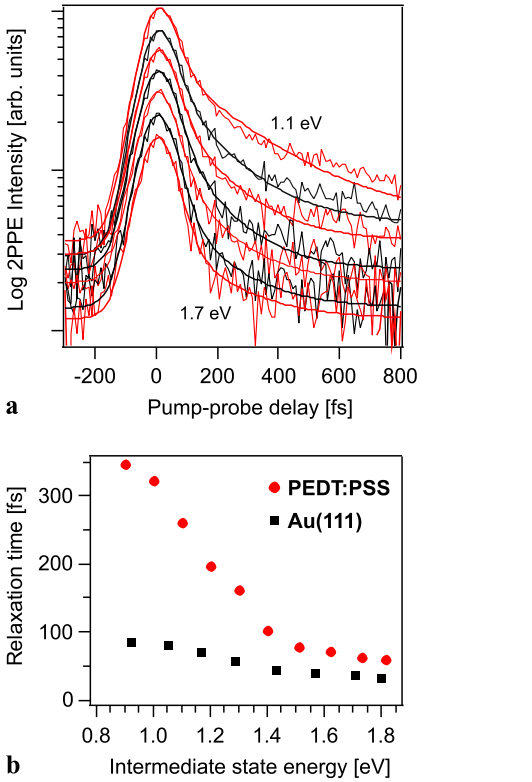

Fig. 3 (**a**) Cross correlation curves for PEDT:PSS recorded at intermediate state energies $E - E_F$ between 1.1 and 1.7 eV. (**b**) Relaxation times of the photoexcited electron distribution for PEDT:PSS and Au(111)

interest, i.e., hot electron distribution, provides the temporal evolution of the electron population, referred to as cross correlation traces as shown in Fig. 3(a). The cross correlation curves are recorded at intermediate state energies $E - E_F$ between 0.9 and 1.8 eV.

In general, several processes contribute to the observed population decay in 2PPE. Relaxation out of a given energy interval above $E - E_F$ is affected by electron–electron (e–e) scattering, electron–phonon (e–ph) or electron–defect scattering and by transport out of the detection volume. The rate of e–e scattering (i.e., the inverse inelastic lifetime) is given by a screened Coulomb interaction and the available phase space depending on the energy above the Fermi level [22]. However generation of secondary electrons by Auger decay of electrons and holes may also increase the population in particular in energy intervals close to E_F. Therefore the measured relaxation times cannot be simply identified with electron lifetimes at least for energies close to E_F.

The relaxation times are determined by fitting the cross correlation curves with a convolution of the pump probe cross correlation with a single exponential decay. For energies above 1.2 eV the fit describes the data well. For lower energies the electron population is more and more dominated by refilling processes with secondary electrons. The relaxation times as a function of intermediate state energy ($E - E_F$) are displayed in Fig. 3(b) together with the corresponding values for Au(111). We would like to indicate two main points: (i) The lifetime, and hence the inelastic mean free path, is strongly energy-dependent. The curve shows a clear increase in relaxation time as E_F is approached. This faster relaxation for higher energies above $E - E_F$ is due to availability of more phase space (see above). (ii) The comparison with Au(111) shows that for intermediate state energies above approximately 1.5 eV the relaxation times for PEDT:PSS and Au are very similar. The relaxation time for PEDT:PSS is less than a factor 2 higher. For metals, the e–e interaction is efficiently reduced by screening, which attenuates Coulomb interactions. For PEDT:PSS, despite a lower charge carrier density, the screening of carrier–carrier Coulomb interaction seems also efficient. Moreover, due to the polaronic nature of the charge carriers in the polymer, electron–phonon interaction is much more efficient than in the case of a metal, leading to comparable relaxation times in the two materials. For intermediate state energies below 1.5 eV the relaxation times in both materials differ significantly; in PEDT:PSS the electrons exhibit much longer lifetimes. We attribute this to refilling effects, viz. the creation of secondary electrons by decay of excited electrons into lower energetic states (cascade electrons) and Auger electrons. Furthermore, polaronic hopping to neighboring weakly localized states reduces the probability of radiative recombination by meeting a polaron of the opposite charge at low carrier excitation density. Note that the small slope change in the relaxation time of electrons in Au(111) around 1.5 eV has been associated with photoexcitation of d-electrons as for copper [15].

Acknowledgements This work has been supported by the Deutsche Forschungsgemeinschaft through the SPP1355. We thank Norbert Koch and Johannes Frisch (Humboldt Universität zu Berlin) for helping us with the sample preparation.

References

1. S.A. Carter, M. Angelopoulos, S. Karg, P.J. Brock, J.C. Scott, Appl. Phys. Lett. **70**, 2067 (1997)
2. X. Yang, D.C. Müller, D. Neher, K. Meerholz, Adv. Mater. **18**, 948 (2006)
3. C.W. Sele, T. von Werne, R.H. Friend, H. Sirringhaus, Adv. Mater. **17**, 997 (2005)
4. P. Cosseddu, A. Bonfiglio, Appl. Phys. Lett. **88**, 023506 (2006)
5. Y. Nishihara, A. Matsuda, A. Fujii, M. Ozaki, E.L. Frankevich, K. Yoshino, Synth. Met. **154**, 102 (2005)
6. H. Neugebauer, J. Electroanal. Chem. **563**, 153 (2004)
7. N. Koch, ChemPhysChem **8**, 1438 (2007)
8. N. Koch, E. Vollmer, A. Elschner, Appl. Phys. Lett. **90**, 043512 (2007)
9. E. Varene, I. Martin, P. Tegeder, J. Phys. Chem. Lett. **2**, 252 (2011)
10. R.U.A. Khan, D. Poplavskyy, T. Kreouzis, D.D.C. Bradley, Phys. Rev. B **75**, 035215 (2007)
11. S.C.J. Meskers, J.K.J. van Duren, R.A.J. Janssen, Adv. Funct. Mater. **13**, 805 (2003)
12. J.R. Goldman, J.A. Prybyla, Phys. Rev. Lett. **72**, 1364 (1994)
13. E. Knoesel, A. Hotzel, M. Wolf, Phys. Rev. B **57**, 12812 (1998)
14. T. Hertel, E. Knoesel, M. Wolf, G. Ertl, Phys. Rev. Lett. **76**, 535 (1996)
15. M. Aeschlimann, M. Bauer, S. Pawlik, R. Knorren, G. Bouzerar, K.H. Bennemann, Appl. Phys. A **71**, 485 (2000)
16. M. Bauer, M. Aeschlimann, J. Electron Spectrosc. Relat. Phenom. **124**, 225 (2002)
17. G. Moos, C. Gahl, R. Fasel, M. Wolf, T. Hertel, Phys. Rev. Lett. **87**, 267402 (2001)
18. M. Lisowski, P.A. Loukakos, U. Bovensiepen, M. Wolf, Appl. Phys. A **79**, 739 (2004)
19. W.A. Tisdale, M. Muntwiler, D.J. Norris, E.S. Aydil, X.-Y. Zhu, J. Phys. Chem. C **112**, 14682 (2008)
20. K.-C. Chang, M.-S. Jeng, C.-C. Yang, Y.-W. Chou, S.-K. Wu, M.A. Thomas, Y.-C. Peng, J. Electron. Mater. **38**, 1182 (2009)
21. S. Hagen, Y. Luo, R. Haag, M. Wolf, P. Tegeder, New J. Phys. **12**, 125022 (2010)
22. P.M. Echenique, J.M. Pitarke, E.V. Chulkov, A. Rubio, Chem. Phys. **251**, 1 (2000)

Appl Phys A
DOI 10.1007/s00339-012-6819-4

Applied Physics A
Materials Science & Processing

RAPID COMMUNICATION

Polaron dynamics in thin polythiophene films studied with time-resolved photoemission

Erwan Varene · Petra Tegeder

Received: 1 February 2012 / Accepted: 3 February 2012

Abstract Femtosecond time-resolved two-photon photoemission spectroscopy is employed to study the dynamics of an excited state in a thin regioregular poly(3-hexylthiophene) (RR-P3HT) film deposited on a conducting polymer poly(3,4-ethylene-dioxythiophene): poly-(styrenesulfonate) (PEDT:PSS) electrode following optical excitation at 2.1 eV. We found that the biexponential decay of this excited state has a fast component (2.6 ps) assigned to bound polaron pairs which recombine quickly or separate to be added to the slow component (7.6 ps). The latter is attributed to polarons generated via charge transfer between adjacent polymer chains.

1 Introduction

Organic photovoltaic cells (OPVC) are one of the most auspicious alternative for traditional silicon-based solar cells [1, 2]. This new generation of solar cells is fabricated using either small molecules or polymers as active semiconductor layers. The latter are favored because of their higher potential for real low-cost and large-area production as thin homogeneous polymer films can be easily made from solution. The best performances for polymer-based OPVCs are obtained using regioregular poly(3-hexylthiophene) (RR-P3HT) as donor material (up to ≈5% efficiency [3]) and poly(3,4-ethylene-dioxythiophene): poly-(styrenesulfonate) (PEDT:PSS) (see Fig. 1) is the electrode of choice for almost all OPVCs due to its transparency in the visible spectrum [4], its high conductivity [5], and work function. In P3HT electrons are usually delocalized on the π-conjugated backbone of the polymer, resulting in a high conductivity in the organic film, which can be increased up to 1000 S/cm when doped with iodine [5]. In this work we are using regioregular RR-P3HT showing self-organization of the chains into a lamellae structure resulting in relatively strong interchain interactions compared to regiorandom (RRa) P3HT that keeps a more chainlike morphology in the film.

In order to optimize device performance, good knowledge of the electronic properties of the polymers is needed. In this study we utilized time-resolved two-photon photoemission (2PPE) in order to gain insight into the excited states dynamics in the polymer film deposited on PEDT:PSS. At present, studies on the dynamics of electronic excitations and charge transfer processes at the adsorbate/substrate interface are limited to rather simple molecular systems (small molecules) adsorbed on single-crystal metal or semiconductor surfaces [6–16]. In the literature only a few 2PPE studies using nanosecond laser pulses on conjugated polymer films on metal substrates [17–24] exist. However, interfaces of direct relevance to OPVCs, i.e., conjugated polymer/polymer electrode have so far not been addressed. Here we show that 2PPE is a suitable tool to probe excited states dynamics in thin polymer films, namely the polaron dynamics in thin P3HT films.

2 Experimental

Two-photon photoemission spectroscopy The experimental setup combines a tunable femtosecond laser system with an ultrahigh vacuum (UHV) chamber for time-resolved

E. Varene · P. Tegeder (✉)
Fachbereich Physik, Freie Universität Berlin, Arnimallee 14, 14195 Berlin, Germany
e-mail: tegeder@physik.fu-berlin.de
Fax: +49-30-83856059

Published online: 23 February 2012

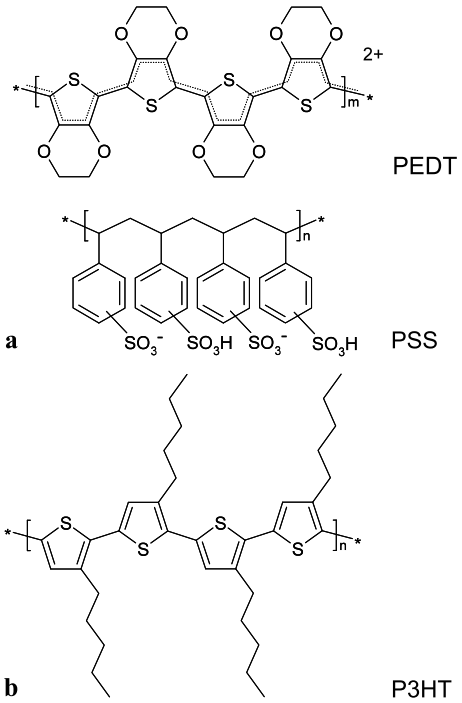

Fig. 1 Chemical structure of (**a**) the conducting polymer mixture PEDT:PSS and (**b**) P3HT

two-photon photoemission spectroscopy and surface science techniques. For the 2PPE measurements, femtosecond laser pulses are generated by a 300 kHz Ti:Sapphire laser system which pumps an optical parametric amplifier (OPA). The visible output with photon energies between 1.7 eV and 2.7 eV is frequency doubled to generate ultraviolet pulses. The frequency doubled pulses $h\nu_2$ and the visible fundamental $h\nu_1$ are delayed with respect to each other (pump and probe pulse) and focused onto the sample. Thereby a pulse duration of around 60 fs is achieved [15]. While the pump pulse excites an electron from below the Fermi level E_F to intermediate unoccupied states at energies $E = E_{\text{kin}} + \Phi - h\nu_2$ (with Φ the work function), the probe pulse photoionizes the sample by lifting the electron above the vacuum level (E_{vac}). Photoelectrons are detected in an electron time-of-flight (TOF) spectrometer and analyzed with respect to their kinetic energy E_{kin}. The energy resolution of the TOF spectrometer depends on the electron energy; in the range of $E_{\text{kin}} \approx 1$ eV, it is around 20 meV.

Film preparation As substrates, indium-tin-oxide (ITO) coated glass substrates (sheet resistance 15–30 Ω) were used. ITO samples were cleaned by ultrasonication in acetone and isopropanol. PEDT:PSS (AI4083, H.C. Stark GmbH and Co. KG) was deposited by spin coating at 1500 rpm and dried at 200°C for 5 min at ambient atmosphere. P3HT (Aldrich $M_n \sim 64.000$) was spin-coated (3000 rpm) in inert atmosphere from chloroform solution with various concentrations (0.5 mg/ml, 1 mg/ml, and 2 mg/ml).

3 Results and discussion

In the following we discuss the results on the charge carrier dynamics in thin regioregular RR-P3HT films on PEDT:PSS obtained by time-resolved 2PPE. In Fig. 2, a false color representation of the photoemission intensity of a 24-nm RR-P3HT film on PEDT:PSS recorded with photon energies of $h\nu_1 = 2.1$ eV for the visible and $h\nu_2 = 4.2$ eV for the UV laser pulses represents the electron distribution as a function of both time delay (horizontal axis) and energy (vertical axis). Depending on the sequence of laser pulses (or formally the sign of the pump-probe delay), the electrons are probed either near E_F or at higher intermediate state energies. Negative delays correspond to populating intermediate electronic states with UV light pulses ($h\nu_2$), while the visible pulses ($h\nu_1$) subsequently probe the excited electron distribution. On the other hand, for positive delays, the electrons are excited to intermediate states close to the Fermi level (hot electrons) with the visible pulses ($h\nu_1$) and are subsequently probed by the UV pulses ($h\nu_2$). Analyzing the two-dimensional data set by extraction of the time-dependent 2PPE photoelectron yield integrated over the energy intervals centered on the state of interest, e.g., unoccupied intermediate state labeled as A, provides the temporal evolution of the electron population, referred to as cross correlation traces as shown in the bottom panel of Fig. 2.

A broad photoemission feature located around $E_{\text{Final}} - E_F = 4.9$ eV, labeled as A, is observed showing a lifetime toward positive pump-probe delay. Hence this unoccupied intermediate state is pumped by the visible photons ($h\nu_1 = 2.1$ eV) and probed by the UV pulses ($h\nu_2 = 4.2$ eV); therefore its energetic position is ∼0.7 eV above E_F (note that the energy scale is referenced to the Fermi level of PEDT:PSS). The cross correlation trace for the energy region of state A is shown in the bottom panel of Fig. 2. Fitting the cross correlation trace with a biexponential decay results in time constants of 2.6 ps and 7.6 ps. In order to assign this unoccupied intermediate state, we have to consider both its energetic position and lifetime. From UPS measurements it is known that the upper valence band (VB) edge of P3HT is located 0.2 eV below the Fermi level of PEDT:PSS [25]. Surprisingly, we do not observe the bottom edge of the conduction band in the 2PPE spectrum. However the commonly accepted optical band gap of P3HT is 1.9–2.1 eV [26]. Thus the unoccupied state labeled as A which we observe in the 2PPE is located 0.9 eV above the VB edge (see Fig. 3), corresponding to 1.0–1.2 eV below the bottom edge of the conduction band (CB).

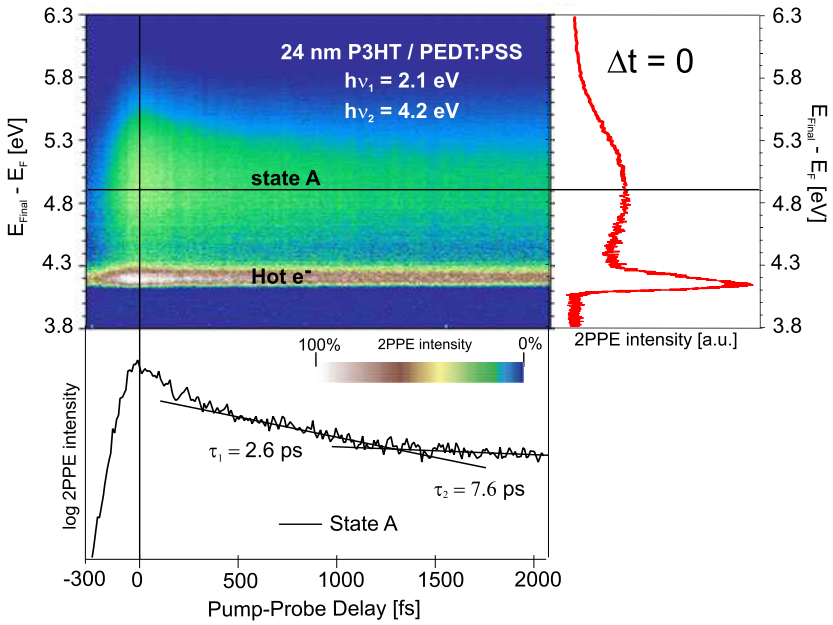

Fig. 2 2D-plot of 2PPE spectra as a function of pump-probe delay of a 24-nm P3HT film on PEDT:PSS. For positive delays, the VIS pulse ($h\nu_1 = 2.1$ eV) arrives at the surface before the UV pulse ($h\nu_2 = 4.2$ eV), and therefore the unoccupied intermediate state labeled as state A is VIS-pumped and UV-probed. The spectrum on the right corresponds to a cut at zero time delay. *The bottom panel* shows cross correlation trace for the energy region of state A

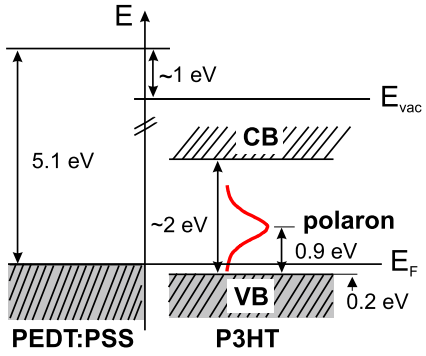

Fig. 3 Energetic position of the polaron in P3HT observed in the present study. The Fermi level of PEDT:PSS serves as reference

It is known that the photoexcitation of π-electrons with photon energies greater than the band gap of P3HT will induce the formation of excitons [27]. An exciton can either meet another exciton and undergo exciton-exciton annihilation or decay to the ground state. Moreover, if the exciton is created close to a dissociation center, for instance, another polymer chain, it can undergo a charge transfer and produce a bond polaron pair with the negative and positive polaron on adjacent chains. Ruseckas et al. [28] have reported that this process is very efficient in polythiophene and takes place within 100 fs after photoexcitation. This bound polaron pair can recombine, be trapped by a defect state, or dissociate into two charge carriers.

The binding energy of the exciton in RR-P3HT reported by Sakamoto et al. [27] is 0.7 eV, and its lifetime in the order of a few hundred femtoseconds [29]. Moreover it is known from the literature that two delocalized polaron bands located at 0.1 eV and 1.85 eV, as well as two localized polaron bands at 0.35 eV and 1.25 eV, respectively, are existent in RR-P3HT [30], viz. in the energy regime where we find the broad 2PPE feature. Therefore we assign the fast component (2.6 ps) to bound polaron pairs, in which positive and negative polarons are bound to each other on adjacent chains by Coulomb interaction. The bound polaron can recombine quickly or separate and be added to the slow component (7.6 ps) assigned to polarons generated by charge transfer between adjacent polymer chains. Due to electronic and geometric disorder in the P3HT films, the broadening of the polaron peak does not allow to differentiate energetically the polarons from the bound polaron pairs. Note that, varying the film thickness from 5 nm to 30 nm did not lead to significant changes in the polaron dynamics. In order to support our assignment, a comparison between the observed charge carrier dynamics in RR-P3HT films forming a lamellae structure with nonnegligible interchain interactions and the dynamics in regiorandom (RRa) P3HT films keeping a chainlike morphology could certainly be useful to gain further insight into the nature of the observed processes. However, our study shows that time-resolved 2PPE is a powerful tool to investigate the excited state dynamics in polymer films.

Acknowledgements Funding by the Deutsche Forschungsgemeinschaft (DFG) through the priority program SPP 1355 "Elementary Processes in Organic Photovoltaics" is gratefully acknowledged.

References

1. Y. Shirota, H. Hageyama, Chem. Rev. **107**, 953 (2007)
2. P. Peumans, A. Yakimov, S.R. Forrest, J. Appl. Phys. **93**, 3693 (2003)

3. M.T. Dang, L. Hirsch, G. Wantz, Adv. Mat. **31**, 3597 (2011)
4. D. Wakizaka, T. Fushimi, H. Ohkita, S. Ito, Polymer **45**, 8561 (2004)
5. R.D. McCullough, S. Tristram-Nagle, S.P. Williams, R.D. Lowe, M. Jayaraman, J. Am. Chem. Soc. **115**, 4910 (1993)
6. C.D. Lindström, X.-Y. Zhu, Chem. Rev. **106**, 4281 (2006)
7. C.H. Schwalb, S. Sachs, M. Marks, A. Schöll, F. Reinert, E. Umbach, U. Höfer, Phys. Rev. Lett. **101**, 146801 (2008)
8. A. Yang, S.T. Shipman, S. Garrett-Roe, J. Johns, M. Strader, P. Szymanski, E. Muller, C. Harris, J. Phys. Chem. C **112**, 2506 (2008)
9. S. Hagen, P. Kate, F. Leyssner, D. Nandi, M. Wolf, P. Tegeder, J. Chem. Phys. **129**, 164102 (2008)
10. S. Hagen, P. Kate, M.V. Peters, S. Hecht, M. Wolf, P. Tegeder, Appl. Phys. A **93**, 253 (2008)
11. M. Wolf, P. Tegeder, Surf. Sci. **603**, 1506 (2009)
12. P. Szymanski, S. Garret-Roe, C.B. Harris, Prog. Surf. Sci. **78**, 1 (2005)
13. E. Varene, L. Bogner, S. Meyer, J. Pennec, P. Tegeder, Phys. Chem. Chem. Phys. **14**, 691 (2012)
14. E. Varene, I. Martin, P. Tegeder, J. Phys. Chem. Lett. **2**, 252 (2011)
15. S. Hagen, Y. Luo, R. Haag, M. Wolf, P. Tegeder, New J. Phys. **12**, 125022 (2010)
16. J.E. Johns, E.A. Muller, J.M.J. Frechet, C.B. Harris, J. Am. Chem. Soc. **132**, 44 (2010)
17. Y. Sohn, J. Richter, J. Ament, J.T. Stuckless, Appl. Phys. Lett. **84**, 76 (2004)
18. Y. Sohn, J.T. Stuckless, Appl. Phys. Lett. **90**, 171901 (2007)
19. Y. Sohn, J.T. Stuckless, ChemPhysChem **8**, 1937 (2007)
20. Y. Sohn, J.T. Stuckless, J. Chem. Phys. **126**, 174901 (2007)
21. Y. Sohn, J.T. Stuckless, Chem. Phys. Lett. **444**, 125 (2007)
22. Y. Sohn, J.T. Stuckless, Chem. Phys. Lett. **436**, 228 (2007)
23. G.D. Hale, S.J. Oldenburg, N.J. Halas, Phys. Rev. B **55**, R16069 (1997)
24. S.G.D. Hale, S.J. Oldenburg, N.J. Halas, Appl. Phys. Lett. **71**, 1483 (1997)
25. F.J. Zhang, A. Vollmer, J. Zhang, Z. Xu, J.P. Rabe, N. Koch, Org. Electron. **8**, 606 (2007)
26. V. Shrotriya, J. Ouyang, R.J. Tseng, G. Li, Y. Yang, Chem. Phys. Lett. **411**, 138 (2005)
27. A. Sakamoto, M. Takezawa, Synth. Met. **159**, 809 (2009)
28. A. Ruseckas, M. Theander, M.R. Andersson, M. Svensson, M. Prato, O. Inganas, V. Sundström, Chem. Phys. Lett. **322**, 136 (2000)
29. X. Ai, M.C. Beard, K.P. Knutse, S.E. Shaheen, G. Rumbles, R.J. Ellingson, J. Chem. Phys. B **110**, 25468 (2006)
30. O.J. Korovyanko, R. Österbacka, X.M. Jiang, Z.V. Vardeny, R.A.J. Janssen, Phys. Rev. B **64**, 235122 (2001)

Ultrafast Exciton Population, Relaxation, and Decay Dynamics in Thin Oligothiophene Films

E. Varene, L. Bogner, C. Bronner, and P. Tegeder*

Fachbereich Physik, Freie Universität Berlin, Arnimallee 14, 14195 Berlin, Germany

(Received 24 February 2012; published 13 November 2012)

Femtosecond time-resolved two-photon photoemission spectroscopy is utilized to determine the electronically excited states dynamics at the α-sexithiophene (6T)/Au(111) interface and within the 6T film. We found that a photoinduced transition between the highest occupied molecular orbital and lowest unoccupied molecular orbital is essential in order to observe exciton population, which occurs within 100 fs. In thin 6T films, the exciton exhibits a lifetime of 650 fs. On a time scale of 400 fs, an energetic stabilization is observed leading to the formation of a polaron or electron trapping at defect states. The lifetime of this state is 6.3 ps. Coverage-dependent measurements show that apart from the excited state decay within the film, a substrate-mediated relaxation channel is operative. The present study demonstrates that two-photon photoemission spectroscopy is a powerful tool to investigate the whole life cycle from creation to decay of excitons in an organic semiconductor.

DOI: 10.1103/PhysRevLett.109.207601 PACS numbers: 79.60.Fr, 71.35.−y, 78.47.jd

Organic semiconductors are being explored for a number of fascinating applications in optoelectronic devices such as organic photovoltaic cells, organic light emitting diodes, or organic thin film transistors [1,2]. A complete knowledge of the electronic structure and the dynamics of electronically excited states in potential molecule-based devices is necessary for improvement and optimization of the device performance. Thereby the exciton formation and decay dynamics at interfaces and within the molecular films are of particular relevance. Recently it was discussed by Koch *et al.* [3] that the choice of the appropriate experimental method to study exciton populations is important. They have emphasized that the existence of exciton signatures in absorption or luminescence spectra are due to a coherent excitonic polarization and are not a fingerprint of a real incoherent exciton population. For excitations above the band gap (interband absorption), fast Coulomb and phonon scattering results in polarization decay and the generation of electron-hole pair population on a femtosecond (fs) time scale [3]. Therefore fs time-resolved two-photon photoemission (2PPE) is a very powerful tool to study these processes. The first pump pulse excites a transition between the highest occupied molecular state and lowest unoccupied molecular state (''interband'' adsorption), while the second pulse probes the electronically excited state. By varying the time delay between the pump and probe pulses from a few fs up to several picoseconds, it is thus possible to resolve the exciton population and decay dynamics.

In the present study we utilized fs time-resolved 2PPE to determine the charge carrier and exciton dynamics at the α-sexithiophene (6T)/Au(111) interface and within the 6T film. Oligothiophenes, π-conjugated chainlike planar molecules, are highly relevant for small-molecule-based solar cells, which are fabricated *via* vacuum deposition. In bulk heterojunction photovoltaic cells they possess very high efficiencies [4]. Several surface science studies focusing on the adsorption behavior of 6T on noble metal surfaces exist, e.g. on Au(111) [5] and Cu(110) [6]. In addition, the occupied band structures of 6T adsorbed on various noble metals have been determined [7–9]. Using 2PPE the electronic structure, i.e., both occupied and unoccupied molecular electronic as well as excitonic states, of 6T adsorbed on Au(111) have been observed. Therein the energetic position of the transport level and the exciton binding energy have been determined [10]. In contrast to time-resolved measurements ranging from femtoseconds to milliseconds to elucidate the decay dynamics of excitons in 6T films (thickness about 50–350 nm) [11–13], investigations on the exciton formation, relaxation, and decay at 6T/Au(111) interfaces and within thin films are not known so far. A recent 2PPE study investigated the charge transport properties of 6T and the dihexyl-substituted 6T (DH6T) adsorbed on Ag(111), respectively, and found a charge localization in DH6T within 230 fs while in 6T no localization was observed. The charge localization has been attributed to the hydrocarbon side chains [14]. The exciton decay dynamics at organic molecule-metal interfaces has been observed so far only for C_{60} films epitaxially grown on Au(111) and Cu(111) using 2PPE [15]. Additionally 2PPE has been used to probe charge transfer excitons on a surface of organic semiconductors, namely, pentacene and tetracene, respectively [16,17].

In this Letter, we investigate the exciton formation and decay in 6T on Au(111) as a function of 6T coverage using 2PPE. We found that an optically induced transition between the highest occupied molecular orbital (HOMO) and lowest unoccupied molecular orbital (LUMO) is the basic prerequisite in order to observe the population of a Frenkel exciton. The exciton generation occurs within 100 fs followed by an energetic stabilization on a time

scale of around 400 fs leading to a polaronic or trap state. Both the excitonic and polaron or trap state exhibit a coverage dependent lifetime, which in each case is associated with two decay channels, an intrinsic and a distance-dependent (external) decay.

In our experiment, the Au(111) crystal was mounted on a liquid nitrogen cooled cryostat that, in conjunction with resistive heating, enables temperature control from 90 to 800 K. The crystal was cleaned by standard procedure of cycles of Ar^+ sputtering and annealing. The 6T was dosed by means of a home-built effusion cell held at 500 K at a crystal temperature of 290 K. The 6T coverage was quantified by temperature-programmed desorption and work function measurements. Tunable fs laser pulses for the time-resolved 2PPE-measurements are supplied from a Ti:Sapphire oscillator in combination with a 300 kHz regenerative amplifier and optical parametrical amplifiers [18].

Using photon energy-dependent 2PPE, we recently determined the electronic structure of 6T adsorbed on Au(111) [10], which is summarized in Fig. 1. The exciton state is found 0.9 eV below the LUMO. Although the exciton is not a single particle state but a quasiparticle formed by a correlated electron and hole bound through Coulomb interaction, in 2PPE the final state being an electron and an ionized molecule, it is often simpler to assign the binding energy to the electron. It is essential to point out that only excitations with photon energies enabling a HOMO-LUMO transition (resonant excitation), i.e., around 2.9 eV, permitted the observation of the exciton generation in 2PPE. This is in accordance with a real

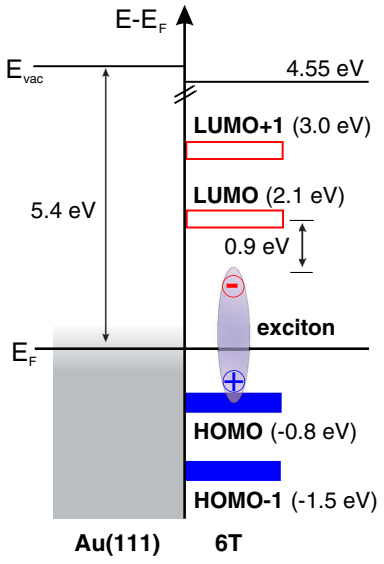

FIG. 1 (color online). Energetic position and assignment of 6T-derived photoemission spectral features at a coverage of 1 monolayer (ML) 6T adsorbed on Au(111). The Fermi level of Au(111) serves as reference. The exciton binding energy is 0.9 eV.

exciton population process [3]. Chan *et al.* [19] have applied 2PPE to study the excited state dynamics in pentacene or fullerene bilayers after optical excitation and observed multiple exciton generation. However, we excite the system with 3 eV photons and observe the feature attributed to a Frenkel exciton at a final state energy of 2 eV above the HOMO; thus, we can rule out the formation of two or more electron-hole pairs from the absorption of one photon. Moreover, our assignment is in very good agreement with the results of Frolov *et al.* [20] who have found that Frenkel excitons in 6T are characterized by a stimulated emission band at 2 eV.

In the following we focus on the excited state dynamics, in particular, the population and decay dynamics of the Frenkel exciton. In the low-coverage regime (1–2 ML), the lifetimes for electrons in the molecular excited states, viz. the LUMO and LUMO + 1, possess values that are below the limit of our experimental resolution ($\tau < 10$ fs). These ultrashort lifetimes point towards a strong electronic coupling between 6T and Au(111), allowing for efficient back transfer of electrons to the metal substrate. At metallic surfaces such short lifetimes of excited states, i.e., in the range of fs, have been found for several adsorbates [15,18,21–23]. In contrast, the exciton exhibits a

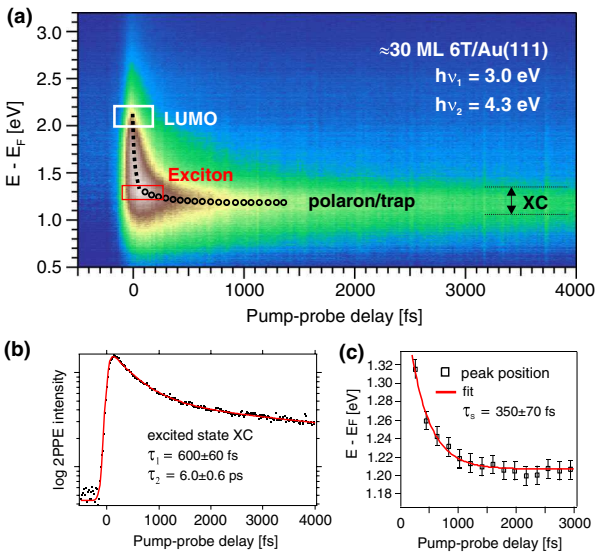

FIG. 2 (color online). Two-dimensional spectrum of time-resolved 2PPE measurements recorded with $h\nu_1 = 3.0$ eV and $h\nu_2 = 4.3$ eV. The dashed line in (a) indicates the energetic stabilization of electrons leading to the formation of the exciton, and the dotted line represents the energetic stabilization of electrons caused by the formation of polarons or at defect sites trapped electrons (see text). (b) Cross correlation traces of the 2PPE intensity integrated over the excited state peak intensities [XC energy range in (a)] with a biexponential fit that gives the indicated lifetimes. (c) Maximum peak intensity of the exciton state as a function of pump-probe delay that yields the indicated energy stabilization time due to polaron formation or localization at defect sites.

pronounced lifetime as can clearly be seen in Fig. 2(a) for 30 ML 6T/Au(111). In this false color two-dimensional representation, the 2PPE intensity at particular energy with respect to the Fermi level, E_F, as a function of time delay (Δt) between the two laser pulses $h\nu_1 = 3.0$ eV and $h\nu_2 = 4.3$ eV is displayed. The cross correlation curve for the energy region of the excited state [XC in Fig. 2(a)] is shown in Fig. 2(b). The solid line corresponds to a fit used to determine lifetimes. The fit model contains a sech^2 function representing the laser pulse duration convoluted with the response function of the intermediate state. The response function is biexponential yielding the indicated lifetime values τ_1 and τ_2, which correspond to two different states. A detailed discussion about the origin of these states will be given below.

Returning to the time-resolved 2PPE spectra shown in Fig. 2(a), a fast energetic stabilization of electrons (dashed line) leading to the formation of the Frenkel exciton is clearly seen. In addition, the excitonic state stabilizes on a slower time scale (dotted line). The first fast process, the stabilization of around 0.9 eV, occurs within 100 ± 20 fs [see Fig. 2(a)]. We interpret this observation as follows: Optical excitation with 3.0 eV photons leads to an intramolecular HOMO-LUMO transition, followed by the decay of the polarization and formation of the exciton population (correlated electron-hole pair) that occurs on a femtosecond time scale [3]. The transition of the electron from a bonding (the HOMO) to an antibonding state (the LUMO) is a very efficient source for the stimulation of molecular vibrations; therefore, the exciton binding energy of 0.9 eV dissipates to molecular vibrations on a time scale of the inverse of a vibrational quantum (≤ 100 fs, for instance the C-S-C ring deformation mode at 700 cm^{-1} [24], which corresponds to a period of 48 fs). On the other hand, coupling of the exciton to molecular vibrations (electron-nuclear interaction) can lead to the generation of a polaron. This process may be responsible for the observed energetic stabilization of around 0.1 eV, which proceeds on a time scale of 350 ± 70 fs [see Fig. 2(c)]. In addition to the decrease in electron energy, this kind of localization due to the polarization in the nuclear coordinates should be accompanied by a time-dependent disappearance of parallel dispersion [14,25]. However, the photoemission of the electron that is intrinsic to 2PPE breaks the exciton, and thus we cannot measure the dispersion of this excitonic state. Besides polaron formation being responsible for the energetic stabilization, the electron may be trapped into a defect site [26]. Localization by defects has been shown to occur on a hundred fs time scale in particular systems [27]. Distinguishing between electrons trapped into a defect site and a self-localizing polaron is difficult because of the similar time scales for both formation processes.

In order to gain further insights into the exciton decay, we investigated the dynamics as a function of 6T coverage. The cross correlation curves for the energy region of the excited state (exciton and polaron or trap) as a function of coverage are presented in Fig. 3. Both lifetime values τ_1 and τ_2 exhibit a clear dependence on layer thickness: τ_1 increases from 40 ± 10 fs at 3 ML to 650 ± 65 fs at 30 ML, τ_2 rises from 200 ± 20 fs (3 ML) to 6 ± 0.6 ps (30 ML). The results of the fits as a function of film thickness are summarized in Figs. 3(b) and 3(c). The solid lines are fits using a simple exponential function. The asymptotic values are 650 ± 50 fs for τ_1 and 6.3 ± 0.6 ps for τ_2, respectively. As it has been discussed for the monoexponential exciton decay in C_{60} adsorbed on Au(111) and Cu(111) [15], respectively, a coverage-dependent decay time indicates that the exciton decays via two relaxation channels, an intrinsic and a distance-dependent channel. The intrinsic decay rate corresponds to the decay in the bulk material and the distance- dependent (external) rate to quenching by the metal substrate. Accordingly for 6T/Au(111), the coverage dependence of both decay times indicate that each of them contains at least two relaxation channels, an intrinsic and an external channel. The intrinsic decays for bulk 6T are

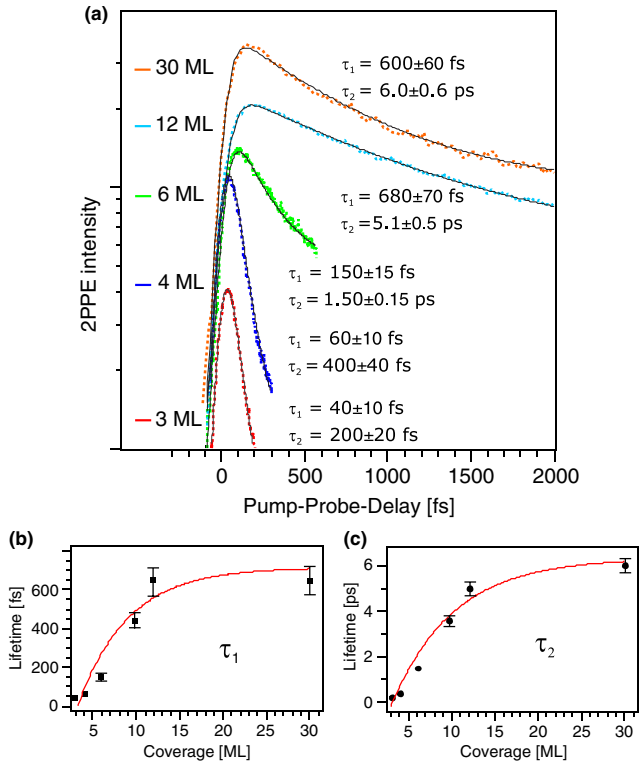

FIG. 3 (color online). (a) Cross correlation traces of the 2PPE intensity integrated over the excited state peak intensities (exciton and polaron or trap) as a function of 6T coverage on a logarithmic intensity axis. The lines represent fits for the biexponential decay, which yields the indicated lifetimes. The dependence on film thickness of the transient lifetime (b) τ_1 and (c) τ_2.

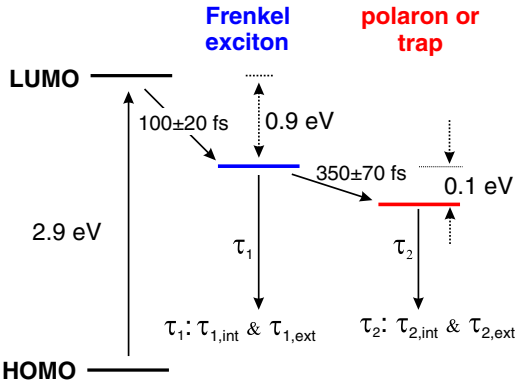

FIG. 4 (color online). Formation and decay processes of a Frenkel exciton in sexithiophene adsorbed on Au(111). τ_{int} indicates the intrinsic (for bulk 6T) and τ_{ext} the external (distance-dependent) lifetime (see text).

related to the asymptotic values of 650 ± 50 fs for τ_1 and 6.3 ± 0.6 ps for τ_2 [Figs. 3(b) and 3(c)].

Figure 4 summarizes the exciton formation and decay processes as determined in our time-resolved photoemission study. We attribute the two lifetime values τ_1 and τ_2 obtained from the biexponential decay (see Fig. 2) to originate from the decay of the singlet Frenkel exciton (τ_1) and the polaron or defect state (τ_2), respectively. As discussed above, both values contain an intrinsic (τ_{int}, for bulk 6T) and external (τ_{ext}, coverage-dependent decay to metal states) decay. Before addressing the coverage-dependent lifetime, we discuss the intrinsic lifetime of the Frenkel exciton and the polaron or defect state in bulk 6T by comparing with time-resolved studies known from literature. Most studies [11–13] determined the dynamical processes after optical excitation of higher lying electronic states compared to the formation and decay of the lowest (first) Frenkel exciton state investigated here. In addition, almost all of these experimental results revealed dynamic processes on much longer time scales. For the singlet Frenkel exciton, we observe a lifetime of $\tau_{1,int} = 650 \pm 50$ fs. In comparison, a value of ≈ 1 ps has been found for the decay in 6T films using picosecond fluorescence spectroscopy [12]. The lifetime of the polaron or defect state is $\tau_{2,int} = 6.3 \pm 0.6$ ps, thus one order of magnitude longer than the first exciton state. The coverage- or distance-dependent lifetime (τ_{ext}) is associated with back-transfer of electrons to the metallic substrate (substrate-mediated quenching). With increasing 6T coverage, the probability density of the excited state (exciton, polaron, or trap) is further away from the metal-molecule interface. As a result, its coupling (wave function mixing) to the Au surface decreases and the electron transfer rate decreases [15].

In conclusion, using fs time-resolved 2PPE we were able to elucidate the exciton population and decay dynamics in sexithiophene adsorbed on Au(111). The formation of the exciton takes place on a femtosecond time scale following optical excitations higher than the HOMO-LUMO gap energy. In bulk 6T, the exciton either recombines, it possesses a lifetime of 650 fs, or energetic stabilization results in generation of a polaron or trapped charge (with a lifetime of 6.3 ps). Both the exciton and the polaron or trap state lifetimes are coverage dependent indicating that an intrinsic (for bulk 6T) and an external relaxation channel exist. Our study shows that 2PPE is a powerful tool to determine exciton population and decay dynamics. Therefore, this method promises to provide a link between optical and electron spectroscopy. The creation and decay of excitons are important elementary processes in organic semiconductors. Precise insight into these processes is certainly essential for optimization of organic-molecule-based optoelectronic devices.

Funding by the Deutsche Forschungsgemeinschaft (DFG) through the priority program SPP 1355 and collaborative research center SFB 658 is gratefully acknowledged.

*Corresponding author.
petra.tegeder@physik.fu-berlin.de

[1] H. E. Katz and J. Huang, Annu. Rev. Mater. Res. **39**, 71 (2009).
[2] K. Walzer, B. Maennig, M. Pfeiffer, and K. Leo, Chem. Rev. **107**, 1233 (2007).
[3] S. W. Koch, M. Kira, G. Khitrova, and H. M. Gibbs, Nature Mater. **5**, 523 (2006).
[4] R. Fitzner, E. Reinhold, A. Mishra *et al.*, Adv. Funct. Mater. **21**, 897 (2011).
[5] M. Kiel, K. Duncker, C. Hagendorf, and W. Widdra, Phys. Rev. B **75**, 195439 (2007).
[6] M. Kiguchi, S. Entani, K. Saiki, and G. Yoshikawa, Appl. Phys. Lett. **84**, 3444 (2004).
[7] I. G. Hill, A. Kahn, Z. G. Soos, and R. A. Pascal Jr., Chem. Phys. Lett. **327**, 181 (2000).
[8] N. Koch, G. Heimel, J. Wu, E. Zojer, R. L. Johnson, J.-L. Brédas, K. Müllen, and J. P. Rabe, Chem. Phys. Lett. **413**, 390 (2005).
[9] M. Grobosch and M. Knupfer, Adv. Mater. **19**, 754 (2007).
[10] E. Varene, I. Martin, and P. Tegeder, J. Phys. Chem. Lett. **2**, 252 (2011).
[11] G. Lanzani, S. V. Frolov, P. A. Lane, Z. V. Vardeny, M. Nisoli, and S. De Silvestri, Phys. Rev. Lett. **79**, 3066 (1997).
[12] K. Watanabe, T. Asahi, H. Fukumura, H. Masuhara, K. Hamano, and T. Kurata, J. Phys. Chem. B **101**, 1510 (1997).
[13] G. Urbasch, H. Giessen, M. Murgia, R. Zamboni, and R. F. Mahrt, J. Phys. Chem. B **104**, 6536 (2000).
[14] J. E. Johns, E. A. Muller, J. M. J. Frechet, and C. B. Harris, J. Am. Chem. Soc. **132**, 15 720 (2010).
[15] G. Dutton, D. P. Quinn, C. D. Lindstrom, and X.-Y. Zhu, Phys. Rev. B **72**, 045441 (2005).

[16] M. Muntwiler, Q. Yang, W. A. Tisdale, and X.-Y. Zhu, Phys. Rev. Lett. **101**, 196403 (2008).
[17] Q. Yang, M. Muntwiler, and X.-Y. Zhu, Phys. Rev. B **80**, 115214 (2009).
[18] S. Hagen, Y. Luo, R. Haag, M. Wolf, and P. Tegeder, New J. Phys. **12**, 125022 (2010).
[19] W. Chan, M. Ligges, A. Jailaubekov, L. Kaale, L. Miaja-Avila, and X.-Y. Zhu, Science **334**, 1541 (2011).
[20] S. V. Frolov, Ch. Kloc, B. Batlogg, M. Wohlgennant, X. Jiang, and Z. V. Vardeny, Phys. Rev. B **63**, 205203 (2001).
[21] A. Yang, S. T. Shipman, S. Garrett-Roe, J. Johns, M. Strader, P. Szymanski, E. Muller, and C. B. Harris, J. Phys. Chem. C **112**, 2506 (2008).
[22] M. Wolf and P Tegeder, Surf. Sci. **603**, 1506 (2009).
[23] C. Bronner, M. Schulze, S. Hagen, and P. Tegeder, New J. Phys. **14**, 043023 (2012).
[24] G. Louran, J. P. Buisson, S. Lefrant, and D. Fichou, J. Phys. Chem. **99**, 11 399 (1995).
[25] A. D. Miller, I. Bezel, K. J. Gaffney, S. Garrett-Roe, S. H. Liu, P. Szymanski, and C. B. Harris, Science **297**, 1163 (2002).
[26] L. G. Kaake, P. F. Barbara, and X.-Y. Zhu, J. Phys. Chem. Lett. **1**, 628 (2010).
[27] U. Bovensiepen, C. Gahl, J. Stähler, M. Bockstedte, M. Meyer, F. Baletto, S. Scandolo, X.-Y. Zhu, A. Rubio, and M. Wolf, J. Phys. Chem. C **113**, 979 (2009).

Bibliography

[1] R. Williams, *J. Appl. Phys.* **1960**, *32*, 15051514

[2] D. M. Chapin, C. S. Fuller, and G. L. Pearson, *J. Appl. Phys.* **1954**, *25*, 676677

[3] http://sharp-world.com/corporate/news/120531.html

[4] Shirakawa, Hideki; Louis, Edwin J.; MacDiarmid, Alan G.; Chiang, Chwan K.; Heeger, Alan J., *J. Chem. Soc, Chem. Com.* **1977**, *16*, 578.

[5] Tang, *Applied Physics Letters* **1986**, *48*, 183

[6] http://www.konarka.com/

[7] http://www.heliatek.com/

[8] Y. Zheng, J. Xue, *Pol. Rev.* **2010**, 50

[9] G. Urbasch, M. Hopmeier, H. Giessen, and R. F. Mahrt, *J. Phys. Chem. B* **2000**, *104*, 12210-12214

[10] F. Petraki, S. Kennou, S. Nespurek, *J. Appl. Phys.* **2008**, *103.*

[11] D.E. Markov, *PhD thesis*, University of Groningen, **2006**.

[12] M. Knupfer, T. Pichler, M. S. Golden, J. Fink, M. Murgia, R. H. Michel, R. Zamboni, C. Taliani, *Phys. Rev. Lett.* **1999**, *83*, 1443.

[13] M. Knupfer, *Appl. Phys. A* **2003**, *77*, 623-626.

[14] G. Wannier, *Physical Review* **1937**,*52*, 191

[15] B. Mauvernay, *PhD thesis*, University of Toulouse, **2007**.

[16] M. Muntwiller, Q. Yang, X.-Y. Zhu, *J. Electron Spectrosc. Relat. Phenom.* **2009**.

[17] X.-Y. Zhu, Q. Yang, M. Muntwiller, *Acc. Chem. Res.* **2009**, *42*, 1779-1787.

[18] H. Frohlich, *Adv. Phys.* **1954**, *11*, 325

[19] L. Bogner, *Master thesis*, Freie Universitaet Berlin, **2011**.

[20] X. Zhu, A. Kahn, *MRS Bulletin* **2010**, *35*, 443.

[21] P. Peumans, A. Yakimov, S.R. Forrest, *J. Appl. Phys.* **2003**, *93*, 3693-3723 .

[22] G. Chidichimo, L. Filippelli, *Int. J. Photoenergy* **2010** .

[23] Kim, J.Y. et al., *Science* **2007**, *317*, 222-225.

[24] T. Ameri, G. Dennler, C. Lungenschmied, C. Brabec, *Energy Eniron. Sci.* **2009**, *2*, 347-363.

[25] N. D. Sariciftci, D. Braun, C. Zhang, V. I. Srdanov, A. J. Heeger, G. Stucky, and F. Wudl, *Appl. Phys. Lett.* **1993**, *62*, 585.

[26] J. J. M. Halls, K. Pichler, R. H. Friend, S. C. Moratti, and A. B. Holmes, *Appl. Phys. Lett.* **1996**, *68*, 3120.

[27] Y. Yi, V. Coropceanu, J.-L. Bredas, *J. Mater. Chem.* **2011**, *21*, 1479-1486.

[28] H.J. Egelhaaf, D. Oelkrug, D. Oeter, Ch. Ziegler, W. Göpel, J. Mol. Struc. 348 (1995) 405; D. Oeter, H.J. Egelhaaf, Ch. Ziegler, D. Oelkrug, W. Göpel, *J. Chem. Phys.* ,**1994**, *101*, 6344.

[29] S. Nagamatsu, K. Kaneto, R. Azumi, M. Matsumoto, Y. Yoshida and K. Yase, *J. Phys. Chem. B*, **2005**, *109*, 9374.

[30] Y.-S. Hsiao, W.-T. Whang, C.-P. Chenb and Y.-C. Chenb *J. Mater. Chem.*, **2008**, *18*, 59485955

[31] M.T. Dang, L. Hirsch, G. Wantz, *Adv. Mat.* **2011**, *31*, 3597.

[32] S. Hagen, *PhD thesis*, Freie Universität Berlin, **2009**.

[33] P. S. Kirchmann, *PhD thesis*, Freie Universität Berlin, **2008**.

[34] Prato, S.; Floreano, L.; Cvetko, D; De Renzi, V.; Morgante, A.; Modesti, S.; Biscarini, F.; Tamboni, R.; Taliani, C. *J. Chem. Phys. B.*, **1999**, *103*, 7788-7795.

[35] Kiel, M.; Duncker, K.; Hagendorf, C.; Widdra, W. *Phys. Rev. B* **2008**, *75*, 195439-1–8.

[36] Duncker, K.; Kiel, M.; Höfer, A.; Widdra, W. *Phys. Rev. B* **2008**, *77*, 155423-1–8.

[37] E. Varene, I. Martin, P. Tegeder, *J. Phys. Chem. Lett.* (2011) 2, 252.

[38] Kiguchi, M.; Entani, S.; Saiki, K.; Yoshikawa, *Appl. Phys. Lett.* **2004**, *84*, 3444–3446.

[39] F. Jäckel, U.G.E. Perera, V. Iancu, K.-F. Braun, N. Koch, J.P. Rabe, and S.-W.Hla, *Phys. Rev. Lett.* **2008**, *100*, 126102.

[40] Chandekar, A.; Whitten, J.E. *Synthetic Metals* **2005**, *150*, 259–264.

[41] Koch, N.; Heimel, G.; Wu, J.; Zojer, E.; Johnson, R.L.; Brédas, J.-L.; Müllen, K.; Rabe, J.P. *Chem. Phys. Lett.* **2005**, *431*, 390–395.

[42] Knupfer, M.; Liu, X. *Surf. Sci.* **2006**, *600*, 3978–2981.

[43] Grobosch, M.; Knupfer, M. *Adv. Mater.* **2007**, *19*, 754–756.

[44] Hill, I.G.; Kahn, A.; Soos, Z.´pß0oiuhzgtfdsaysxdfghjkio.; Pascal Jr., *Chem. Phys. Lett.* **2000**, *327*, 181–188.

[45] J.E. Johns, E.A. Muller, J.M.J. Frechet, C.B. Harris, *J. Am. Chem. Soc.*, **2010**, *132*, 15720.

[46] G. Dutton, D.P. Quinn, C.D. Lindstrom, X.-Y. Zhu, *Phys. Rev. B* , **2005**, *72*, 045441.

[47] M. Muntwiler, Q. Yang, W. A. Tisdale, and X.-Y. Zhu, *Phys. Rev. Lett.*, **2008**, *101*, 196403

[48] Q. Yang, M. Muntwiler, and X.-Y. Zhu, *Phys. Rev. B.*, **2009**, *80*, 115214.

[49] E. Varene, L. Bogner, C. Bronner, P. Tegeder, *Phys. Rev. Lett.*, **2012** *109* 207601.

[50] S. W. Koch, M. Kira, G. Khitrova, H. M. Gibbs, *Nat. Mat.*, **2006**, *5*, 523.

[51] Yang A, Shipman ST, Garrett-Roe S, Johns J, Strader M, Szymanski P, Muller E, Harris C.B. J. Phys. Chem. C **112** 2506 (2008).

[52] M. Wolf, P Tegeder, Surf. Sci. **603**, 1506 (2009).

[53] Hagen S, Luo Y, Haag R, Wolf M, Tegeder P 2010 *New. J. Phys.*, **2010**, *12*, 125022.

[54] G. Louran, J.P. Buisson, S. Lefrant, D. Fichou, *J. Phys. Chem.*, **1995**, *99*, 11399

[55] U. Bovensiepen, C. Gahl, J. Stähler, M. Bockstedte, M. Meyer, F. Baletto, S. Scandolo, X.-Y. Zhu, A. Rubio, M. Wolf, *J. Phys. Chem. C*, **2009**, *113*, 979

[56] H. Inoue, G. Yoshikawa, and K. Saiki, Jpn. *J. Appl. Phys.*, **2006**, *45*, 1794.

[57] G. Yoshikawa, M. Kiguchi, S. Ikeda, and K. Saiki, *Surf. Sci.*, **2004**, *77*, 559.

[58] A.J. Makinen, J.P. Long, N.J. Watkins, Z.H. Kafafi *J. Phys. Chem.*, **2007**, *109*, 5790.

[59] M. Kiel, K. Duncker, C. Hagendorf and W. Widdra, *Phys. Rev. B: Condens. Matter*, **2007**, *75*, 195439.

[60] L. Rossi, G. Lanzani, and F. Garnier, *Phys. Rev. B*, **1998**, *58*, 6684.

[61] P. Lang, C. Nogues, S. Verneyre, F. Demanze, P. Srivastava, F. Garnier, J. C. Wittmann, B. Lotz, and C. Straupe, *J. Chim. Phys. Phys.-Chim. Biol.*, **1998**, *95*, 1286.

[62] A. Stabel and J. P. Rabe, *Synth. Met.*, **1994**, *67*, 47.

[63] A. Yassar, G. Horowitz, P. Valat, V. Wintgens, H. Hmyene, F. Deloffre, P. Srivastava, P. Lang, F. Garnier, *J. Phys. Chem.* **1995**, *99*, 9155

[64] J.E. Johns, E.A. Muller, J.M.J. Frechet, C.B. Harris, *J. Am. Chem. Soc.* **2010**, *132*, 15720

[65] H. Glowatzki, S. Duhm, K.-F. Braun, J. P. Rabe and N. Koch, *Phys. Rev. B: Condens. Matter*, **2007**, *76*, 125425.

[66] G. Koller, S. Berkebile, J. Ivanco, F. Netzer and M. Ramsey, *Surf. Sci.*, **2007**, *601*, 5683.

[67] T. Kakudate, S. Tsukamoto, N. Nakaya and T. Nakayama, *Surf. Sci.*, **2011**, *605*, 1021.

[68] E. Varene, L. Bogner, S. Meyer, J. Pennec, P. Tegeder, *Phys. Chem. Chem. Phys.*, **2012**, *14*, 691-696.

[69] E. Varene, J. Pennec, P. Tegeder, Chem. Phys. Lett. 515 (2011) 141.

[70] S.A. Carter, M. Angelopoulos, S. Karg, P.J. Brock, J.C. Scott, *Appl. Phys. Lett.*, **1997** *70*, 2067.

[71] X. Yang, D.C. Müller, D. Neher, K. Meerholz, *Adv. Mater.*, **2006**, *18*, 948.

[72] C.W.Sele, T.vonWerne, R.H.Friend, H.Sirringhaus, *Adv.Mater.*, **2005**, *17*, 997.

[73] P.Cosseddu, A.Bonfiglio, *Appl.Phys.Lett.*, **2006**, *88*, 023506.

[74] Y. Nishihara, A. Matsuda, A. Fujii, M. Ozaki, E.L. Frankevich, K. Yoshino, *Synth. Met.*, **2005**, *154*, 102.

[75] H. Neugebauer, *J. Electroanal. Chem.*, **2004**, *563*, 153.

[76] N. Koch, E. Vollmer, A. Elschner, *Appl. Phys. Lett.*, **2007**, *90*, 043512.

[77] J.R. Goldman, J.A. Prybyla, *Phys. Rev. Lett.*, **1994**, *72*,1364.

[78] E. Knoesel, A. Hotzel, M. Wolf, *Phys. Rev. B*, **1998**, *57*, 12812.

[79] T. Hertel, E. Knoesel, M. Wolf, G. Ertl, *Phys. Rev. Lett.*, **1996**, *76*, 535.

[80] K.-C. Chang, M.-S. Jeng, C.-C. Yang, Y.-W. Chou, S.-K. Wu, M.A. Thomas, Y.-C. Peng, *J. Electron. Mater.*, **2009**, *38*, 1182.

[81] E. Varene, P. Tegeder, *Appl. Phys. A* **2012**, *106*, 803.

[82] Y. Sohn, J. Richter, J. Ament, J.T. Stuckless, *Appl. Phys. Lett.*, **2004**, *84*, 76.

[83] Y. Sohn, J.T. Stuckless, *Appl. Phys. Lett.*, **2007**, *90*, 171901.

[84] Y. Sohn, J.T. Stuckless, *ChemPhysChem*, **2007**, *8*, 1937.

[85] Y. Sohn, J.T. Stuckless, *J. Chem. Phys.*, **2007**, *126*, 174901.

[86] Y. Sohn, J.T. Stuckless, *Chem. Phys. Lett.*, **2007**, *444*, 125.

[87] Y. Sohn, J.T. Stuckless, *Chem. Phys. Lett.*, **2007**, *436*, 228.

[88] G.D. Hale, S.J. Oldenburg, N.J. Halas, Phys. Rev. B 55 (1997) R16069.

[89] G.D. Hale, S.J. Oldenburg, N.J. Halas, Appl. Phys. Lett. 71 (1997) 1483.

[90] F.J. Zhang, A. Vollmer, J. Zhang, Z. Xu, J.P. Rabe, N. Koch, *Org. Electron.*, **2007**, *8*, 606.

[91] V. Shrotriya, J. Ouyang, R.J. Tseng, G. Li, Y. Yang, *Chem. Phys. Lett.*, **2005**, *411*, 138.

[92] E. Varene, P. Tegeder, *Appl. Phys. A* **2012**, *107*, 13.

[93] A. Sakamoto, M. Takezawa, *Synth. Met.*, **2009**, *159*, 809.

[94] A. Ruseckas, M. Theander, M.R. Andersson, M. Svensson, M. Prato, O. Inganas, V. Sundström, *Chem. Phys. Lett.*, **2000**, *322*, 136.

Acknowledgments

First of all I would like to express all my gratitude to Prof. Petra Tegeder. It has been a real pleasure to work in her group during the last four years. Her door was always open, and she was always in a good mood and ready to take time for a discussion. Vielen Dank!

I also want to thank Prof. Katharina J. Franke for accepting to be the second referee of this work.

I would like to thank Prof. Martin Wolf who has allowed me to start my PhD at the FU, as Prof. Petra Tegeder was still a member of his group.

I thank Sebastian, who has taught me how to use the whole experimental setup within the first 15 min of my PhD. I think that Micha and Mathieu will never forget my face expression that day.

I want to thank Lea who has been a very good colleague and friend since she as joined the group.

Thank you Chris. You have been a great flatmate during a few months, even after we almost died during our ski tour in the Alps.

Thank you Stephan for the daily morning glass of wine in Grenoble.

I want to thank all the group for the very nice working atmosphere: Micha, Micha, Felix, Anton, Isabel, and Mathias. As well as Dietgard Mallwitz and Peter West for their great support for diverse problems related to administration.

Thank you to all my friends, and especially to Filip who even came back from holidays when I needed his help. Djakuem!

Thank you Marcia for being the perfect roommate, I will visit you in Rio again!

And of course I want to thank my family for supporting me and accepting my decision to live far away from them. Merci!

And finally, thank you Kasia "kochany kasku" Kajma for making my life nicer everyday with your smile and your support. Dziekuje! Kocham moja Slicznotka!

Curriculum Vitae

For reasons of data protection,
the curriculum vitae is not included in the online version

Erklärung der Urheberschaft

Ich erkläre hiermit an Eides statt, dass ich die vorliegende Arbeit ohne Hilfe Dritter und ohne Benutzung anderer als der angegebenen Hilfsmittel angefertigt habe; die aus fremden Quellen direkt oder indirekt übernommenen Gedanken sind als solche kenntlich gemacht. Die Arbeit wurde bisher in gleicher oder ähnlicher Form in keiner anderen Prüfungsbehörde vorgelegt und auch noch nicht veröffentlicht.

Ort, Datum Unterschrift